Margarita Mármol

Development of a new bearing geometry to reduce friction losses

Maschinenelemente und Getriebetechnik Berichte

Development of a new bearing geometry to reduce friction losses

Vom Fachbereich Maschinenbau und Verfahrenstechnik
der Technischen Universität Kaiserslautern
zur Erlangung des akademischen Grades

Doktor-Ingenieur (Dr.-Ing.)
genehmigte
Dissertation

von
Frau Margarita Mármol M.Sc.
aus Madrid, Spanien

Dekan: Prof. Dr.-Ing. Tilmann Deck
Prüfungsvorsitzeder: Prof. Dr.-Ing. Oliver Koch
Berichterstatter: Prof. Dr.-Ing. Bernd Sauer
Prof. Dr.-Ing. Roman Teutsch

D386

Preface

This thesis was written while I was working as a research assistant at the Chair of Machine Elements, Gears and Tribology (MEGT) at the Technical University of Kaiserslautern. The dissertation is based on the work carried out within the framework of the research project "Reibungsverlustoptimiertes Wälzlager zur Substitution von hochbelasteten Kegelrollenlagern" (DFG reference SA 898/19-1) of the Deutsche Forschungsgemeinschaft e.V. (DFG). I would like to take this opportunity to thank the DFG for funding the project.

I would especially like to thank my doctoral supervisor Prof. Dr.-Ing. Bernd Sauer. The always valuable advice from his wealth of experience and the stimulating technical discussions have contributed greatly to the success of this dissertation. I am particularly grateful for the great trust placed in me for the success of my work.

I would like to thank Prof. Dr.-Ing. Roman Teutsch, Head of the Institute for Mechanical and Automotive Design (iMAD) at the Technical University of Kaiserslautern, for supervising my work. I would like to thank Prof. Dr.-Ing. Oliver Koch, Head of the Institute of Machine Elements, Gears and Tribology, for chairing the examination board.

I would like to thank my colleagues for their support. Special thanks goes to Dr.-Ing. Timo Kiekbusch, Dr.-Ing. Sebastian Wiesker, Jun. Prof. Dr.-Ing. Stefan Thielen, Dr.-Ing. Rahul Dahiwal, Seiedardeshir Sebteini, M.Sc., Dipl.-Ing. Lukas Rüth, Simon Graf M.Eng. and Dipl.-Ing. Patrick Wingertszahn for the always helpful discussions and their support of my work at MEGT.

I would also like to express my gratitude to my numerous research assistants as well as students and graduates over the years.

My special thanks go to my family and personal environment, who have supported and encouraged me at all times on my life's journey. The support I have received from you has made this work possible in the first place. My very special thanks goes to my dear husband René, for believing in me and for his patience and support over the past years. I would also like to thank my parents and brother, Flor, Fernando and Nacho for their constant support and encouragement during my academic career: "Gracias por vuestro apoyo".

Kaiserslautern, July 2022

Abstract

The choice of the optimal rolling bearing depends on the boundary conditions and the requirements of the application. This way, the rolling bearings are designed in terms of their requirements of carrying capacity, the resulting frictional losses or the velocity limit among others. The optimization of the internal geometry of rolling bearings for specific applications is still a focus of study. Moreover, new rolling bearings, based on the existing geometries have been developed in the recent years and are on continuous development up to now.

One of the most commonly used rolling bearings for combined load when high load carrying capacity is needed is the tapered roller bearing (TRB). Although this type of rolling bearing has been used in widespread application, its relatively high friction losses occurring at the rib contact are a spotlight for the engineers on this area of work. A solution for reducing the frictional losses appearing at TRBs for applications where a high load carrying capacity is needed is still being searched for. Many recent studies focus on the optimization of the contact between the roller end and the raceway rib surface. On the contrary, this work focuses on the development of a new type of rolling bearing, based on the existing TRB, but where a rib contact is no longer needed.

First of all, the geometrical parameters defining the internal geometry of the rolling bearings, more specifically the contact between the roller and the raceways, have been studied. Moreover, several patents defining new geometries of rolling bearings have been analyzed. Based on the correlations observed between the different geometrical parameters, types of geometries and outcomes, the geometry of a new type of rolling bearing has been developed. In order to study its behavior, a Multi-Body-Simulation (MBS) Model of the new type of rolling bearing has been generated. Moreover, in order to validate the model, a prototype of the geometry under study has been manufactured and experimentally tested. The results obtained have been compared with the simulated results as well as with a TRB of same main dimensions. After the validation of the model, several simulations have been conducted in order to understand better the behavior of the new rolling bearing design. To do so, a sensitivity analysis has been conducted. Within the analysis, the main geometrical parameters defining the roller-raceway contact have been varied and their influence on main outcomes examined. Finally, an application example of an axle-gearbox for heavy-duty trucks is presented and its result compared with those of a tapered roller bearing.

Kurzfassung

Die Auswahl des optimalen Wälzlagers wird durch die Randbedingungen und die vorherrschenden Anforderungen der entsprechenden Anwendung bedingt. Also gibt es unterschiedliche Ausprägungen von Wälzlager was unter anderem die Anforderung an Tragfähigkeit, die Reibungswiderstände und die Grenzdrehzahl angeht. Die Optimierung der internen Geometrie eines Wälzlagers gilt nach wie vor nicht als abgeschlossen. In den vergangenen Jahren wurden weiter neue Wälzlager auf Basis der bereits vorhandenen Geometrien entwickelt. Bis zum heutigen Tage finden neue Entwicklungen in diesem Bereich statt.

Ein typisches Wälzlager für kombinierte Belastung die eine hohe Tragfähigkeit aufweisen sind Kegelrollenlager. Obwohl diese Art von Lager bereits in einer Vielzahl von Anwendungen zum Einsatz kam stellt der relativ hohe Reibungsverlust des Lagers, der am Bordkontakt auftaucht, den Fokus vieler Überlegungen von Ingenieuren aus diesem Bereich dar. Eine Lösung des genannten Problems der hohen Reibungsverluste eines Kegellagers am Bordkontakt, bei der Anforderung eine hohe Tragfähigkeit aufzuweisen, konnte bislang nicht gefunden werden. Der Fokus von vielen neueren Studien in diesem Bereich liegt auf der Optimierung des Kontaktes zwischen dem Rollen und den Bord des Innenrings. Im Gegensatz zu diesem Ansatz befasst sich die vorliegende Arbeit mit der Entwicklung eines neuen Wälzlagers welches auf dem Kegelrollenlager basiert, bei dem jedoch kein Bordkontakt mehr nötig ist.

Zunächst fand eine Untersuchung der geometrischen Parameter, welche die interne Geometrie eines Wälzlagers bestimmen, genauer gesagt welche den Kontakt zwischen dem Wälzkörper und der Laufbahn bestimmen, statt. Darüber hinaus wurden verschiedene Patente, welche neue Geometrien von Wälzlagern offenbaren analysiert. Letztlich wurde die Geometrie eines neuen Wälzlagers entwickelt basierend auf den Korrelationen, die zwischen den verschiedenen geometrischen Parametern und den verschiedenen Geometrien und deren Ergebnissen, aufgezeigt werden konnten. Um Verhaltensmuster der neuen Art von Wälzlager studieren zu können, wurde ein Mehrkörpersimulation (Multi-Body-Simulation, MBS) Modell angefertigt. Des Weiteren wurde ein Prototyp der zu untersuchenden Geometrie hergestellt und experimentell getestet mit dem Ziel der Validierung des Modells. Die so generierten Daten wurden sowohl mit den simulierten Ergebnissen als auch mit einem Kegelrollenlager mit den gleichen Hauptabmessungen verglichen. Nach der Validierung des Modells fanden mehrere Simulationen statt mit dem Ziel das Verhalten des neuen Wälzlagertyp besser zu verstehen. Um dies zu ermöglichen wurde eine Sensitivitätsanalyse

durchgeführt. Während des Analysevorgangs wurden die Hauptgeometrischen Parameter die einen Wälzkörper-Laufbahn Kontakt ausmachen variiert und deren Einfluss auf das Hauptergebnis untersucht. Letztlich werden die Ergebnisse des Vergleichs eines Anwendungsbeispiels bei einem Achsgetriebe in Schwerlastfahrzeugen mit dem neuen Wälzlager und einem Kegelrollenlager dargestellt.

Contents

List of Symbols

Variable	Description	Unit
aA	Distance from the BA to the PA	mm
aP	Distance between contact points	mm
aPk	Distance from one contact point to the roller end	mm
B	Rolling bearing width	mm
BA	Bearing axis	mm
b_m	Load rating coefficient	-
C_0	Dynamic load rating	N
C_0	Static load rating	N
d	Rolling bearing bore diameter	mm
D	Rolling bearing outside diameter	mm
D_{pw}	Pitch diameter	mm
D_{we}	Roller diameter	mm
e	Calculation factor for the dynamic load ratings	-
F	Force	N
F_a	Axial force	N
f_c	Load rating coefficient	-
F_N	Normal force	N
F_r	Radial force	N
F_R	Frictional force	N
$F_{T,L,s}$	Lubricant sliding force	N
$F_{T,S,s}$	Solid body sliding force	N
h_0	Lubricant film height	mm
h_{min}	Minimum lubricant film height	mm
i	Number of roller rows	-
L_{10}	Nominal fatigue life	10^6 revolutions
L_{we}	Effective roller length	mm
M	Frictional torque	Nmm
$M_{T,hys}$	Material hysteresis torque	Nmm
$M_{T,L,r}$	Lubricant rolling torque	Nmm
$M_{T,L,s}$	Lubricant sliding torque	Nmm
$M_{T,S,r}$	Solid body rolling torque	Nmm

$M_{T,S,s}$	Solid body sliding torque	Nmm
n	Rotational velocity	rpm
$\vec{n}$	contact normal	-
n_C	Rotational velocity of the cage	rpm
n_{IR}	Rotational velocity of the inner ring	rpm
n_{OR}	Rotational velocity of the outer ring	rpm
n_R	Rotational velocity of the roller	rpm
$\vec{p}_R$	contact normal to the slice	-
$\vec{p}_{RW}$	contact normal to the raceway	-
p	Calculation factor for the nominal fatigue life	-
P	Equivalent dynamic load	N
P_0	Equivalent static load	N
p_{EHL}	Pressure distribution in EHL contacts	MPa
p_H	Hertzian pressure distribution	MPa
PA	Axis of the center of curvature	mm
$\vec{p}$	contact point	-
$\vec{p}_R$	contact point vector on the roller	mm
$\vec{p}_{RW}$	contact point vector on the raceway	mm
$\vec{p}_S$	central point vector of a slice	mm
$P(x_k)$	Profile function	mm
r	Rolling bearing bore radius	mm
R	Rolling bearing outside radius	mm
R_0	Radius of a circular crowned profile	mm
re	transverse raceway radius	mm
re_c	circumferential raceway radius	mm
r_S	Slice radius	-
s	Geometrical parameter defining the osculation	mm
S_0	Static load-bearing safety	-
u	Circumferential velocity	m/s
u_0	Summation of the circumferential velocities of two bodies in contact	m/s
u_C	Circumferential velocity of the cage	m/s
u_{IR}	Circumferential velocity of the inner ring	m/s
u_R	Circumferential velocity of the roller	m/s
u_{rel}	Difference of the circumferential velocities of two bodies in contact	m/s
W	External load	N
X	Dynamic radial load factor	-
X_0	Static radial load factor	-

x_k	Distance from the center of the slice k to the center of the rolling element	mm
Y	Dynamic axial load factor	-
Y_0	Static axial load factor	-
Z	Number of rollers	-
α	Contact angle	°
β	Load angle	°
δ	Penetration	mm
γ	Taper angle	°
κ	Osculation	-
κ_1	Misalignment factor parameter for toroidal roller bearings	-
μ	Coefficient of friction	-
μ_{min}	Point of minimal friction	-
ω	Angular velocity	s^{-1}
Φ	Solid load-bearing component	-
Λ	Specific lubricating film hight	mm
θ_a	Tilting angle of the shaft	°

Abbreviations

Abbreviation	Description
3D	Three dimensional
AST	Alternative Slicing Technique
BA	6 Bearing Axis
BEAST	Bearing Simulation Tool
BRAIN	Bearing Analysis in NSK
Caba3D	Computer Aided Bearing Analyser 3D
CAD	Computer Aided Design
CARB	Compact Aligning Roller Bearing
CFD	Computational fluid dynamics
CoDaC	Calculation of Drag and Churning
COF	Coefficient of Friction (μ)
CPD	Contact Potential Difference
DIN	Deutsches Institut für Normung
EHL	Elastohydrodynamic Lubrication
FEM	Finite Element Model
GBLM	Generalized Bearing Life Model
MBS	Multi-Body Simulation
MEGT	Chair of Machine Elements, Gears and Tribology
PCR	Profile curve radius
PCR_{LB}	Profile curve radius of the raceway
PCR_R	Profile curve radius of the roller
SRR	Slide-to-Roll ratio
TRB	Tapered roller bearing
TSRB	Tapered spherical roller bearing

1 Introduction

The main goal when designing a rolling bearing is to connect two components that move relative to one another and the associate transfer of forces while minimizing the total frictional torque between the parts. Because of their versatility, low friction and high power density, rolling bearings are one of the most frequently used machine elements.

The relative movement of two bodies in contact is always associated with a resistance that counteracts this movement. This resistance is the resultant of the friction that takes place in the contact between the two bodies. Rolling bearings are made up of several mechanical elements mounted and in contact with each other. The various contacts between these elements are subject to different types of friction, depending on the type of relative velocity between the elements. Since the reduction of the overall losses is the ultimate goal when designing a mechanical element, in order to minimize the friction taking place, the design of all its components is carefully studied and constantly optimized.

Depending on the direction of movement between the two components, rolling bearings can be separated between translational (linear motion) and rotatory movement (e.g. shaft and housing). Based on the main load direction, rolling bearings can as well be differentiated into radial or axial bearings. This work is focusing on rotary radial bearings.
Generally speaking, rotary radial bearings consist of two concentric rings, provided with raceways, between which the rolling elements are embedded and allowed to roll. Both inner and outer ring are firmly connected to the relatively moving components, in most of the cases shaft and bearing housing. In some cases, the rolling elements are guided by a cage, maintaining a constant distance between them. A scheme of a rolling bearing structure is shown in Figure 1.1 [Wan15]. The function of the rolling elements is to ensure the relative movement of the two rings by rolling. Due to elastic deformation, in addition to pure rolling, sliding takes place between the contact partners. This combination of pure rolling and sliding motion results in the characteristic rolling motion of all rolling bearings, which is associated with low resistance and, therefore, low frictional losses.
Depending on the shape of the rolling elements, according to DIN 611 [DIN10b], rolling bearings can, likewise, be divided into ball (e.g. deep groove ball bearings or angular contact ball bearings) and roller bearings. The shape of the roller and its profile is a complex and extensive research field. Broadly speaking, rollers are divided into cylindrical, tapered and barrel rollers. Nevertheless, due to the profiling of the rollers, we can find both

cylindrical and tapered rollers with a spherical or logarithmic profile. The different types of profiling, as well as other geometrical characteristics of the rollers are explained in section 2.1.2. Depending on the size of the rollers and their arrangement, the rolling bearings with rollers as rolling elements can be divided into: cylindrical and needle (cylindrical rollers), tapered (tapered rollers), barrel, spherical and toroidal (barrel rollers) roller bearings. An overview of the most common rolling bearing types is shown in section 2.2.
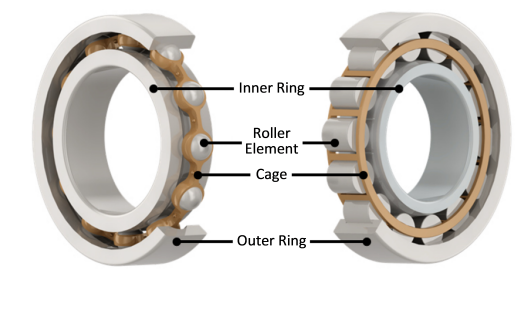
Figure 1.1: Structure of an exemplary rolling bearing of a deep groove ball bearing (left) and a cylindrical roller bearing (right).[Wan15]

The selection of the best rolling bearing type for a specific application is usually made taking the existing operating conditions into account. Above all, the static and dynamic load ratings of the rolling bearing play an important role in the selection process. Other parameters listed in the rolling bearing catalogs, like the size or limit speeds can be used as auxiliary variables.

These variables are all strongly influenced by the geometric parameters defining the rolling elements and are the basis for determining the rolling bearing life.

The design and dimensioning of rolling elements based on the operating conditions, its influence on the static and dynamic behavior of the rolling bearing and ultimately on the total frictional losses and bearing life, is the main focus of this thesis work.

2 State of the art

The field of rolling bearings is very extensive. This section focuses on the principles relevant for this work. An overview of this section is shown in Figure 2.1. Since the work focuses on the variation of the roller and raceway geometries, the first subsection (2.1) focuses on the parameters defining those geometries and their influence on the contact between them. Special attention goes to the definition of the rib contact and its influence in the behavior of rolling bearings, described in section 2.1.3. Afterwards, the way those parameters influence the lifetime and kinematic of the rolling bearing is presented in sections 2.1.4 and 2.1.5.

This work focuses on the reduction of the frictional torque resulting on the contact between roller and raceway. Therefore, section 2.3 describes the types of friction and friction conditions relevant for rolling bearings.

An overview of the standard rolling bearing types, their geometrical definition as well as their applications is summarized in section 2.2.1. The fundamentals of the dynamic simulation of rolling bearings, the basis of the simulations conducted within this work, is presented in section 2.4.
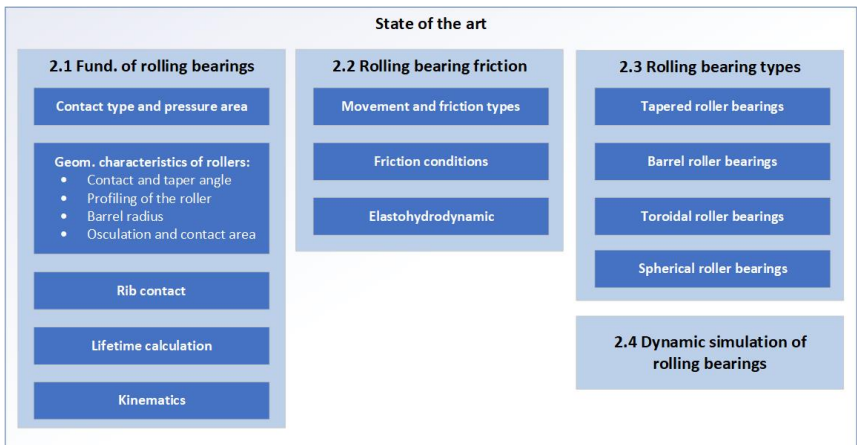
Figure 2.1: Overview of the chapter State of the Art

2.1 Fundamentals of rolling bearings

2.1.1 Contact type and pressure distribution

The transmission of forces between inner and outer ring takes place via the rolling elements. These forces generate loaded contact areas, especially between the rolling elements and the raceways. At these areas, elastic deformation takes place in form of a flattening or depression. As a result, a contact pressure distribution appears around the contact point. Theoretically, an elliptical contact area results from the point contact with ball bearings (see Figure 2.2 left). On the other hand, a rectangular contact area results from the line contact with roller bearings (see Figure 2.2 right). The theoretical pressure distribution in the rolling element resulting from both types of contact is represented with red lines.

Compared to a ball, the rollers have a larger contact area perpendicular to the roller axis. As a result, it can transmit higher forces, has greater rigidity and it allows the application of smaller rolling elements under the same load. For cases with a line contact, the longer the contact length along the roller axis is, the higher the resulting rolling friction is.
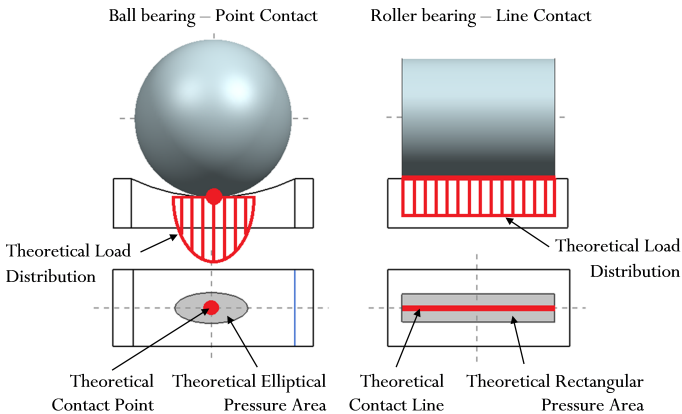
Figure 2.2: Point vs. Line contact.(Wang)

The geometry of the rolling element and the raceways defines the contact behavior at the rolling element-raceway contact. This contact is, for the majority of the situations, the most important in terms of friction losses, being primarily responsible of the resultant total friction (in cases of mixed friction, the rib contact plays and important role and has to be as well studied (see section 2.1.3). Within this work, the focus lays on the geometry of the rollers. There are many geometrical parameters defining the geometry of a roller. The next section gives an overview of the most important geometrical parameters of a roller.

2.1.2 Geometrical characteristics of rollers

Contact and taper angle   The contact angle α indicates the orientation of the contact line. The contact line is in turn defined by the perpendicular to the tangent between the rolling elements and the raceways. According to the contact angle and thus the preferred load direction, a distinction is made between two types of rolling bearings. This is: axial bearings, where the contact angle is bigger than 45° and radial bearings, where the contact angle is smaller than 45°. Depending of the type of roller bearing, radial roller bearings might be as well subjected to a high external axial force (e.g., tapered roller bearings). The angle that the resultant of the external bearing radial force F_r and the axial force F_a forms to the vertical, is called the load angle β. Furthermore, this angle determines the direction of the external force. It should not be confused with the contact angle α, which defines the direction in which the bearing force is transmitted between the outer and inner ring [HB96] (see Figure 2.3).
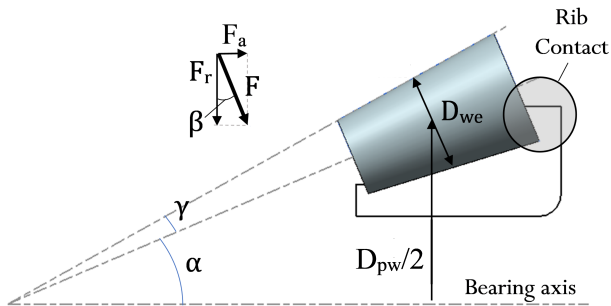
Figure 2.3: Contact angle α and taper angle γ defining the geometry of a tapered roller bearing. Load angle β between the radial force F_r and the axial force F_a

When choosing a bearing and its corresponding contact angle, two parameters have to be taken into consideration in order to maximize the life time: the dynamic bearing load, and the load rating. Both parameters are highly influenced by the contact angle of the bearing. In general terms, the highest load-bearing capacity for a bearing is obtained when $\alpha \approx \beta$. The influence that the contact angle has in the dynamic bearing load and the load rating and thus, the life time of the bearing, is explained in section 2.1.4. The contact angle is influencing the resultant velocities of both cage and rollers as later explained in section 2.1.5.

When the contact angle is bigger than zero, the surface lines of the rollers should intersect at a point at the bearing axis in order to provide an optimal kinematic behavior by minimizing the slippage and drilling friction. This way, an even distribution of pressure

with its maximum on the middle of the rolling surface can be obtained for purely radially loaded bearings and non-tilted rolling elements. Furthermore, it allows for a symmetrical pressure distribution of the rollers and ultimately reduces slippage [Neu17][Nak76]. The geometrical constrain of the surface lines intersecting at a point at the bearing axis turns into a taper angle γ of the rollers that can be defined in terms of the contact angle (α), the diameter of the roller (D_{we}) and the pitch diameter of the rolling bearing (D_{pw}) as follows:

$$\gamma = atan\left(\frac{D_{we}}{D_{pw}/sin\alpha}\right) \tag{2.1}$$

With the taper angle defined before, the rolling elements have a characteristic cone-shaped geometry. This geometry is characterized by symmetrical taper angles of the inner and outer ring raceways in relation to the rolling bearing axis. When the rolling elements are loaded, because of this cone-shaped inner geometry, the forces acting on the outer ring F_O and the inner ring F_I result into a normal force acting on the flange of the inner ring F_R (see Figure 2.4). In order to absorb this resulting axial force, a rib in the inner ring has to be provided.

The geometry of the roller end and the rib surfaces in a tapered roller bearing (TRB) is such, that a point contact and the resulting elliptical contact area existing between them. Figure 2.4 illustrates the load situation and the contact point and pressure area appearing at the contact. [KD11; Kor11]
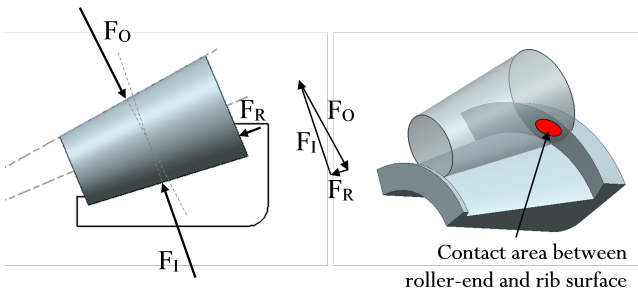
Figure 2.4: Forces on a tapered roller bearing

For geometries where the contact angle is zero, the raceway contact will not be able to carry axial loads. In cases where axial forces appear, a rib contact has to be as well provided. The contact between the rolling elements and the rib of the inner ring is of great importance in terms of transmission of forces and friction behavior. The friction appearing at this contact is pure sliding, with a relatively higher coefficient of friction compared to the roller-raceway contact. This friction plays a particularly important role in TRB, being the reason of the high friction losses appearing in mixed friction regime for this type of

rolling bearing. Therefore, the need of a rib contact should, if possible, be avoided. The proportion of this friction to the total friction losses of the roller bearing depends on many factors e.g., rotational speed, load, lubrication; all affecting the lubrication condition at the flange. In cases of mixed friction, the friction losses at the flange are at its maximum and dominate over the others.

Profiling of the roller   In section 2.1.1, for the case of a roller, an even pressure distribution in the longitudinal direction is presupposed. In reality, however, there is a pressure peak due to the stress concentration and thus a widening of the pressure area in the edge area of an unprofiled cylinder [Reu87] (see Figure 2.6a). These stress peaks have a decisive influence on the load-bearing capacity and the service life. In order to avoid these stress peaks, cylindrical and tapered rollers are nowadays manufactured with a profile. This way, the outer surface of the roller is not longer purely cylindrical or conical, but with a certain curvature. The stress distribution at the contact area between the rollers and raceways is thus determined by the contact profile of the rollers. This profiled surface leads to a more even distribution of pressure compared to the unprofiled surface. The profiles of the different rolling bearing manufacturers can differ from one another. As a general reference for the profiling of the roller, the logarithmic profile described by LUNDBERG [Lun39] can be set. The logarithmic profile and the corresponding equations for cylindrical and tapered rollers are described in DIN 26281 [DIN11] as follows:

For cylindrical roller bearings:

If $L_{we} \leq 2,5 \cdot D_{we}$:

$$P(x_k) = 0,00035 \cdot D_{we} \cdot ln \left[\frac{1}{1 - \left(\frac{2 \cdot x_k}{L_{we}} \right)^2} \right] \tag{2.2}$$

If $L_{we} \geq 2,5 \cdot D_{we}$ and $|x_k| \leq \frac{L_{we} - 2,5 \cdot D_{we}}{2}$:

$$P(x_k) = 0 \tag{2.3}$$

If $L_{we} > 2,5 \cdot D_{we}$ and $|x_k| > \frac{L_{we} - 2,5 \cdot D_{we}}{2}$:

$$P(x_k) = 0,0005 \cdot D_{we} \cdot ln \left[\frac{1}{1 - \left[\frac{2 \cdot |x_k| - (L_{we} - 2,5 \cdot D_{we})}{2,5 \cdot D_{we}} \right]^2} \right] \tag{2.4}$$

For tapered roller bearings:

$$P(x_k) = 0,00045 \cdot D_{we} \cdot ln \left[\frac{1}{1 - \left(\frac{2 \cdot x_k}{L_{we}} \right)^2} \right] \tag{2.5}$$

Another commonly used profile type is the circular crowned profile. This profile sets the basics for the geometrical definition of a barrel roller bearing. Figure 2.5 shows a graphical representation of a circular crowned profiled for a tapered roller. With the parameters represented on it, the circular crowned profile follows the equation:

$$P(x_k) = R_0 - \sqrt{R_0{}^2 - x_k{}^2} \tag{2.6}$$
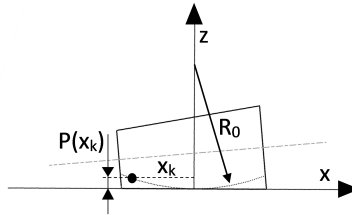
Figure 2.5: Geometrical dimension of crowned tapered roller/raceway contact.

Figure 2.6 shows some examples of contact profiles and their resulting pressure distribution compared to an unprofiled cylinder. In the first column of pictures, a lower load is applied to the roller. In the middle column, a higher load is applied, so that for every type of contact profile the whole contact length is loaded. In the third column, the load is not applied in the middle of the roller but displaced, so that an uneven distribution of pressure takes place along the contact length.
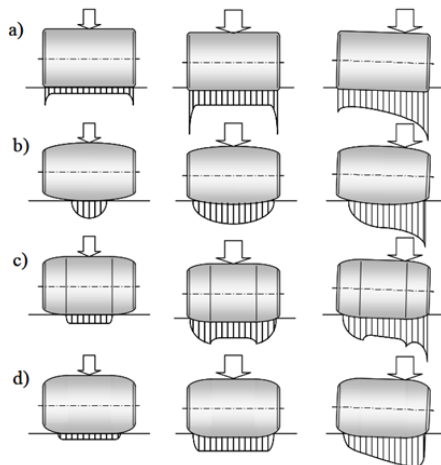
Figure 2.6: Influence of the rolling profile on the load distribution for cylindrical (a), spherical (b), cylindrical-spherical (c) and logarithmical (d) profiles [Reu87].

It can be observed, that stress concentrations can however still appear in profiled rolling elements under various circumstances: when the load increases, when an eccentric force is applied or when the rolling bearing is tilted. For this reason, a very precise calculation of the stress distribution in linear contacts has to be done. For this propose, slice models will be used. More information about the existing slice models and its implementation in the Multibody Simulation Model is explained in section 5.2.1.

Barrel radius   A barrel roller is ultimately a completely profiled cylinder roller. Its profile follows equation (2.6), where the total length of the roller has a profile defined by a profile curve radius ($R_0 = PCR$). An example of a barrel roller is shown in Figure 2.6.b. This type of roller is commonly used for compensating angular misalignment where skewing takes place between the outer and the inner ring. For rollers where the contact surface is barrel-shaped, different behaviors can be observed depending on how the radius of the roller is defined. In these terms, we have barrel or spherical roller bearings (where the center of the PCR lays at the bearing axis) and toroidal roller bearings (where the center of the PCR lays at an axis further apart from the roller than the bearing axis). The location of the center of the PCR for toroidal rollers is represented in Figure 2.7 by the bigger PCR on the right side of the picture. By the fact that the PCR of the raceways and the rollers in such bearings are considerably greater than corresponding radii in e.g., spherical roller bearings with corresponding radial measures, the rollers can be made longer than what is possible in such spherical bearings. This characteristic enhances the radial load carrying capacity of the rolling bearing. Other geometries, where the profile curve radii of the raceways are smaller than for spherical roller bearings (smaller radius on the left side of Figure 2.7), have been described in different patents [Gre19][KKL16], and are yet to be studied.
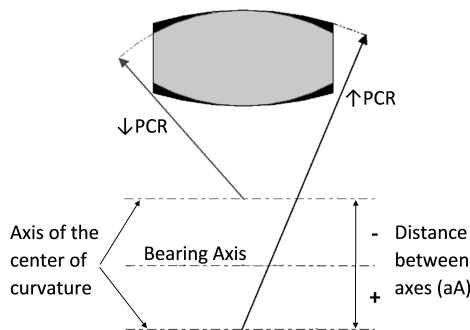
Figure 2.7: Different profile curve radii (PCR) of the roller

As in every angular-contact ball bearing, a drilling friction results from a contact diameter that is not orthogonal to the axis of rotation of the roller. This turns into a bigger drilling

friction, the smaller the PCR is. This, as well as other types of frictions, are explained in section 2.3.1.

When varying the PCR of the rollers, their crowning changes. When increasing the PCR, a flatter roller results, increasing the axial displacement of the roller. This behavior is due to the fact that the angle between the acting axial load and the roller surface absorbing this load is decreased. Figure 2.8 shows two rollers with different PCR: a roller with lower PCR (a), therefore higher angle between the acting axial load and the roller surface absorbing this load and a roller with higher PCR (b), therefore lower angle between the acting axial load and the roller surface absorbing this load.
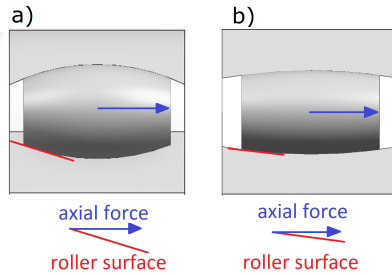
Figure 2.8: Influence of the PCR on the resulting angle between the acting axial load and the roller surface absorbing this load for an example with zero contact angle

Osculation and contact area   For all rolling bearings with a curved raceway profile in the axial section, the profile of the raceway has a slightly larger radius than the profile of the rolling element. This difference in the curvature in the axial plane is characterized by the osculation. For barrel, toroidal and spherical roller bearings, the osculation is defined as the ratio between the PCR of the rollers and the PCR of the raceway. It follows the equation:

$$\kappa = 1 - \frac{PCR_{LB} - PCR_R}{PCR_R} \tag{2.7}$$

The length of the contact area existing between rollers and inner and outer ring is highly influenced by the osculation. In these terms, a narrower osculation ($\kappa \to 1$) turns into a bigger contact length. The size of the contact area directly affects parameters like frictional torque, maximum pressure and load ratings. Figure 2.9 shows a plain representation of different osculations and its resulting contact length for a ball bearing and a barrel roller bearing.
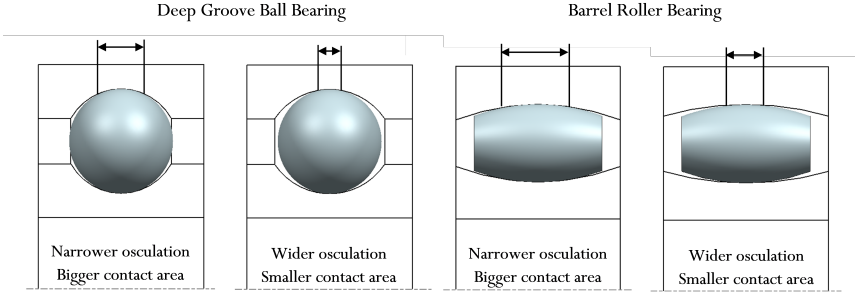
Figure 2.9: Influence of the osculation in the resulting contact length

2.1.3 Rib Contact

At the contact between the roller-end and the raceway rib, all three types of friction types occur superimposed: sliding friction, rolling friction and drilling friction. Furthermore, the frictional forces on the rib result in a moment that causes the rolling element to skew.

The contact between the roller-end and the raceway rib surface plays a particularly important role in tapered roller bearings. This contact supports both, the external axial force as well as the axial force component resulting from an external radial force acting on the different taper angles of the inner and outer ring. Although the external axial force has a bigger effect on the rib load, an axial force is always present, event for pure radial loads. As a result, this contact point has a decisive influence on the functionality and losses of this type of rolling bearing, especially in mixed friction regime.

A kinematic property of rolling bearings with significant rib forces is the rolling element skew caused by them (see Figure 2.10). This skew movement is mainly caused by the resulting friction at the rib surface. Since the forces that occur depend on the lubrication conditions, load, speed and surface properties, it is not possible to determine the skew based on the geometry alone. The rolling element skew is very difficult to measure.
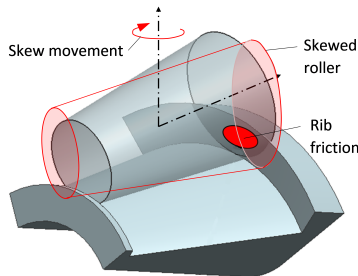
Figure 2.10: Skew movement of the roller resulting from the friction occurring at the rib contact

YANG et al. developed a measuring method using contact potential difference (CPD) with which you can successfully measure the rolling element skew [YDH99; YDH00a; YDH00b]. Their measurements show that the skew changes during operation and that there is a noticeable scattering between the rolling elements. The authors presented an empirically derived equation which relates the rolling element skew to basic bearing data. The tests show a skew in the range between 0.15 and 0.6 °. YANG et al. come therefore to the conclusion that the correct description of friction in the rib contact is of essential importance for mapping the bearing behavior.

In [ZQH88], ZHANG et al. developed a EHL (Elastohydrodynamic Lubrication) model for the contact between the roller end and the raceway rib surface in tapered roller bearings. The investigations come to the conclusion that the non-Newtonian behavior plays a decisive role in the prediction of the frictional torques and that at high speed the influence of the temperature on the minimum lubricant film height and the frictional torque cannot be neglected. As part of his work, KOCH developed the three-dimensional quasi-static calculation model Zyroax for combined loaded cylindrical roller bearings [Koc08] in which both the description of the raceway and the rib contacts are based on discretized contact models. It describes the interactions between raceway and rib contact and their influence on the service life. The frictional forces on the rib cause the rolling elements to tilt and therefore sets a mutual influence on the pressures in the contact points.

An extension of the rolling bearing calculation tool of the Forschungsvereinigung Antriebstechnik e.V. (LAGER2) to include rolling bearing friction torques is shown in [WJO15], these are the basics described in [WP13]. The friction in the rib contact is also dealt with. A comparison with test bench measurements on tapered roller bearings of type 31312A shows good accordance between the calculation model and the test results. At the same time, the influence of the rib friction, which dominates in mixed friction regime, due to the prevailing sliding friction is also evident (see Figure 2.11).
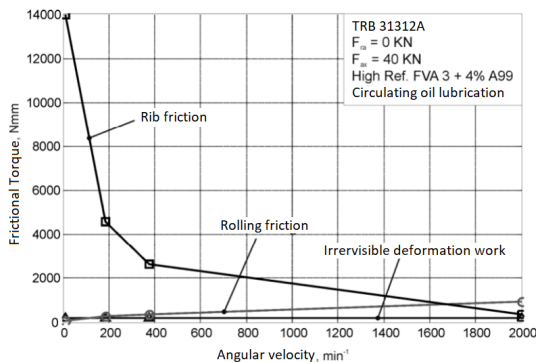
Figure 2.11: Calculation of the frictional torque components for a TRB 31312A [WP13]

KIEKBUSCH simulated in his work [Kie17] different geometries combinations for the raceway-end rib surface contact. In contrast to Koch's approach, who defined the rib contact through a single point contact, within the framework of his work, KIEKBUSCH discretized the rib contact surface using a cell model, allowing the correct consideration of the non-elliptical contact surface. Overall, the results of the developed models could be confirmed with the results from [Koc08], which proves the correct modeling of the resulting rib forces.

2.1.4 Lifetime calculation

With sufficient lubrication and cleanliness as well as medium to high loads, the bearing life ends due to fatigue damage that progresses from the inside of the material to the running surface. Likely, the fatigue process begins with material inhomogeneities when the shear threshold strength is exceeded. The tensions appearing in the material below the contact surface are decisive for their mechanical stress. Nevertheless, coefficients with force dimensions are being used in the bearing calculation. These are: the equivalent static (P_0) or dynamic load (P) for the stress and the static (C_0) or dynamic load rating (C) as a measure of the load capacity. The terms static and dynamic do not relate to changes in the external load, but to the angular velocity of a bearing. The basic load ratings as defined in [DIN09b] and [DIN10a] are as follows:

Static load ratings
If a bearing stands still, pivots or rotates slowly, it is considered to be statically stressed. If high, static or shock loads occur, the raceways and rolling elements may undergo plastic deformation. This deformation limits the static load carrying capacity of the rolling bearing with respect to the permissible noise level during operation of the bearing. In this case, the static load-bearing safety (S_0) is also a coefficient to be checked. The static bearing load P_0 is defined as the load that induces the same load at the center point of the most heavily loaded contact point between the rolling element and raceway as the combined load occurring in practice. The static bearing load can be obtained from the following equation:

$$P_0 = max\,(X_0 \cdot F_r + Y_0 \cdot F_a, F_r) \tag{2.8}$$

For roller bearings with one row of roller, as it is the case under study in this work, the parameters X_0 and Y_0 can be calculated as follows:

$$\begin{aligned} X_0 &= 0,5 \\ Y_0 &= 0,22 \cdot cot\alpha \end{aligned} \tag{2.9}$$

The basic static load rating C_0 is defined as the load under which the Hertzian pressure at the most heavily loaded point between the rolling elements and raceways reaches the

value of 4000 N/mm^2 for roller bearings. The following equation can be used in order to obtain the static load rating:

$$C_0 = 44 \cdot \left(1 - \frac{D_{we} \cdot cos\alpha}{D_{pw}}\right) \cdot i \cdot Z \cdot L_{we} \cdot D_{we} \cdot cos\alpha \tag{2.10}$$

Where D_{we} is the roller diameter, α the contact angle of the roller, D_{pw} the pitch diameter of the rolling bearing, i the number of roller rows, Z the number of rollers and L_{we} the effective roller length. The effective roller length is the length of the roller that is loaded. Under normal contact conditions, this load causes a permanent deformation at the contact points of approx. 1/10000 of the rolling element diameter. As previously mentioned, in addition to dimensioning on the basis of the fatigue life, it is advisable to check the static load safety factor S_0. The relation between the shock loads occurring during operation and the permissible value of S_0 is listed in [DIN09b] for different types of rolling bearings.

$$S_0 = \frac{C_0}{P_0} \tag{2.11}$$

Dynamic load ratings

The basic dynamic load rating C applies to rotating bearings. The equivalent dynamic bearing load P of the bearing results from the radial and axial mean force F_r and F_a of the load spectrum for the corresponding rotor speed. It can be calculated as follows:

$$
\begin{aligned}
P = X \cdot F_r + Y \cdot F_a \quad &\text{if} \quad \frac{F_a}{F_r} \leq e \\
P = F_r \quad &\text{if} \quad \frac{F_a}{F_r} > e
\end{aligned} \tag{2.12}
$$

For roller bearings with one row of rollers, the parameters e, X and Y can be calculated as follows:

$$
\begin{aligned}
e &= 1,5 \cdot tan\alpha \\
X &= 0,4 \\
Y &= 0,4 \cdot cot\alpha
\end{aligned} \tag{2.13}
$$

The basic dynamic load rating C is defined as the load of constant magnitude and direction which a sufficiently large number of apparently identical bearings can endure for a basic rating life of one million revolutions. In the case of radial bearings, this is a purely radial load, while in the case of axial bearings it is a purely axial load. The following equation can be used in order to obtain the dynamic load rating C:

$$C = b_m \cdot f_c \cdot (i \cdot L_{we} \cdot cos\alpha)^{7/9} \cdot Z^{3/4} \cdot D_{we}^{29/27} \tag{2.14}$$

Where D_{we} is the roller diameter, α the contact angle of the roller, Z the number of rollers and L_{we} the effective roller length. b_m and f_c are calculation factors. The first one depends on the rolling bearing type and the second one on the geometrical parameters

of the roller. Their values are listed in [DIN10a]. In addition to aspects such as rigidity or installation space, the bearings are usually selected with regard to the fatigue life according to [DIN10a]. The number of revolutions of the bearing rings relative to each other until failure due to material fatigue is the so-called bearing life. The bearing life varies considerably even under identical load (mainly due to irregularities in the material structure), so that it is not possible to calculate a service life in advance for a specific bearing.

The basic dynamic load rating was therefore defined as the equivalent load at which 90% of a larger number of similar bearings survive one million revolutions under standard conditions.

According to the standard DIN ISO 281 [DIN10a], the nominal fatigue life of the rolling bearing is defined as the basic rating life in millions of revolutions, that is reached or exceeded by 90% of a sufficiently large number of apparently identical bearings before the first indications of material fatigue appears. The nominal fatigue life is then calculated as:

$$L_{10} = (C/P)^p \tag{2.15}$$

The test results with a large number of bearings are showing that the value for the exponent p = 3 for ball bearings or p = 10/3 for cylindrical roller bearings is suitable for mathematically mapping the corresponding service life [DIN10a]. The fatigue life also depends on other parameters such as the degree of cleanliness of the lubricant, the oil viscosity or the oil temperature in the bearing. To take these additional influences into account, the equation for calculating the fatigue life is modified. There are various tools for determining the service life, allowing the designer to determine the respective bearing service life in the application. The modified nominal reference service life described in [DIN10a] allows to take into account parameters like the internal load condition, the lubrication conditions, the contamination conditions and materials deviating from the standard. Through the service-life correction factors introduced, the surface initiated fatigue can be estimated as well. The goal of this work is a first estimation in the search of an optimal geometry, therefore, only the nominal fatigue life will be taken into account.

The Generalized Bearing Life Model Recently, the company SKF introduced a new way of calculating the rolling bearing life, the so-called Generalized Bearing Life Model (GBLM) [MEG15]. The previous models for the estimation of the rolling bearing life are based on the consideration of an equivalent stress, originated beneath the contact surface, that is applied to the stressed volume of the rolling contact. Through the years, fatigue surface-originated fatigue, resulting from reduced lubrication or contamination, has been incorporated, by means of a multiplication factor, into the estimation of the bearing life, resulting into the expanded adjusted rating life. In the SKF GBLM, this issue is addressed by developing a general approach for rolling contact life in which the

surface-originated damage is explicitly formulated into the basic fatigue equations of the rolling contact. In these terms, the calculation of the lifetime is separated into the surface and the subsurface of the material. Therefore, different physical models can be applied for those two regions. On one hand, subsurface rolling contact fatigue can be treated following the classic dynamic capacity model. On the other hand, the surface needs more advanced tribological models, which can take care of the complex physical interactions occurring in highly stressed concentrated Hertzian contacts, such as lubrication, friction, wear, fatigue or running-in. This new formulation gives the power to better represent the tribology of rolling bearings in rating life calculations. Furthermore, it gives a better knowledge of the surface endurance that dominates the field performance of rolling bearings. [MEG15]

Influence of the contact angle Figure 2.12 shows the relation between the dynamic bearing load and the contact angle for different ratios axial to radial load. We can observe, that as soon as the load angle ($\beta = atan(F_a/F_r)$, see Figure 2.3) increases, the equivalent dynamic bearing load increases faster, the smaller the contact angle is. In other terms, smaller contact angles are more susceptible to an increase of the axial load. The nominal life time for different contact angles, compared to the load angle β is shown in Figure 2.13. It can be seen, that for each load angle, an optimal contact angle can be defined in order to maximize the lifetime. In general terms, for smaller contact angles, the longest lifetime of a bearing is obtained when $\alpha \approx \beta$. For the example represented in Figure 2.13, the geometrical parameters and dimensions of a TRB 32208 have been considered ($C = 79kN$ for α=14°).
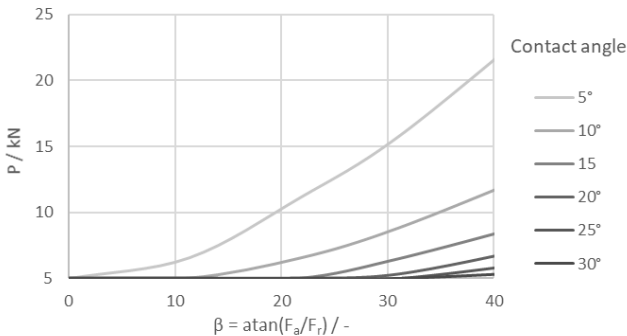
Figure 2.12: Influence of the load angle β on the dynamic bearing load P for different contact angles
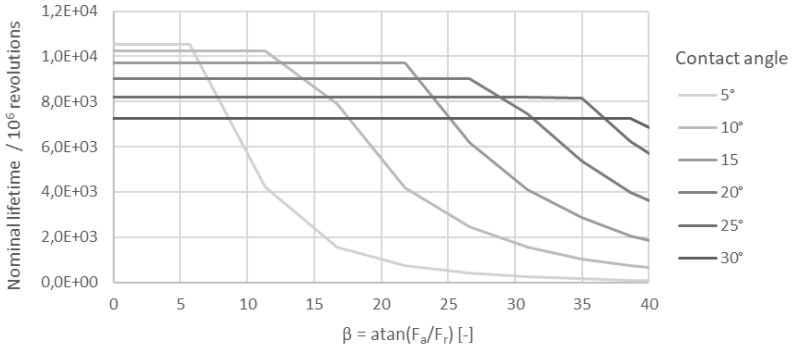
Figure 2.13: Influence of the load angle β on the nominal lifetime for different contact angles

2.1.5 Kinematics

The investigation of the effects occurring in rolling bearings requires the understanding of the rolling bearing kinematics. Assuming slip-free rolling bearing behavior, the rotation of the rolling elements and the cage can be calculated in terms of the rotation of the bearing rings with simple mathematical means according to [BEH95]. In these terms, the velocity of the rollers, cage and hence the dynamic of the rolling bearing is highly influenced by the geometry of the roller.

First of all, the fundamentals of kinematics, defining the difference between the angular velocity ω, the rotational velocity n and the circumferential velocity u have to be explained. The relation between these three velocities is as follows:

$$\omega = \frac{\pi n}{30} \tag{2.16}$$

$$u = R \cdot \omega = R \cdot \frac{\pi n}{30} \tag{2.17}$$

Where R is the radius of the rotational body (i.e. roller, cage or rings). Assuming a fixed outer ring and a rotating inner ring, for rolling bearings with slip-free behavior, the following relation can be assumed for the roller-inner ring contact:

$$u_R = u_{IR} \tag{2.18}$$

The circumferential velocity and the rotational velocity of a rolling element around the rolling bearing axis correspond to the circumferential and rotational velocities of the cage respectively (u_C, n_C). They can be calculated as follows:

$$u_C = \frac{\pi \cdot D_{pw}}{60} \cdot \left[\left(1 - \frac{D_{we} \cdot cos\alpha}{D_{pw}} \right) \cdot \frac{n_{IR}}{2} + \left(1 + \frac{cos\alpha}{D_{pw}} \right) \cdot \frac{n_{OR}}{2} \right] \tag{2.19}$$

$$n_C = \left(1 - \frac{D_{we} \cdot cos\alpha}{D_{pw}}\right) \cdot \frac{n_{IR}}{2} + \left(1 + \frac{D_{we} \cdot cos\alpha}{D_{pw}}\right) \cdot \frac{n_{OR}}{2} \tag{2.20}$$

where n_{IR} and n_{OR} are the inner and outer ring rotational velocities, D_{pw} the pitch diameter, α the contact angle of the roller and D_{we} the rolling element diameter as shown in Figure 2.3. In order to calculate the rotational velocity of the rolling elements u_R around their own axis of rotation and the resulting circumferential velocity n_R, the following equations can be used:

$$u_R = \frac{\pi \cdot D_{pw}}{60} \cdot \left(\frac{D_{pw}}{D_{we}} - \frac{D_{we} \cdot cos^2\alpha}{D_{pw}}\right) \cdot \frac{n_{OR} - n_{IR}}{2} \tag{2.21}$$

$$n_R = \left(\frac{D_{pw}}{D_{we}} - \frac{D_{we} \cdot cos^2\alpha}{D_{pw}}\right) \cdot \frac{n_{OR} - n_{IR}}{2} \tag{2.22}$$

2.2 Rolling bearing types

Rolling bearings can be divided into several types based on several features. An overview of the most common rolling bearing types is shown in Figure 2.14. Depending on the primary shape of the rolling elements, according to DIN 611 [DIN10b], rolling bearings can be divided into two main groups: ball bearings (e.g. deep groove ball bearings or angular contact ball bearings) and roller bearings. Furthermore, based on the size of the rollers and their arrangement, the rolling bearings with rollers as rolling elements can be divided into: cylindrical and needle (cylindrical rollers); barrel, spherical and toroidal (barrel rollers) or tapered (tapered rollers) roller bearings. Certain types of rolling bearings are of special interest for this work. The following sections give an overview of the most important characteristics, advantages and disadvantages as well as applications of these types of rolling bearings.
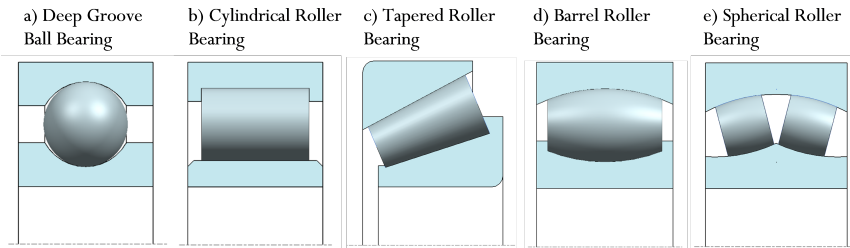

Figure 2.14: Overview of common roller bearing types.

2.2.1 Tapered roller bearings

Tapered roller bearings (TRBs) consist of an outer and inner ring with tapered raceways and tapered rollers in a window cage [DIN78]. Because of the conical shape of the rollers, the forces acting on it result into a normal force in the axial direction, turning into the need of a rib at the inner ring as shown in Figure 2.4. A profiled contact between the rollers and the raceways ensures optimum stress distribution at the contact points. As a result, the bearings can tolerate certain angular misalignments and give better support of moment loads.

TRBs can support both high radial and high axial loads thanks to the line contact taking place between rollers and raceway. Because of its geometrical characteristics, TRB can however only support axial loads in one direction. The axial load carrying capacity of the bearing is dependent on the nominal contact angle α. In most bearing series of the rolling bearing manufacturers this angle varies between 10° and 20° [DIN78; Sch17; SKF14]. In special series, α is approximately 28° to 30°. The greater this angle, the higher the axial load to which the bearing can be subjected.

The biggest disadvantage of TRBs is the great frictional torque taking place in mixed friction regime and the resulting high losses. Although the roller-raceway contact is optimized and its friction minimized, the roller-to-rib contact has a significant influence on the frictional torque of TRBs, especially in mixed friction regimes. For this reason, alternative bearings with lower load carrying capacity resulting in lower friction losses are used when lower loads are applied.

Given all these attributes, TRBs are commonly used when high radial and axial loads occur and combined loads must be supported, as well as when high bearing stiffness is required (e.g. differential gears). Specially for cases where the load carrying capacity of angular contact ball bearings is no longer sufficient and the higher speed suitability of angular contact ball bearings is not required.

In order to improve the behavior of a TRB, several adjustments and optimizations are being studied and implemented. The most important ones are regarding the rib contact and its influence in the total frictional torque. In these terms, the Generation D of the company SCHAEFFLER can be mentioned [SRW21]. The focus of this optimization is the location of the contact ellipse at the roller-rib contact, see Figure 2.4. The further from the bearing axis it is, the higher is the frictional torque due to the larger lever arm. Therefore, the goal must be to have a roller-rib contact as close as possible to the inner ring raceway. However, the pressure ellipse of the contact can not get too close to the undercut between the raceway and the rib. If the contact ellipse would run into this undercut, high edge stresses would arise having an important influence in the service life of the rolling bearing. This behavior is, therefore, to be avoided.

Another improvement yet to be studied and carried out is to optimize the geometry of

the roller for each specific application. One example would be the generation D+ of the company SCHAEFFLER [SRW21].

In general terms, in order to obtain an even distribution of the pressure at the roller, the surface lines of the rollers must intersect at a point at the bearing axis, see Figure 2.3. This way, the rollers are symmetrically loaded, ultimately avoiding slippage. However, once a TRB is mounted, the rollers and raceways are deformed and tilted. Because of this, the surface lines of the loaded bearing might not intersect at a point on the bearing axis anymore. A solution for this problem is described in the patents [Neu17][Nak76][PO12]. In the geometry defined in these patents, the surface lines of the rollers lay at different points of the bearing axis. Furthermore, the distance between the intersection points is calculated for the specific geometry. With this arrangement, at first, a non optimal solution for bearings that are neither mounted or loaded is proposed. However, once the rolling bearing is mounted and loaded, the rollers and raceways are deformed and tilted in such a way that the surface lines finally intersect at a point of the bearing axis. Thus an optimal geometry is achieved. A deeper description of the approach defined in these patents is explained in Section 4.1.3.

TONG and HONG have studied the influence that the profiling of the raceways has in the behavior of tapered roller bearings [TH15], specially on the resulting stiffness, axial displacement and pressure distribution. Based on its results, they developed an optimization of partially crowned roller profiles based on the resulting bearing fatigue life and the bearing stiffness [TH17].

2.2.2 Barrel roller bearings

Barrel roller bearings are composed of an outer ring with a concave raceway, a concave inner ring with two ribs, barrel rollers and a cage. The resulting roller-raceway contact is a line contact. As a result, barrel roller bearings have high radial load carrying capacity. However, axial loads are directly absorbed by the rib contact at the inner ring. In turn, barrel roller bearings have only a low axial load carrying capacity in both directions. Due to the concave contact between the rollers and the raceways, barrel roller bearings are suitable for compensating angular misalignments. This misalignment results from a skewing movement between the outer and the inner ring i.e., between the axle and the housing. Under normal conditions, in cases where the inner ring rotates, barrel roller bearings can swivel up to 4° from the central position.

The roller-raceway contact behavior is governed, among others, by the PCR of the roller. The PCR of a barrel roller is such, that the center of the PCR lays at the bearing axis. This way, the PCR of a barrel roller, as defined in DIN 635-1 [DIN94], follows the formula:

$$PCR_{roller} = 0.25 \cdot (d+D) + 0.125 \cdot (D-d) \tag{2.23}$$

Where d is the rolling bearing bore diameter and D is the rolling bearing outside diameter. The ratio roller length to roller diameter L_{we}/D_{we} is set to 1 for this type of roller. The roller ends are thus long enough to carry low axial loads through the roller-end rib contact. However, this limited length of the roller length, narrows as well the roller-raceway contact length and thus the radial load carrying capacity.

2.2.3 Toroidal roller bearings

Several years ago, the company SKF developed a new type of bearing. It was officially presented in 1995 under the name of CARB bearing (Compact Aligning Roller Bearing). The geometry of this rolling bearings is based in the patent of KELLSTRÖM of 1985 [Kel85], which sets the basics for rolling bearings with concave and convex rollers. The CARB bearing is a single row roller bearing with relatively long, slightly crowned rollers. The inner and outer ring raceways are correspondingly concave and symmetrical. The outer ring raceway geometry is based on a torus, which is why it is commonly known as toroidal roller bearing.

The idea for this bearing came from the need of compensating great misalignment with a minimum resulting friction. The existing spherical roller bearings could not accommodate important axial displacements within the bearing. If great axial displacements were taking place, it was necessary for one of the rolling bearings of a bearing arrangement to move axially on its seating in the housing. This axial movement would result in considerable friction and thus internal axial forces in the bearing arrangement. In order to be able to compensate great misalignment, toroidal roller bearings are not provided with ribs. Therefore, they can not carry axial loads in any direction, and can consequently fundamentally be used as a floating bearing in certain applications.

The main geometrical characteristic of a toroidal roller is a profile curve radius (PCR) of the raceways and the rollers considerably greater than the corresponding radii in barrel or spherical roller bearings. In this way, the rollers can be made longer than what is possible when it comes to such rolling bearings. Therefore, the radial load carrying capacity is as well enhanced, and thus a much longer service life is achieved. The PCR of the toroidal rollers can be calculated from the misalignment factor parameter κ_1 following the equation:

$$PCR_{roller} = \kappa_1 \cdot B \cdot \frac{180}{\pi} \tag{2.24}$$

Where κ_1 is a geometrical parameter given by the manufacturer. It can be found on the bearing catalogs [SKF14]. The company SCHAEFFLER refers at it as κ_φ [Sch17], where $\kappa_\varphi = \kappa_1 \cdot B$.

The internal geometry of toroidal roller bearings is still being studied and optimized. KELLSTRÖM et al. focus on the applications where great axial misalignment have to be compensated as well as axial loads be supported. In this way, they have developed an

angular contact self-aligning toroidal roller bearing as described in their patent [KKL16]. The rolling bearing defined in this patent consists of toroidal rollers having a contact angle that varies between 10° and 45°. It is designed as a locating bearing that allows for the self-alignment of the rollers, similar to the ability of spherical roller bearings. This approach allows for more compacts bearings, decreasing the load capacity and avoiding a commonly over-dimensioned rolling bearing solution. A deeper description of the angular contact self-aligning toroidal roller bearing and a method for determining its dimensional parameters are explained in Section 4.1.2.

2.2.4 Spherical roller bearings

A spherical roller bearing consists of two rows of barrel rollers inclined in relation to the bearing axis and symmetrically aligned, sharing an outer and an inner ring. The outer ring has a curved raceway shared by the two rows of rollers. The inner ring, however, has two different raceways, one for each row of rollers, each of them symmetrically inclined relative to the bearing axis. The symmetrical barrel rollers are guided by a cage. This type of bearing is used for cases where a misalignment of the shaft relative to the housing has to be compensated, as well as high radial and axial loads occur. Spherical roller bearings can compensate up to 2° of angular misalignment. Depending on the size of the rolling bearing, the contact angle of the rollers varies from 4,6° to 15,6° [Sch17; SKF14].

In terms of the geometry of the rollers, some optimizations are still being studied and its implementation continues on today.

A widely known optimization for spherical roller bearings relates to the asymmetry of the roller rows. This enhancement is required for applications where uneven loads tend to act on the left and right rows of spherical rollers. This asymmetry has to be optimized for an specific application in order to minimize the slippage of the row of rollers tending to receive the light load, and the associated friction wear. This is the case described in [NHM10] by Nakagawa et al. Within the patent, they define the geometry of an axial asymmetric double-row self-aligning roller bearing optimized for supporting the main shaft of a wind turbine generator.

For cases where symmetrical loads have to be supported, one of the most important friction losses taking place in spherical roller bearings, is the one related to the skewing movement of the rollers within their raceways. If a reduction in the total friction is to be sought, the skewing friction has to be the focus.

While for TRB, the skewing of the rollers is mainly governed by the friction at the roller end-rib flange interface, in the case of toroidal and spherical rollers, the skewing is a more complex behavior. The skew angle is defined as the angle between the axis of rotation of the rolling element and a plane normal to the path of relative motion of the raceways (see section 2.3.1). Positive skewing compared to negative skewing turns into a reduction of

friction and therefore increase in the bearing life.

KELLSTRÖM and BLOMQVIST propose in [KB76] several solutions in order to obtain higher friction and thus higher skew moment in the outer ring compared to the inner ring, so that a positive skewing is obtained. A deeper description of the different approaches described by KELLSTRÖM and BLOMQVIST are explained in Section 4.1.1.

FIEDLER et al. studied in the influence that the inner geometry of the rollers has in the resulting pressure distribution and frictional torque in spherical roller bearings. The results were presented in [FKS12] and [FKS11]. The study focused on different number of rollers, as well as the osculation of the rollers with the raceways. As expected, the study showed a slightly higher friction torque for narrower osculation, especially at low loads, where the contact surface is significantly higher.

2.3 Rolling bearing friction

The total friction appearing in a rolling bearing is one of the main focus when optimizing its geometry and the main focus of this work as well. The shape, size, and profile of the rolling elements are of main influence on the resulting friction. Depending on the bearing type, the total frictional torque is calculated as the aggregate of the friction taking place at the following locations:

- Rolling element and raceways

- Rolling element and cage (for rolling bearings with cage)

- Rolling elements and ring rib (for rolling bearings with guidance rib)

- Between rolling elements (for full complement rolling bearings)

- Cage and raceways

Not all contacts are relevant for every rolling bearing. The contact calculation between the rolling elements is only necessary for full complement rolling bearings. Similarly, the cage-raceway contact only takes places in bearings that have a ring-guided cage. To which extent each contact contributes to the overall friction varies as well depending on the rolling bearing type and boundary conditions, having the contact between the rolling elements and the raceways usually the biggest contribution. The profile and geometry of the roller highly influence the roller-raceway contact and its resulting friction. With the goal of minimizing the friction taking place between bodies, and thus the losses, the geometries of rollers, raceways and cages have been improved throughout the years. The numerical description of the effects of the friction plays a decisive role in the dynamic simulation of rolling bearings.

2.3.1 Movement and friction types

Friction can be divided into static or dynamic friction. The static friction is a force acting tangentially between two bodies which counteracts a tangential load without the existence of relative movement between the body surfaces. The dynamic friction is the force counteracting a relative movement between two elements. According to [SS12], the dynamic friction can be divided into three different types of movement or friction, depending on the relative movement between the two bodies:

- Sliding / sliding friction: sliding friction takes place when the surface velocity of the two bodies differ. In turn, there is a relative velocity between the two surfaces. This velocity is almost identical over the entire contact area.

- Rolling / rolling friction: rolling friction is characterized by the fact that the surface circumferential velocities of both bodies in the contact area are identical and in the same direction. Therefore, there is no relative velocity between the two surfaces.

- Drilling / drilling friction: drilling friction occurs when a body rotates relative to its contact partner around an axis that is perpendicular to the surface of the other body.
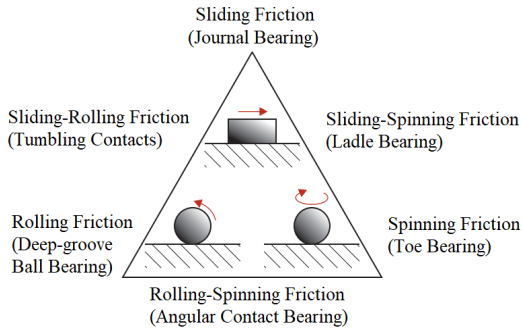
Figure 2.15: Main types of friction with superimposed forms by type of relative motion [CH15]

A schematic illustration of the types of friction, the underlying movements as well as an example for each type can be found in Figure 2.15. In real contacts there is often a superposition of the three basic types of friction.

The combination of pure rolling and sliding is called sliding-rolling friction. This type of friction is the one presented in rolling bearings, as there is usually a rolling movement with (macroscopic) sliding components in the contacts between the rolling elements and the raceway. Depending on the type of bearing, drilling also occurs in rolling bearings. If

the rolling elements of ball bearings run under a load angle, for example, drilling friction occurs. On the other hand, sliding friction occurs between the rolling elements and the cage or between the cage and the bearing rings. In the contact between the roller end and the raceway rib, all three types of movement occur superimposed. Therefore, it is important to correctly describe all states of motion and friction when simulating the dynamics of rolling bearings.

The rolling motion can be characterized by using the Slide-to-Roll ratio SRR. The SRR can be calculated from the relative u_{rel} and the mean surface velocities u_0:

$$S = \frac{u_{rel}}{u_0} = 2 \cdot \frac{u_1 - u_2}{u_1 + u_2} \tag{2.25}$$

The velocities u_1 and u_2 are the surface velocities of the two bodies in contact as defined in Section 2.1.5, equation (2.17). In general, the deviation from kinematic rolling in rolling contact is also referred to as *slip*. In other words, if the surface velocities of the two bodies in contact differs from each other, slip will take place. If a slip-free rolling bearing behavior takes place ($SRR = 0$), the surface velocity of the roller in the middle of the contact length can be mathematically calculated in terms of the rotational speed of the inner ring as defined by equation (2.21). The Slide-to-Roll ratio has established itself as a meaningful description of the various slip conditions. The movement states that might take place at the rolling bearing contacts are summarized in Table 2.1.
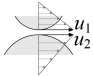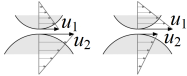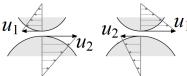
Type of movement	Graphical representation	SRR	Velocities
Rolling		$S = 0$	$u_1 = u_2$
Sliding-Rolling		$0 < |S| < 2$	$sgn(u_1) = sgn(u_2)$
Sliding		$2 \leq |S| < \infty$	$sgn(u_1) \neq sgn(u_2)$

Table 2.1: Parameters defining the new geometry and their value for different bearings

Drilling friction and the profile curve radius of the roller The drilling movement of a roller is defined as the rotation of the roller around an axis that is perpendicular to the surface of the raceway. In other words, a drilling movement results from a contact normal direction perpendicular to the axis of rotation of the roller.

For cylindrical rollers, the axis of rotation of the roller is perpendicular to the contact normal direction, therefore, no drilling movement takes place (Figure 2.16.a). For tapered

rollers (Figure 2.16.b) and barrel or toroidal rollers (Figure 2.16 c and d) the axis of rotation of the roller is not parallel to the surface contact. Therefore, the rolling motion of the roller results in a drilling movement. Furthermore, the bigger the crowning and the contact angle are, the bigger the drilling friction is. This results into bigger drilling movement for barrel rollers (Figure c), than for toroidal rollers (Figure 2.16.d). This type of friction plays an important role in both angular-contact ball bearing and barrel roller bearing.
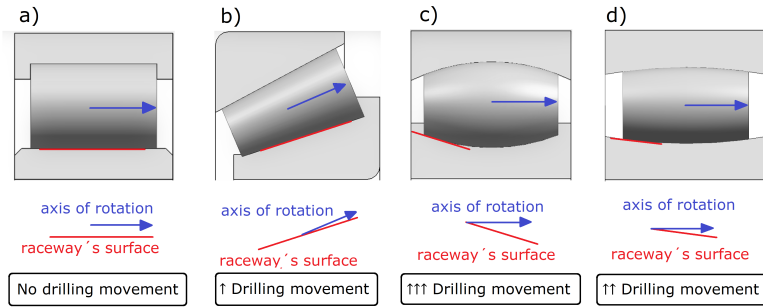
Figure 2.16: Drilling movement for different rolling bearing types

Skewing friction and the profile curve radius of the roller The skewing movement of a roller is defined as the rotation of the roller along its z-axis. The z-axis of the roller is defined as the axis that forms from connecting the center of the rolling bearing to the center of the roller as shown in 2.17.

The linear velocity of a point of the roller at its contact is determined by the angular velocity multiplied by the radius from the center of rotation of the roller (equation 2.17). The angular velocity of the roller is constant along the contact line. However, depending on the profiling of the roller, its tapered angle for conical rollers and/or its profile curve radius (PCR) for barrel and spherical rollers, the radius of the roller might vary along its length. For a cylindrical roller, without profiling, the linear velocity is thus constant along the contact length. Furthermore, the linear velocity of the roller and the raceway might not be of the same magnitude, resulting in a sliding-rolling movement as shown in Figure 2.17.a. Because of the crowning profile of barrel, toroidal and spherical rollers, different surface velocities take place along the contact line. Hence, for a pure radial load, when no slip takes place, the linear velocity of the roller at its contact line is only the same as the one of the raceway at two rolling points, as indicated in Figure 2.17.b. In that case, the roller velocity of each point in between the roller points along the contact line is higher than the raceway velocity. On the other hand, the roller velocities of all other points along the contact line until the roller end is lower than the raceway velocity. In the example of Figure 2.17.b, the velocities compensate each other in the x-direction. As a rule, however,

the forces acting on the roller in a roller bearing are such, that the rolling points are not symmetrical in relation to the center of the roller, as shown in Figure 2.17.c. In this case, the velocities do not compensate each other in the x-direction anymore, leading to an undesired skewing movement along the x-axis. The more accentuated the crowning of the roller (smaller PCR), the bigger differences of velocities along the contact line resulting in a bigger skewing movement and friction. An example of the linear velocities with a smaller PCR of the roller is shown in 2.17.d. [KB76].

The examples shown in Figure 2.17 are for a theoretical behavior with no external axial load and no slippage occurring. In real applications, where axial loads are applied as well, the skew moment resulting from the rib forces dominates over the others.
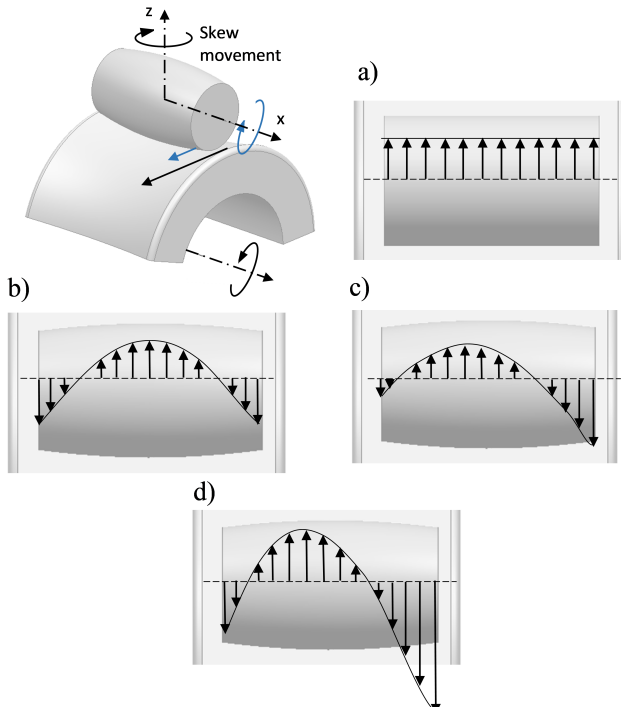
Figure 2.17: Relative motion between roller and raceway for different PCR and pure radial load. a) Velocity distribution with cylindrical roller, b) Velocity distribution with symmetrically loaded crowned roller, c) Velocity distribution with asymmetrically loaded crowned roller, d) Velocity distribution when reducing the PCR of the roller compared to c).

2.3.2 Friction conditions

The lubricant with its rheological properties is a decisive factor influencing friction and damping. A reliable functionality and a sufficient service life of rolling bearings are inconceivable without lubrication. Lubricants are used primarily for the cooling of the machine elements as well as to minimize the friction and wear appearing at the contact points in rolling bearings by completely or partially separating the contact surfaces [SS08]. Depending on the type of separation between the two bodies, four different states of friction can be distinguished. These are schematically represented in Figure 2.18. The four types of friction according to [CH15] are:

- Solid friction: friction between two solid bodies

- Boundary friction: solid body friction, with wetting of the surfaces with a molecular lubricating film

- Fluid friction: friction between two bodies that are completely separated by a fluid lubricating film

- Mixed friction: transition state between solid or boundary friction and fluid friction
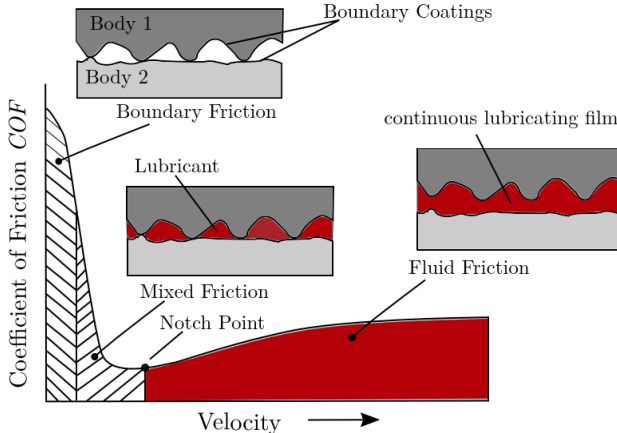
Figure 2.18: Qualitative representation of the Stribeck-Curve [BK12].

In addition to the state of friction, there are many other variables having an influence on the friction or its magnitude. The coefficient of friction (COF) μ is often used to calculate the frictional force. The COF μ is calculated as the quotient of the frictional force F_R and the acting normal force F_N ($\mu = \frac{F_R}{F_N}$). At the beginning of the 19th century, STRIBECK

published a diagram in which he showed the coefficient of friction over the relative velocity of the bodies (for plain bearings). This representation is also known as the Stribeck curve. Figure 2.18 shows an example of a typical Stribeck curve, where the coefficient of friction is shown as a function of the relative velocity with the different friction conditions at a constant load. For rolling bearings, instead of the relative velocity, is the bearing rotational velocity the decisive factor for the resulting lubricating film. The four friction states mentioned are represented here. Starting with the solid friction coefficient μ_s, the coefficient of friction remains almost constant in the boundary friction with a slightly decreasing tendency. With the transition to fluid friction, a lubricating film increasingly builds up due to the higher speed. This lubricating film separates the surfaces and reduces friction. In the area of mixed friction there is also the point of minimal friction μ_{min}. If the speed continues to increase beyond this point, with completely separate surfaces, the shear losses of the lubricant continue to increase leading to an increasing coefficient of friction.

2.3.3 Elastohydrodynamics

When lubricating roller bearings with greases or oils, a hydrodynamic lubrication (HL lubrication) occurs. This happens because the viscous lubricating oil is conveyed into the narrowing lubrication gap due to the movement of the two contact bodies. Under these circumstances, a liquid lubricating film forms, separating the two contact bodies due to the built-up hydrodynamic pressure. Because of the high contact pressure appearing between rolling elements and raceways, the lubrication state of a rolling bearing is usually an elastohydrodynamic lubrication (EHL). EHL can be characterized by the fact that the elastic deformation of the lubricated surfaces of rolling elements and raceways is of an order of magnitude comparable to the height of the built-up hydrodynamic lubricating film. Therefore, the elastic deformation of the surfaces must be taken into account when simulating the dynamic behavior of a rolling bearing. The dependency of the viscosity of the lubricant on the temperature and pressure must as well be taken into account when calculating the contact. Furthermore, if the materials of the two bodies in contact have a high modulus of elasticity (e.g. steel-steel), the term used then is *hard-EHL*. In this case, very high contact pressures of around 0.5 GPa to 4 GPa occur (for rolling bearings, typical values are 1,5 GPa to 3 GPa).

Figure 2.19 shows the pressure distribution in the EHL lubricating film. The pressure distribution in the EHL contact p_{EHL} is similar the the Herzian distribution p_H but deviates from it especially in the inlet region (where no contact takes place, not considered in the Herzian distribution, but very important for the rolling friction) and the outlet region (Petrusevich pressure peak).
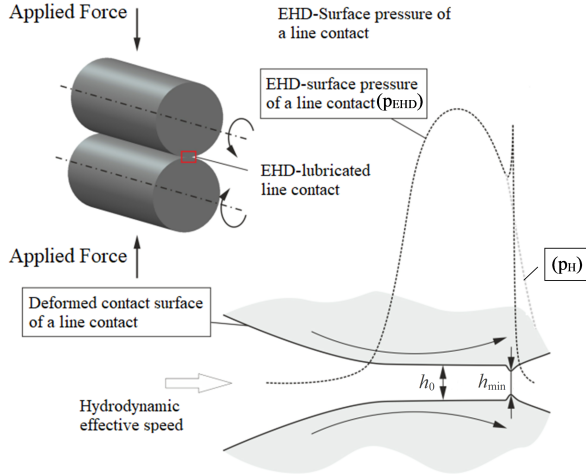
Figure 2.19: Distribution of the pressure and the height of the lubricating film for an EHL-lubricated line contact [Wan15]

In principle, the pressure distribution in an EHD contact shows a similar course as the Hertian pressure. The elastic deformation of the contact surfaces caused by the contact pressure results in an approximately parallel gap. This gap results in turn in a relatively constant central lubricant film height h_0 over a large part of the contact zone. Characteristically, there is a second local pressure maximum at its exit, which is caused by the local constriction of the lubricating film. In this area, the lubricating film height is at its minimum h_{min}. This behavior was first predicted by PETRUSEVICH using numerical simulations [SS08; Mag12]. The central lubrication gap height is an essential characteristic of the contact. The most well-known equation for the isothermal calculation of the minimum lubricating film height h_{min} of a line contact with smooth surfaces was published by DOWSON and HIGGINSON in 1961 [DH61]. It establishes a connection between the dimensionless minimum lubricating film height h_{min} and the dimensionless parameters for the material G, the load W and the speed U:

$$h_{min} = 1,6 \cdot G^{0,6} \cdot U^{0,7} \cdot W^{-0,13} \tag{2.26}$$

The value of h_{min} determines both the mixed friction conditions and the shear gradient in the lubricating film. Both are essential input variables for the calculation of the friction in the contact.

Furthermore, the specific lubrication height Λ is calculated from the central lubrication

height h_{zen} and the squared mean roughness σ of the contact partners according to [Tal67] as follows:

$$\Lambda = \frac{h_{zen}}{\sigma} \tag{2.27}$$

Based on the specific lubrication height, the mixed friction range is considered to be in the range between $0.5 < \Lambda < 3$ [ZH91].

2.4 Dynamic simulation of rolling bearings

In addition to an experimental analysis, the dynamic simulation of rolling bearings offers the possibility of a better understanding of this machine element and the internal processes taking place in it thanks to the computing power available nowadays. Some examples include the prediction of the lubrication conditions, the cage dynamics or the wear calculation. In addition, it is possible to study a contact area with very high resolution. When experimental testing, this is only possible to a limited extent or comes with a great deal of effort. With all this said, the dynamic simulation of rolling bearings enables saving time and resources. In general, the tasks to be dealt with when performing a dynamic simulation can be divided into several sub-areas [Kie17]:

- Contact description or calculation

- Calculation of normal forces

- Calculation of the tangential forces

- Establishing and solving the equation of motion

The contact detection is an important part of the simulation of rolling bearings and influences both the required computing time and the stability of the calculation. To this end, it is to be examined to what extent the well-known contact models for the calculation of the static load and the pressure distribution can be coupled with numerically effective methods for the contact calculation. In terms of the calculation of forces, in order to achieve plausible results in the context of a dynamic simulation, suitable damping models must be included in addition to the normal force and friction models.

With the help of dynamic simulation, many output variables are obtained, on the basis of which an assessment of many types or causes of damage is possible. Some of the types of damage that can be predicted are, for example, slippage, wear and tear, cage instabilities or cage breakage.

Among the years, numerous models for the dynamic simulation of rolling bearings have been developed both at research institutes and at rolling bearing manufacturers. This shows that the dynamic simulation of rolling bearings is a very suitable tool for analyzing

and evaluating bearing behavior under a wide variety of boundary conditions. Across all bearing types, the correct contact and friction description of all contact points are found to be essential aspects that are elementary for its dynamic simulation.

The multi-body simulation (MBS) offers a suitable basis for investigating dynamic processes in roller bearings. The implementation of the model in a commercial program has the advantage that existing modules can be directly used. In this manner, the Chair of Machine Elements, Gears and Tribology (MEGT) started developing dynamic models of bearings for over a decade. To this end, several models developed within the commercially available software MSC.Adams were combined with self-written user routines [Teu05; Hah05]. From its origins, the models have been further developed over the years [Woh10; Aul14; Kie17]. These models are parametrically implemented, so that modifications in the geometry, mass properties, and operating parameters can easily be adjusted to the requirements. Furthermore, individual parameters of the inner geometry of the rolling bearing can be varied and optimized comparatively easily, saving time and resources.

3 Motivation, Objectives and Strategy

3.1 Motivation

The minimization of the rolling bearing losses occurring in any type of machine has been a focus of study during many years. This issue is specially important in widespread applications as it is the case of vehicle powertrains. In the attempt of reducing the fuel-consumption and the CO2-emissions of any kind of vehicle, each rolling bearing system is thought over and optimized. In general, any application where an adjusted bearing arrangement is solved using tapered roller bearings, this is of special interest. This is due to the relatively high friction losses occurring at the rib contact of this type of rolling bearing.

Based on several researches, a tandem angular contact ball bearing appears to be an optimal substitution for cases with low to moderate loaded rolling bearings. This bearing, while having the same size and grease chamber than tapered roller bearings, has the advantage of considerably less friction losses. Tandem angular contact ball bearings have been successfully used as an alternative to tapered roller bearings for several applications, including the axle gear of passenger cars [Pla11; Boh12; Sch21]. Figure 3.1 shows the resulting frictional torque for the two types of bearings under various load conditions and angular velocities.

Ball bearings have, however, the disadvantage of less carrying capacity than TRB. Therefore, although it is a better solution for the case of passenger cars (with a weight limitation of 4 tons and 2 axes resulting in 2 tons of axle load), its load rating is insufficient to be used in the case of highly loaded rolling bearings, such as heavy-duty trucks (with a maximum permissible total mass of 40 tons and 5 axes resulting in 8 tons of axle load).

A new concept of bearing as a substitution for the commonly used TRB, aiming to reduce the frictional torque and resulting losses, while keeping its high carrying capacities is still been searched for.
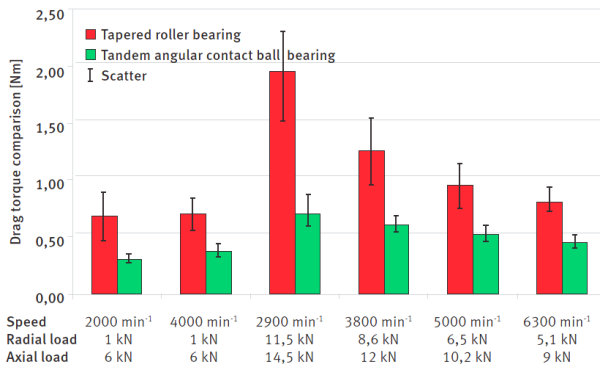
Figure 3.1: Resulting torque for tapered roller bearing compared to tandem angular contact bearing [Sch21]

3.2 Aim of the work

With the aim of reducing the frictional torque of tapered roller bearings, the most recent studies have focused on the optimization of the rib contact. The friction behavior at the contact between the rib of the inner ring and the rolling elements of TRBs is of great importance. Because of the velocities appearing at their surfaces, the friction arising at their contact is pure sliding. This turns into a relative high coefficient of friction and therefore great losses in mixed friction regime. The weight of this friction to the total friction losses of the roller bearing depends on many factors e.g. rotational speed, load, lubrication; all affecting the lubrication condition at the flange. In the cases of mixed friction, the friction losses at the flange are at its maximum and dominate over the others [BH05][Sch21]. The optimization of this contact is, however, very limited.

This work focuses on the total disposal of the rib contact and its resulting friction. By this means, the total frictional torque appearing at the rolling bearing will be considerably reduced, being its main proportion the resulting frictional torque at the roller-raceway contact. In this terms, a new roller geometry based on the existing geometry of a tapered roller will be developed. The original geometry of the roller will be modified in a way, that the appearing axial forces will be directly supported by the roller-raceway contact, avoiding the need of a rib at the inner ring. In order to achieve this statement, a crowning-shaped roller combined with a contact angle will be defined.

The main disadvantage of this geometry will be its resulting drilling friction. As it is the case for every crowned profiled roller, a contact diameter that is not orthogonal to the axis of rotation of the roller causes a drilling movement of the rollers relative to the inner

ring, resulting in an undesired drilling friction. Consequently, the bigger the profile curve radius and the contact angle are, the higher the resulting drilling friction is.

With all this, the choice of the geometrical parameters is aim to be so, that the resulting drilling friction of the roller does not outweigh the friction at the rib contact when using TRB. In other words, the total resulting frictional torque is reduced. In these terms, the limit of the less crowned surface possible, so that no flange is needed is to be searched. To do so, the axial displacement of the rollers will be, among others, a key output to be studied.

3.3 Approach

As a first step, several patents and existing roller geometries will be studied in order to establish key features for the definition of the searched geometry. Based on these characteristics, the basics of a new roller geometry will be defined. Withing this geometry, key parameters can be varied, influencing the roller-raceway contact while maintaining the fundamentals of the geometry as explained in the previous section. Afterwards, the geometrical definition of the roller will be implemented in a MBS model.

In addition to an experimental analysis, dynamic simulations of roller bearings allow an in-depth analysis of the processes in the machine element. One of its advantages and the most important for this study is that individual parameters of both the geometry and the boundary conditions can be varied and thus optimized comparatively easily, saving time and resources. In addition, it is possible to study a contact area with very high resolution. This is only possible to a limited extent in an experiment or with a great deal of effort. Compared to a static simulation, such as investigations with the FEM, more complex effects such as cage-rolling element interactions can also be treated. There are several models available for the dynamic simulation of rolling bearings. Among the best known are BEAST (Bearing Simulation Tool) of the SKF company [SFN99; SF01; ISF05; Nak06], BRAIN (Bearing Analysis in NSK) of the NSK company [Ara97; ANS97], Caba3D (Computer Aided Bearing Analyser 3D) of the SCHAEFFLER company [KPW09a; KPW09b; HSN15] and CAGEDYN of the TIMKEN company [Hou09a; Hou09b; Hou10]. There is only a little detailed information about these programs, as they are part of the company's know-how. Therefore, these models are not accessible for general research.

For the simulation accomplished in this work, commercial MBS-Software will be used. A MBS-Software serves as a user interface, solving equations of motion and creating the balance of forces between the bodies. The basis of this software will be supplemented with self-developed calculation routines, both for computation and evaluation. The calculation routines for TRB already developed at the MEGT chair will be the starting point of the work. These routines are contained in and access from a MBS model. Within them,

advanced slice models are used for the calculation of the highly loaded EHL contacts. These existing MBS and routines, as well as its procedure of computation and evaluation, have been validated and presented in several studies [AAH07; SK17; KS17; KFS15; Kie17; Teu05; Dah16]

In order to create the calculation routines for the new geometry, the main focus is to change its geometrical definition as well as the calculation routines obtaining the penetration, the location of the contact points and the contact directions. The penetration is defined as the negative distance between the two contacting surfaces. In other words the theoretical penetration depth of the undeformed surfaces. Once these changes have been fulfilled, the existing routines obtaining velocities, forces and friction torques considering damping and lubrication can be directly transferred from the existing TRB model.

The geometry of rolling bodies, inner and outer rings, as well as cage, together with the boundary conditions and loads, define a MBS Model configuration. The model configuration will be fully-parametric implemented. By this means, the geometries of the single bodies, as well as boundary conditions and loads will be transferred from the parameter set into an input file.

Once both, the self-developed calculation routines and the MBS model configuration, are created, an exemplary geometry defined by a set of parameters will be chosen. Furthermore, a prototype of this geometry will be manufactured. In order to validate the model, the prototype of the new optimized geometry will be experimentally tested, together with a tapered roller bearing of the same main dimensions. The experimental testing will take place in a frictional torque test rig. Through the use of this test rig, it is possible to realistically reproduce the loads and misalignment occurring on a rolling bearing.

After the model has been validated, a sensitivity analysis of the parameters defining the geometry will be conducted. Within it, the influence that input parameters have in specific output parameters will be analyzed. The main input parameters to be changed are the osculation, the crowning or the contact angle of the roller. On the other hand, the main output parameters to investigate are the axial displacement of the roller, the total frictional torque or the pressure distribution at the contact area. Based on the observed correlations, a workflow defining a path for choosing the geometrical parameters can be conceived.

4 Geometrical Definition

In this section, the geometrical parameters that will characterized the geometry of the rollers and raceways of the new rolling bearing type are established. The selection of these parameters and, therefore, the roller-raceway contact defined by them, is based on several aspects. First of all, on the previously defined geometrical parameters (section 2.1.2) and their influence on specific output values such as frictional losses or lifetime. Furthermore, this selection is based on several patents and theoretical foundations with regard to the behavior of rolling bearings. Both the patents and the foundations are presented in section 4.1.

4.1 Foundations

The behavior of rolling bearings is a complex field. The movement that the roller follows among the raceways varies, mostly depending on its geometry, but also on the boundary conditions. Within this section, very specific behaviors and geometries, not applicable for most of the standard bearings, are presented. These foundations are described in several prototypes of rolling bearings, which are as well introduced in this section. An overview of the described patents, as well as their characteristics considered for the definition of the geometry under study is presented in section 4.1.5.

4.1.1 Skew movement

As mentioned in Section 2.3.1, the dynamic friction is the force counteracting a relative movement between two elements. When a barrel or spherical roller rolls among the raceways of inner and outer ring, a relative linear velocity between the roller and the raceways takes place. The relative sliding speeds resulting from the crowning of the roller as explained in Section 2.3.1 and represented in Figure 2.17 create friction forces between the roller and the raceway. The friction forces on the rolling element in a given contact are opposite in direction to the ones on the raceway of that contact.

This behavior is deeply explained by KELLSTRÖM and BLOMQVIST in their patent of 1976 [KB76]. There they explained the forces and resulting friction appearing in a crowned roller in terms of skewing. Furthermore, they presented solutions in order to minimize this

friction. Figure 4.1 shows a drawing of the patent, illustrating the direction of the friction forces at the contact between the rolling element and the raceway. These forces arise from the relative motion between roller and raceway as previously explained in Figure 2.17.d, resulting in turn from the angular velocities of the inner ring (moving away from the reader) and the outer ring (moving towards the reader). The friction forces are distributed in such a way, that they do not neutralize each other; rather they create a moment which tends to skew the roller along its z-axis (AA-axis in Figure 4.1). Since the moments of the inner and outer raceway are directed opposite to each other, the greatest moment predominates over the other skewing the roller in a certain direction. This moment is called skew moment and it is the resultant ot the moment taking place at the outer ring minus the one taking place at the inner ring. A positive skewing takes place when the friction force components acting on the roller in the axial direction are directed co-directional (add onto) to the axial component of the normal contact force acting on the roller-raceway contact. Since zero skewing is impossible to achieve, it is of great interest to avoid having negative skewing. As for the example displayed in Figure 4.1, a preferred positive skewing takes place when the moment taking place at the outer ring contact is predominant over the moment from the inner ring. Positive compared to negative skewing turns into a reduction of the friction and therefore an increment in the bearing life.
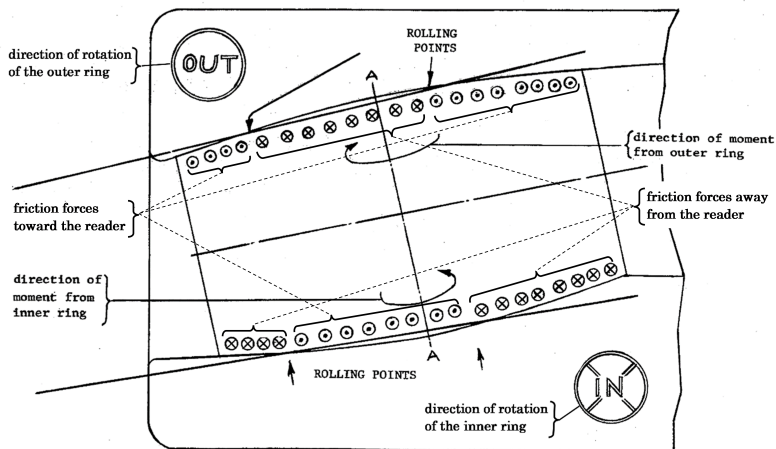
Figure 4.1: Frictional force patterns and resulting skew movements [KB76]

For spherical roller bearings, it has been determined, that an optimum performance is obtained when the skew angle is in a positive range between 0° and 2°. It is known that the skew movement created by the inner ring tends to skew the roller in the negative direction. This is why the outer ring skew moment has to be predominant. KELLSTRÖM

and Blomqvist provide in [KB76] an improved rolling element wherein the sum of the moments acting on the rolling element as a result of the friction forces at the contact causes the rolling element to assume a positive or zero skew angle. They present several solutions in order to obtain higher friction and thus higher skew moment in the outer ring compared to the inner ring. These can be described as:

- Manufacturing a rougher contact surface at the outer ring turning into a higher friction.

- Having a different geometrical definition for the inner raceway than for the outer raceway in terms of radius of curvature. A bigger PCR of the inner ring, in other words, a wider osculation, will turn into a more concentrated area of contact at about its median. Therefore, resulting in less friction. An illustrating example is shown in the left row of Figure 4.2.

- With an outer ring defined in a way that the contact point is not at the middle anymore, but the roller is in contact with the raceway at two different contact points (by mechanizing a relief groove). This way the roller engages the outer raceway at a higher pressure than at its median. An illustrating example is shown in the right row of Figure 4.2.

Figure 4.2: Different solutions in order to achieve a positive skewing: reducing the friction of the inner raceway (left) and increasing the skew movement of the outer ring (right)

4.1.2 Angular toroidal roller bearing

Kellström et al. described in [KKL16] the geometrical definition of an angular toroidal roller bearing. As a baseline for the geometry, they established two main parameters: the

transverse and the circumferential raceway radii. The transverse raceway radius is defined as the radius of the outer raceway in the direction transverse to the rolling direction of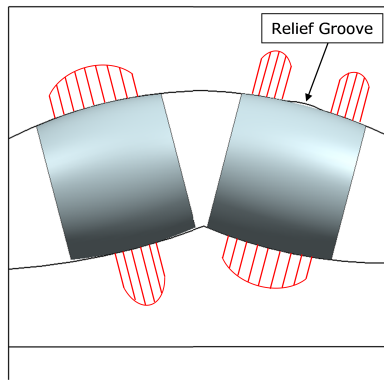 the rollers (re in Figure 4.3). In other words, the transverse raceway is the profile curve radius of the outer raceway (PCR) as defined in Section 2.1.2. Likewise, the circumferential raceways radius may be defined as the radius of the outer raceway in the rolling direction of the rollers at the contact point between the rollers and the outer raceway (re_c in Figure 4.3). In other words, the distance, perpendicular to the roller surface at the contact point, between the bearing axis and the outer raceway. Based on this, the patent defines two different geometries: whether the transverse radius is bigger than the circumferential raceway radius (positive offset, see Figure 4.3 left), or on the other hand, the transverse radius is smaller than the circumferential raceway radius (negative offset, see Figure 4.3 right).

A method for determining the dimensional parameters of an angular toroidal rolling element is also explain in [KKL16]. This way, on the basis of three input parameters, the contact angle will be first determined. These three input parameters are: the outer diameter of the bearing D, the diameter of the axle d, and the load condition P. The contact angle is key for providing sufficiently high axial load carrying capacity of the bearing. Afterwards, the following parameters can be determined as: roller diameter D_{we}, number of rolling elements Z, and pitch diameter of the bearing D_{pw}.
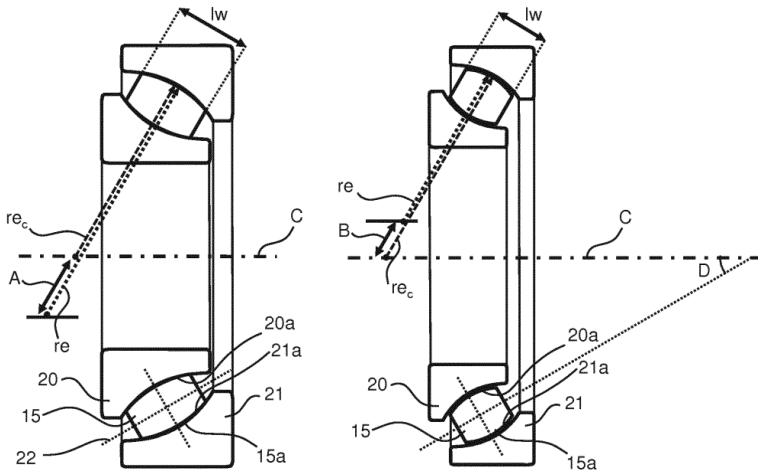

Figure 4.3: Roller designs of an angular toroidal roller bearing [KKL16]

The three input parameters, together with the four determined parameters, can be used as the basis for determining the transverse radius of the rollers. Afterwards, the roller length will be determined based on a ratio between the roller transverse radius and the roller

length. KELLSTRÖM et.al define a range for this ratio, as well as several relations between the design parameters. These associations between parameters are listed below:

- The ratio between the roller transverse radius (PCR_R) and the roller length lw is recommended to be smaller than 10 in order to ensure axial self-orientation of the roller during operation. This association is independent of the bearing pitch diameter. The smaller the ratio, the higher the provided self-orientation ability of the rollers. This ratio is also influenced by the coefficient of friction between the contacting surface of the roller and the raceway of the inner or outer ring.

- The contact angle is recommended to be between 10° and 45°.

- The osculation, in this case defined as the ratio between the roller and the raceway transverse radius (PCR_R/PCR_{LB}) is recommended to be between 0,965 and 0,995.

- For a bearing configuration with positive offset, it is recommended to define a transverse raceway radius of between 1,65 and 1,0 times the circumferential raceway radius.

- For a bearing configuration with negative offset, it is recommended a transverse raceway radius of less than 1,0 times the circumferential raceway radius, but not less than 60% of the roller length.

In 2019 Grehn describes a similar design [Gre19]. In this patent, the barrel roller has a negative offset, this is a smaller PCR than a common barrel roller as defined in DIN 625-1 [DIN94]. With this configuration, the load-bearing capacity of the roller-raceway contact is expected to increase and prevents at the same time the rolling elements from blocking. For this design, a range for the distance between the center of the PCR and the bearing axis is defined. This is, bigger than 0,01 times the distance from the outer raceway to the bearing axle, and smaller than the difference between this distance and the height of the roller. Furthermore, the roller length L_{we} is defined to be equal or bigger than twice the roller diameter D_{we}. The osculation of the outer and inner ring, which might be different from each other, is recommended to be between 0,97 and 0,99.

4.1.3 Corrected geometry for loaded rollers

With the goal of reducing the friction losses taking place in a rolling bearings, several improvements have been made during the years in terms of optimizing the different contact areas. The optimization of a rolling bearing geometry usually takes place for an unloaded static scenario. Like this, however, depending on the application, the rolling bearing will suffer from different geometrical changes, leading to undesired friction and losses. Once a rolling bearing is mounted in a housing or shaft, the outer and inner ring are deformed,

and therefore the rollers tilted. Furthermore, when a rolling bearing is loaded, the rollers experience axial displacement to a greater or lesser degree. This movement turns into a different contact situation than the one searched for when optimizing its geometry.

Therefore, in order to achieve even further improvements, it has been realized, that a designed geometry optimized for its specific application can result into a decrease of the total frictional losses. In particular for applications where TRB is used, an optimized geometry for the specific boundary conditions might result in a significant decrease of the total friction. This optimization puts the focus on the individual friction contacts and the influence that the load condition has on these.

As already mentioned in Section 2.2.1, the surface lines of the rollers of a TRB must intersect at a point at the bearing axis in order to obtain an even distribution of the pressure at the roller. This way, the rollers are symmetrically loaded, ultimately avoiding slippage. However, once a TRB is mounted, both the outer and inner ring are deformed because of the forces appearing at their contact with the housing and shaft. This deformation slightly changes the contact angle of the raceways, so that the surface lines of the loaded bearing might not intersect at a point at the bearing axis anymore. This means, that the internal geometry of the bearing no longer corresponds to the ideal optimized geometry. Therefore, the frictional losses are increased and the bearing life is shortened.

A solution for this problem is first described by Nakamura in 1976 [Nak76]. A TRB used as the support bearing for the semi-floating rear axle of a motor vehicle is the starting point of the patent as shown in the left side of Figure 4.4. The external load W causes the axle to tilt with an angle θ_a with respect to the bearing axis. Therefore, the inner ring is also tilted with respect to the outer ring. As a result, their surface lines do not intersect at a point of the bearing axis anymore. In these terms, the patent describes an optimized geometry for this application. By means of changes in the internal geometry of the rolling bearing, within the mounted and loaded bearing, the surface lines will intersect at the bearing axis. The right drawing of Figure 4.4 shows the optimized geometry. The definition of the internal geometry of the outer ring, the inner ring and the rollers is shown in Figure 4.5. The patented geometry is defined by an outer raceway which is inclined at a specific angle (Δt) with respect to the roller profile. Therefore, while the surface lines of the inner ring and the roller intersect at a point of the bearing axis P_1, the outer ring intersects with the bearing axis at a different point P_2. Furthermore, the distance between the two different intersection points is previously calculated for the specific application and is influenced by the tilting angle of the shaft θ_0. This way, the geometry is not the optimal one for an unloaded unmounted rolling bearing, but for the specific application.
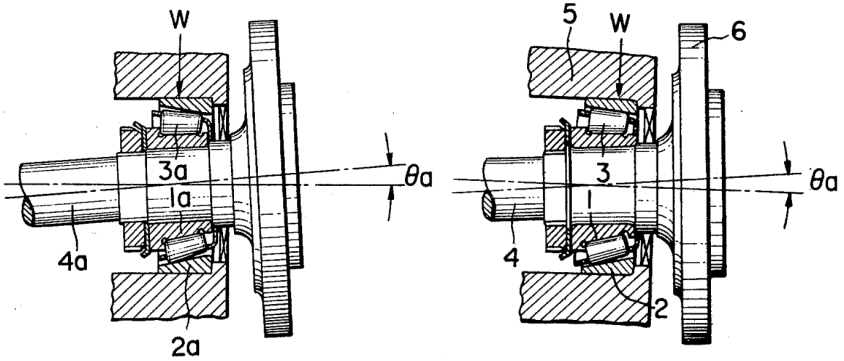
Figure 4.4: Semi-floating rear axle of a motor vehicle when mounted with a standard TRB (left) and with a TRB as described in [Nak76] (right)
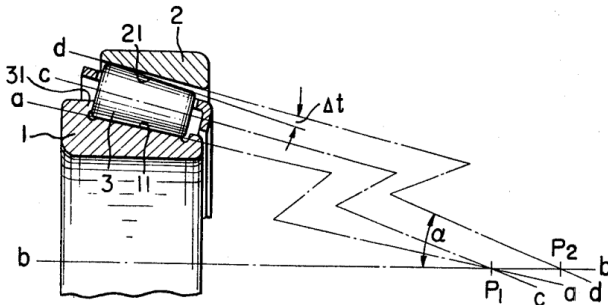
Figure 4.5: Geometry of a TRB as described in [Nak76]

A similar invention was made by Pabst and Oswald in 2012 [PO12]. In this case, the geometry of a TRB was optimized for the mounting of a differential cage in a differential gear. Otherwise, the basics of the definition of the internal geometry of the rolling baring is very similar to the patent of NAKAMURA.

In 2017, NEUKIRCHNER defined a TRB based on the same lines as described by NAKAMURA and PABST [Neu17]. In this case, the definition of the inner geometry is made more general, so that it could be used for different applications. It is not specified, whether the geometry of the outer ring, the inner ring or both are to be changed. The required inclination of the conical raceway surfaces is to be calculated and determined by suitable analysis methods. The angle of inclination results from the specific application and boundary conditions. For this propose, parameters like the bearing assembly, the operating temperature, the mounting temperature, the operating loads, the clamping forces and the screw tensioning

forces have to be known. The ideal bearing geometry is therefore only obtained when the bearing is fully assembled in the housing and the shaft. In other words, when it is exposed to the operating load and temperature. Figure 4.6 shows a comparison of a standard TRB and the geometry defined in the patent. On the left a TRB with surface lines of the inner and outer ring displayed according to the standard is represented. Thus, the surface lines intersect at a point at the bearing axis (5,6). On the right, a TRB according to the invention is represented. In this case, the surface lines cut the bearing axis at different points (thus, the points 5 and 6 are apart from each other).
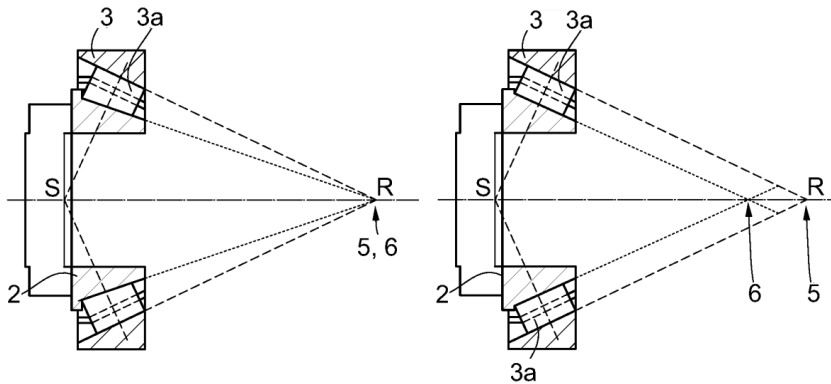
Figure 4.6: Standard TRB and TRB with corrected running surface [Neu17]

Another example of an optimization of the inner geometry for an specific application is the generation D+ of the company SCHAEFFLER [SRW21]. After reaching a limit in the reduction of the frictional losses with the generation D of bearings (through general modifications of the geometry in order to optimize the contact, particularly the rib contact), the attention lays in an application-focused optimization. The so called "tailored design" of a TRB is conceived in such a way that all requirements of the application in terms of pressure, service life, rigidity, etc. are still being met, while the friction is kept as low as possible. As of yet, no specific definitions have been made by the company SCHAEFFLER on how this "tailored design" of the generation D+ is to be achieved. However, its expected advantages in comparison to the standard geometry have been published. By this means, the e-axle of a light commercial vehicle with an empty weight of 2185kg and an engine output of 85kW (peak) is used as an example application. Within this example, two of the three shafts of the eAxle drive system were equipped with two friction-optimized TRB of the generation D+. In other words, four out of six bearings were exchanged. While with the generation D a reduction of 18% in the bearing friction compared to a standard TRB was achieved, with the generation D+ a drop-off of up to 56% was observed. This

shows the potential of optimizing the internal geometry of rolling bearings for a specific application.

4.1.4 Four point contact

Starting from a commonly known spherical roller bearing as defined in DIN 625-2 [DIN09a], and a barrel roller bearing as defined in DIN 625-1 [DIN94], several patents are describing the advantages of splitting the contact area occurring between the roller and both the inner and the outer raceways in two contact zones. In the common designs described in the standard norms, the roller either rests on the running track over their entire length, or just rest on it with their central circumference. When the contact is split in two, four contact points and areas are obtained, instead of two. These are divided into two for the outer raceway and two for the inner raceway. By this means, the self-locking effect of the rollers is avoided.

In 1928, REICHLE set the basis for this type of roller geometry in [Rei28] based on a standard spherical roller. He defined the roller by means of two contact rolling circles of different diameters. Moreover, the contour of the two arcs are connected with each other by a straight line. These diameters form, in turn, the contour lines of two cones with the same contact angle. These cones are such, that the surface lines of the rollers intersect at a point at the bearing axis. A drawing of the geometry defined by Reichle is shown in Figure 4.7.
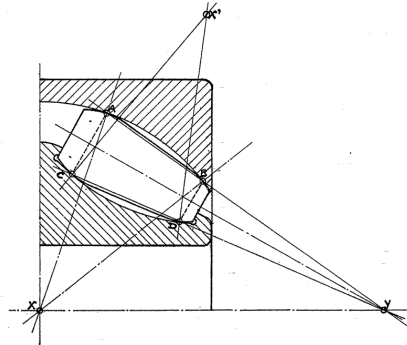
Figure 4.7: Draft of a spherical roller bearing with four contact points as defined by Reichle in [Rei28]

Such rolling elements are significantly better suited to transfer axial loads without the risk of wedging than the commonly used spherical rollers. If necessary, they also can be used as a single row of rollers, in contrast to a spherical roller bearing. This attribute is due to the fact that, thanks to the peculiar shape of the rollers, the angle between

the acting axial load and the roller surface absorbing this axial load is increased in comparison to a spherical roller. Furthermore, oppositely inclined surfaces are available on each roller so that axial loads in both axial directions can be absorbed by the same roller.

In the case of barrel roller bearings, the division of the contact area of the roller in two separate areas is first mentioned in [Soc31]. In this case, the splitting does not take place in terms of a more complex profile of the roller, but as a manufacturing process. In this sense, a common barrel roller is first divided in two halves. Afterwards, these two halves are attached together through a middle component like a pin or a spring. Furthermore, the two halves are separated by a flexible intermediate piece. This compensates for any inaccuracies in the manufacture by absorbing the small forces generated by the bearing load. By this means, in addition to the roller-raceway contact, a new contact takes place between the two halves through the intermediate piece. Therefore, the main disadvantage of this configuration, is the increase in the frictional losses, due to the increase in the contact area. Additionally, there is a risk that the contact points will enter the self-locking area in the event of load changes.

Based on this patent, Jacob described in 1992 [Jac92] a different, improved way of obtaining a four contact point from a barrel roller geometry. Thanks to a cylindrical section manufactured in the middle of the roller, the two carrying areas, rotationally symmetric with respect to the rolling body axis, are in turn divided in two. The width of the section manufactured in the roller and, therefore, the size and location of the two contact areas, are highly influenced by the equivalent angle for the self-locking effect. By this means, the contact points are relocated in order to lay at a bigger angle than the self-locking angle and within the resulting contact length of the corresponding contact area. With the commonly used material pairings, the angle for the self-locking takes a value of around 7°. The position of the contact points are therefore preferably to be selected in such a way that the angle which they form with respect to the central plane of the roller is bigger than 7°. A drawing of this configuration, where the angle defining the location of the contact points is represented as α, is shown in Figure 4.8. By this means, Jacob defines a roller having four contact points, laying outside the self-locking area, whereby the jamming of the rolling elements is excluded.

In addition, the cylinder section ensures that no contact can occur in the central area. Furthermore, the roller can be made longer, with a ratio roller diameter to roller length bigger than 1:2. This configuration, with a longer guiding length, spares the need of a rib for guiding the roller elements.
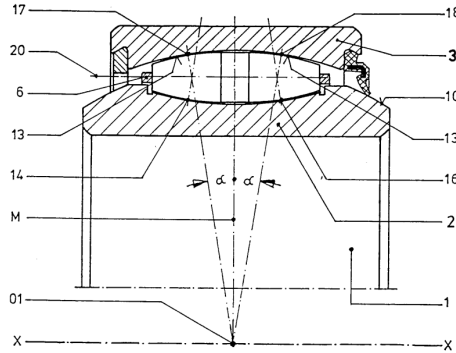
Figure 4.8: Draft of a barrel roller bearing with four contact points as defined by JACOB in [Jac92]

According to [Jac92], for barrel rollers with four contact points, particularly favorable load-bearing conditions take place when the relation between the PCR of the rollers and the PCR of the raceways follows the formula:

$$S = \frac{PCR_{LB}}{2 \cdot PCR_R} \tag{4.1}$$

Where S may take a value between 0,51 and 0,75. In terms of the previous definition of the osculation as establish by the equation 2.7, this means a range for κ between 0,5 and 0,98.

Based on his own patent of 1992, JACOB defined a new geometry of a roller bearing in 2008 [Jac08]. In this case, he defines the basics for the geometrical definition of what he names a "Tonnenschräglager", a combination of german words for a barrel angular roller bearing. The main goal of this geometry is to improve the previous geometry of a four point barrel roller as defined in [Jac92] in terms of increasing its axial load capacity. This patent describes a barrel roller having four contact points instead of two long contact areas, as it is the case of a commonly used barrel roller. Furthermore, the roller is inclined in relation to the bearing axle via a contact angle, such as for TRB. A draft drawing of this geometry is shown in Figures 4.9 and 4.10.

Similar to the geometry referred in [Jac92], the two osculation contact points of each raceway (P) are preferably laying outside the self-locking area. This is achieved through an offset angle of 7° or more between the perpendicular to the roller rotation axle and the location of the osculation points in the osculation region. To assure that no contact between the rollers and the raceways takes place in the self-locking area, a relief channel is provided in the region between the two osculation regions (7).
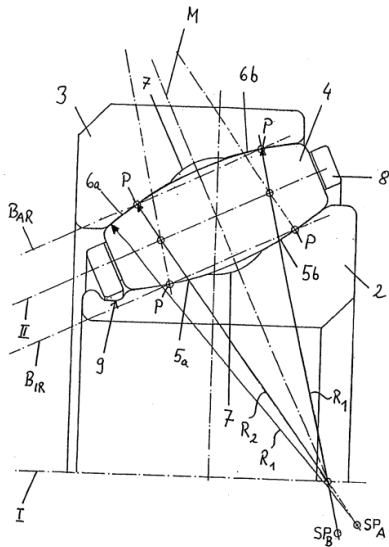
Figure 4.9: Draft of a barrel angular roller bearing with four contact points as defined by
          JACOB in [Jac08]
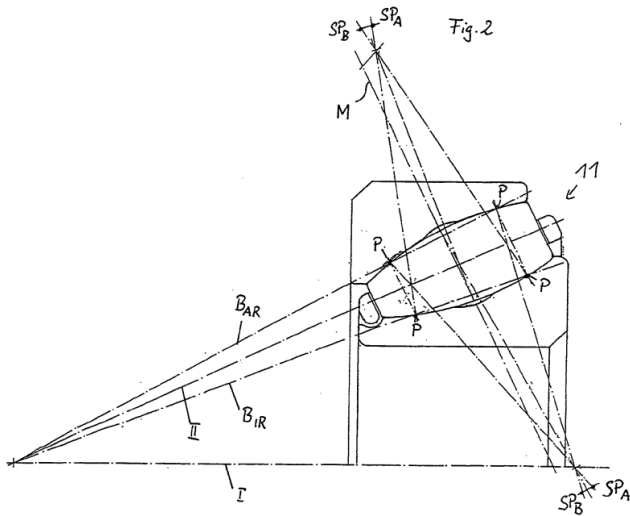
Figure 4.10: Draft of a barrel angular roller bearing with four contact points as defined by
          JACOB in [Jac08]

The two resulting osculation regions per raceway are each formed by a circular section with a constant radius (R_1). Their centers of curvature (SP_A and SP_B) lie outside the center plane of the rolling body (M) and the bearing axis (I) with an offset with respect to each other. On the contrary, the center of curvature of the roller with radius R_2 lies on the bearing axis, resulting in an osculation between the roller and the raceways. In other words a bigger PCR of the raceways compared to the PCR of the roller ($R_1 > R_2$). By this means, rollers are formed as conical barrels. Furthermore, as it is the case for TRBs, the contact tangents of the osculation contact points of the inner and outer rings (B_{IR} and B_{AR}) intersect at a point on the bearing axis, as shown in Figure 4.9. With this configuration, the typical drilling movement, characteristic of barrel rollers, is expected to be minimized. In addition, the ratio of the roller diameter to the roller length is defined to be less than approximately 1:2.

The patent of JACOB also defines a cage to guide the rolling bodies parallel to each other and in the defined alignment to the bearing axis. The cage is held in a groove-like cage guide as represented in Figure 4.9 by point 9.

With the above geometrical definition, a barrel angular roller bearing is defined to have a high load capacity in both axial and radial directions and low resulting friction compared to a TRB. It is expected to combine the advantages of a barrel rolling bearing, such as lower friction thanks to the absence of rib contact and low sensitivity to edge stresses; and those of a TRB including high load capacity under combined load conditions.

4.1.5 Summary

The geometries previously introduced, based on several patents, defined the foundation on which the geometry under study is based. An overview of these patents is listed in Table 4.1. The geometry defined in the patent, as well as its main characteristics are summarized. Most important, the last column presents the characteristics described in the patent that are considered for the design of the geometry under study, defined in the next section.

Table 4.1: Summary of the patents considered for the definition of the geometry under study

Patent	Rolling bearing type	Geometry characterized by	Considered for the geometry under study
[KB76]	Crowned roller (Spherical, barrel, toroidal)	How to influence the resulting skewing by modifying the profiling	Influence of the osculation and PCR on the resulting friction
[KKL16]	Angular toroidal roller bearing	Positive and Negative offset. Definition of dimensional parameters and method for determining them	Associations between parameters
[Gre19]	Angular toroidal roller bearing	Negative offset. Increase of the load-bearing capacity. Prevent from blocking	Associations between parameters
[Nak76; PO12; Neu17; SRW21]	Tapered roller bearing	Geometry optimization for a specific application	Influence of the boundary conditions on the output parameters
[Rei28]	"Conical" spherical roller bearing	Four contact point contact. Division of contact based on a more complex profile of the roller and raceway	
[Soc31]	Barrel roller bearing	Four contact point contact. Division of the contact based on a manufacturing process	
[Jac92]	Barrel roller bearing	Four contact point contact. Division of the contact based on a manufacturing process	Preferable location of the contact points. Osculation values
[Jac08]	Barrel angular roller bearing	Barrel roller bearing with increase axial load capacity	Basic geometry definition

4.2 Geometry under study

The influence that the geometrical parameter of the rollers and raceways has on specific output values such as frictional losses or lifetime has been described in Section 2.1.2. Based on it and on the different patents mentioned in Section 4.1, a new geometry of rolling bearing has been developed. The internal geometry of the new rolling bearing has been defined within 13 variables of lengths and angles, as shown in Figure 4.11. It fulfills the main requirements of a tapered spherical roller bearing (TSRB), also to be called a barrel/toroidal angular roller bearing. This is, a barrel or toroidal roller inclined in relation to the bearing axis via a contact angle, such as for TRB. Furthermore, the roller has four contact points instead of two long contact areas as in the case of commonly used barrel roller. By means of a crowning-shaped roller combined with a contact angle nonzero, the angle between the resulting axial load and the roller surface absorbing this axial load is increased in comparison to a TRB. As a result, the distribution of forces is such, that a flange is no longer needed. By this means, the bearing friction is expected to be reduced in comparison with a standard TRB.

The roller-raceway contact of a TRB is optimal and, therefore, its resultant frictional torque is at its minimum. On the other hand, for the geometry under study, as it is the case for every angular-contact ball bearing, having a contact diameter that is not orthogonal to the axis of rotation of the roller results in an undesired drilling friction. Therefore, the resulting losses at the roller-raceway contact of the new geometry will always be higher than those of a TRB. Considering all this, the ultimate goal when selecting the geometrical parameters is that the resulting drilling friction is smaller, than the friction at the flange when using TRB. In other words, the increase on the frictional losses appearing at the roller-raceway contact of the geometry under study will compensate the frictional losses at the roller-rib contact.

An additional characteristic of the geometry under study as represented in Figure 4.11 is the presence of two osculation contact points on each raceway instead of a line contact among the whole length. By means of a point contact instead of line contact, the contact length is decreased and, therefore, the resulting friction reduced. Another key feature that is fulfilled with this geometry is that the surface lines (Sl_1, Sl_2) of the raceways of the outer and inner ring intersect at the bearing axis (BA). Consequently, an even distribution of pressure is expected, allowing for the rollers to be loaded symmetrically and ultimately avoiding slippage.

A MBS model of the geometry under study will be created (the process will be explained in Section 5), defining the geometry of rolling elements and races depending on the value given to the parameters shown in Figure 4.11. The dynamical behavior of the bearing as well as its lifetime will be affected by the value that these input parameters take.
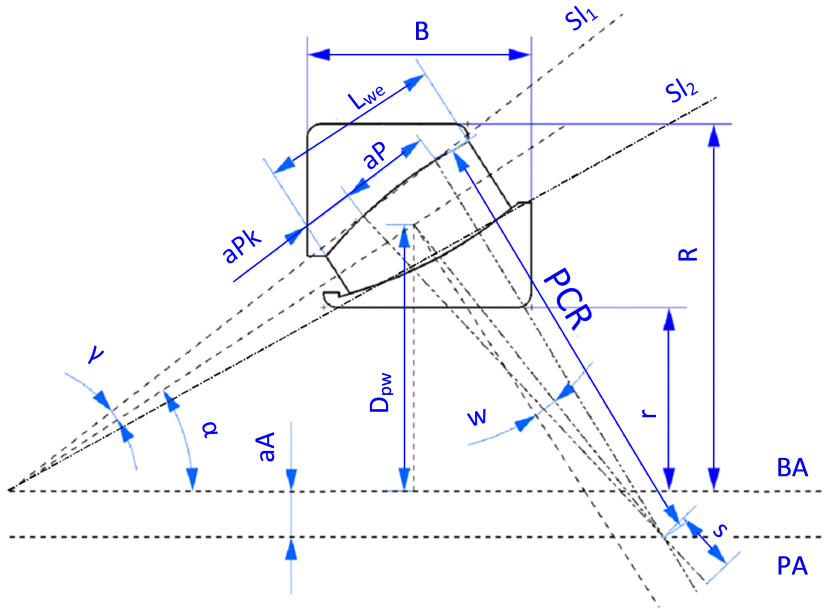
Figure 4.11: Geometrical variables defining the new rolling bearing under study

The ultimate goal when searching for an optimal geometry is to reduce the total frictional losses while keeping a carrying capacity and lifetime comparable to those of a TRB of the same main dimensions. To achieve this goal, the pressure distribution, the maximum pressure and the mean pressure at the contact will be closely monitored.

To this end, the dependency of the input geometrical parameters on the resultant frictional torque and maximum pressure has been studied and presented in Section 7.2. The main parameters to be changed according to its influence in the friction losses are:

- α and γ: The bigger the contact angle (α) of a bearing is, the bigger its axial load capacity is. Therefore, the contact angle will be chosen in accordance with the requirements of load conditions. As previously explained in Section 2.1.2, in order for the surface lines of the raceways to intersect at the bearing axle, the tapered angle (γ) is a direct function of the contact angle (α). It follows thus the equation 2.1.

- aA and PCR: In case of a standard barrel rolling bearing, the center of curvature of the rollers lays at the bearing axle. In other words, the distance between the bearing axis (BA) and the axis of the center of curvature (PA) is zero. As explained

in Section 2.1.2, Figure 2.7, when changing the position of the center of curvature we have two scenarios. In case of negative offset ($-aA$ in Figure 2.7), the axis of the center of curvature (PA) is closer to the raceway of the inner ring. Apart from its mentioning in different patents ([KKL16; Gre19]), non standard bearing follows this description. In case of positive offset ($+aA$ in Figure 2.7), the axis of the center of curvature (PA) is farther apart from the raceway of the inner rings. This is the case with toroidal roller bearings. As soon as the distance between the two axes (aA) is bigger than zero (as it is the example case represented in Figure 4.11), the PCR of the raceways and the rollers can be made considerably bigger (bigger PCR). Therefore the rollers can be made longer (bigger L_{we}), which enhances the radial load carrying capacity. The PCR of the rollers is a key parameter for the search of an optimal solution. The goal is to be maximize it, so that the drilling friction is minimized. Yet it has an upper limit in terms of the axial displacement of the roller. When the PCR is increased, the angle between the resulting axial load and the roller surface absorbing this axial load is reduced, therefore the axial displacement increases. If the axial displacement increases above a limit, a rib at the inner ring will be then needed. This remains to be avoided.

- s, aP and aPk: s is directly related to the osculation (κ), which, as mentioned in Section 2.1.2, affects the size of the contact area at about its contact points. The wider the osculation, the smaller the contact area. This, together with the location of these points, defined by the distance between them (aP) and the distance from the points to the roller edge (aPk), have a major influence on the contact pressure distribution and the possible skewing of the rollers as explained by KELLSTRÖM and BLOMQVIST in [KB76]. For the starting point of the sensitivity analysis described in Section 7.2, as well as for the majority of the cases studied, it has been assumed that the contact points are symmetrical to the roller middle plane as well as its rotation axis. This means, centered along its contact length, as well as equal for the inner and outer race. Therefore, the parameters aP and aPk follow the equations:

$$aPK = \frac{L_{we}}{2} \tag{4.2}$$

$$aPK = \frac{(L_{we} - aP)}{2} \tag{4.3}$$

- L_{we}: In order to maximize the carrying capacity of the rolling bearing, the length of the roller (L_{we}) has to be maximized. Since the need of a rib contact at the inner ring is eliminated, there is no limitation in the roller-end-length needed. In these terms, the ratio of roller diameter to roller length can be made lower than 1:2. Another relation between parameters that will be considered is the ratio between the roller transverse radius PCR_R and the roller length. This ratio is influenced

by the coefficient of friction of both roller and ring at the raceway contact. The lower the ratio, the better is the self-orientation ability of the roller. With all this in consideration, the ratio PCR_R to roller length is recommended to be lower than 10 in order to ensure axial self-orientation of the roller during operation.

The main parameters B (width), r (bore radius), R (outside radius) and D_{pw} (pitch radius) define the external geometry and will be chosen regarding the size of a TRB that will be compared to. This way, a better comparison can be achieved. The angle parameter w, whereby the roller acquire their tapered form, is directly proportional to the other parameters and is calculated for each case.

A standard TRB and a standard Toroidal Roller Bearing with an outer diameter of 80 mm and a bore diameter of 40 mm will be taken as a reference. With this purpose, the value that the input geometrical parameters defined in Figure 4.11 take for these two rolling bearings is listed in Table 4.2. In the first row, the parameters for a TRB 32208 of the SCHAEFFLER company are listed [Sch17]. In the second row, the parameters defining a Toroidal Roller Bearing CARB 2208 of the SKF company are enumerated [SKF14].

Table 4.2: Parameters defining the new geometry and their value for different bearings

Parameter	Description	TRB 32208	CARB 2208
α	Contact angle	14°	0°
γ	Taper angle	2,29°	-
aA	Distance from the bearing axis to the center of the PCR_R	-	
aP	Distance between contact points	-	-
aPk	Distance from contact point to the edge	-	-
B	Rolling bearing width	24,75 mm	23
D_{pw}	Pitch diameter	60 mm	61,2 mm
D_{we}	Roller diameter	10 mm	10 mm
L_{we}	Roller length	17 mm	15,9
PCR	PCR_R	-	122,55 mm
r	Rolling bearing bore radius	20 mm	20 mm
R	Rolling bearing outside radius	40 mm	40 mm
s	Osculation ($PCR_{LB} - PCR_R$)	-	5 mm
w	Angle proportional to the tapered angle	-	-
Z	Number of rollers	17	16

5 Simulation Modeling

In this section, the simulation model developed for the parameter study, sensitivity analysis, and ultimately profound analysis of the new geometry under study is presented. Using the parameter set defined in Figure 4.11, a parameterized multi-body simulation (MBS) model of the new geometry is built via the commercial software MSC.Adams. Within the model, the geometry of rolling elements, the races and the cage is created depending on the value given to the geometrical parameters. By means of a parametric study or a sensitivity analysis (see section 7.2), the influence that these parameters have in specific main outputs such as the frictional torque can be studied. In section 5.1, the internal structure of the MBS model created, as well as the interaction between its modules, is presented. The mathematical description of the contact between the individual rolling bearing elements and the raceways of the outer and inner ring are carried out using self-developed calculation routines in the Fortran programming language. A detailed description of the contact calculation routine is described in detail in chapter 5.2.

A brief description of the TRB model developed and validated by KIEKBUSCH [Kie17] is also explained in Section 5.5. This model was used to evaluate the influence of the newly developed bearing geometry on relevant parameters such as the frictional torque as well as to compare it with a standard tapered roller bearing.

Figure 5.1 shows the representation examples of a TRB Model (left) and a model of the new geometry as defined in Figure 4.11.
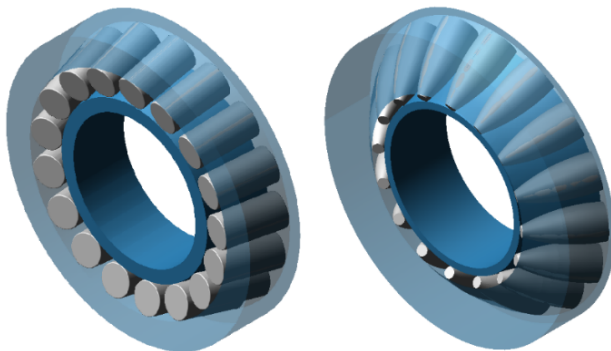
Figure 5.1: Representation of two simulations models. On the left a 32208 tapered roller bearing. On the right an example of the geometry under study.

5.1 Model structure

The MBS model of the new geometry is based on existing dynamic models of different bearings and self-written user routines developed and improved over the past years at the Chair of Machine Elements, Gears and Tribology (MEGT) [Teu05] [Hah05] [Woh10] [Aul14] [Kie17]. Within the model, a coupling of a commercial software and self-programmed calculation routines is used. A simplified diagram of the procedure followed within the MBS Model is shown in general form in Figure 5.2.
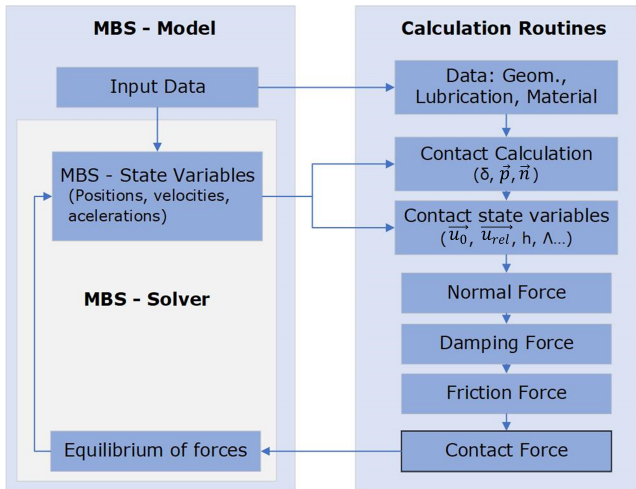
Figure 5.2: Rolling bearing dynamic simulation at the MEGT Chair.

In order to define the bodies, markers, forces and boundary conditions, scripts built in the ADAMS / View Command language are used. These scripts are built parametrically using the input data previously defined. By this means, modifications in the geometry, material properties, and boundary conditions can be adjusted easily. This allows for an uncomplicated generation of new models of different bearing types. In addition, a new geometry and the influence of its geometrical parameters in the output can be achieved, which is the goal of this work.

Once the geometry has been generated, the input data is transferred from the scripts to the calculation routines. Within the routines, the seeking of the contact points will be the focus. After the contact points are found, the penetration on each contact, as well as their corresponding normal direction to the contact are defined. Subsequently, the calculation of the velocities, forces and torques at the specific contact point can be implemented.

The routine for the calculation of the contact point δ, contact normal $\vec{n}$ and penetration $\vec{p}$ is the only routine immediately affected by the modifications in the geometrical definition of the roller-raceway contact. Therefore, the definition of the contact calculation is the most important for this work. A description of the contact calculation taking place within the generated MBS model can be found in the following section.

Once the contact has been defined in terms of its three variables (δ, $\vec{n}$, $\vec{p}$), the geometrical definition of the contact does not influence the calculation of the normal force, damping force and friction force. Therefore, since their calculation is not affected by the internal geometry of the rolling bearing, the corresponding routines can be directly transferred from the existing models [Kie17] .

5.2 Contact calculation

The main role of rolling bearings is guiding the machine elements and transferring the forces. This is mainly conducted by the contact between the rolling elements and the raceways. This contact is therefore the most important for the simulation. The definition of the roller-raceway contact in roller bearings is significantly more complicated than for ball bearings. The rollers and the raceways in contact with them are still rotationally symmetrical, but the profiles are usually more complex. As a solution, discretized models must be used in order to obtain an accurate image of the contact and, thus, be able to calculate the contact conditions. In these terms, a so called "Slice model" will be used. A description of this model can be found in Section 5.2.1.

The main task of the contact calculation routine is to determine the penetration, the contact normal and the contact point. Their calculation is based on the geometry of the two bodies in contact. These parameters are the basis for the further calculation steps. The three parameters can be defined as follows:

- The **penetration** δ (also rigid body penetration) can be understood as the negative distance between the two contacting surfaces. In other words, the theoretical penetration depth of the undeformed surfaces.

- The **contact normal** $\vec{n}$ is the direction of action of the normal force occurring in the contact. It is calculated from the mean of the two surface normals.

- The **contact point** $\vec{p}$ is the location at which the normal force acts. This point is located in the middle of the volume enclosed by the rigid body penetration.

5.2.1 Discretization models

In order to properly define the contact situation between two bodies in contact, the area of contact must be discretized. Depending on the type of contact, this discretization might be along the length of the contact in terms of slices (as it is in the case of a roller-raceway contact), or for an area of contact in terms of a cell (as it is in the case of a roller-end-rib contact). Both discretization models are explained in detail hereunder

Slice Model The integral approach, successfully applied for the point contact of a ball bearing [Kie17] is not suitable for correctly determining the contact parameters in roller bearings. Due to the profiling of the rolling elements and the raceway, a closed solution to the contact problem is not reasonable. With the help of a slice model, the rolling element is discretized into a finite number of individual slices in the direction of the contact line. Subsequently, the contact calculation takes place in the middle of each slice. By this means, the imaging accuracy of the slice model and the required computing time will be influenced by the number of slices in which the roller is discretized. The choice of the number of slices is therefore one of the decisive factors for the quality of the result and the numerical effort. Figure 5.3 shows a simplified representation of the slice model of the contact between a profiled rolling element and a plane as well as the parameters to be obtained for the calculation of the contact.
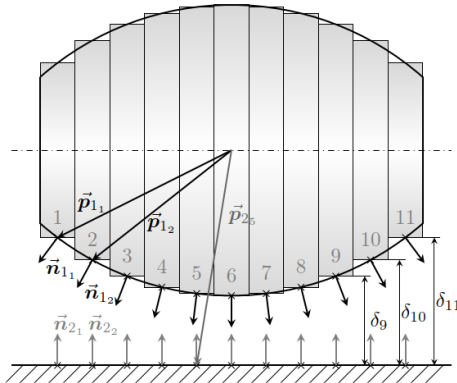
Figure 5.3: Section plane of the slice model of a barrel roller in contact with a plane (contact point $\vec{p}_{j_i}$, contact normal $\vec{n}_{j_i}$ and penetration δ_i) of a body j and a slice i [Kie17]

A conventional slice model is defined in [DIN11]. Within this model, while the radial deformation of the slices are independent of each other, the slices stick together in a torsionally rigid manner. The deformation of each slice can be thus determined by its

penetration with the contour of the opposite slice of the other body. The distribution of pressure according to a conventional slice model is shown in Figure 5.4.b. It can be observed, that the conventional slice model does not properly represent the real pressure distribution of a roller in terms of edge stresses.

The *Alternative Slicing Technique* (AST) implemented in the MBS Model used in this work was first presented by TEUTSCH in [TS04] and subsequently implemented by KIEKBUSCH in [Kie17]. Thanks to the consideration of the mutual influence of the slices, more precise results can be achieved when implementing the alternative slice model. By this means, a pressure distribution closer to the real distribution, as shown in Figure 5.4.a, can be obtained.
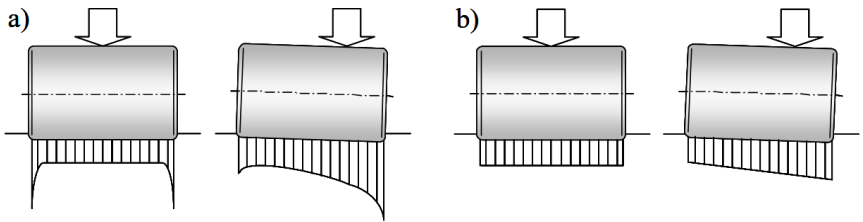
Figure 5.4: Qualitative pressure distribution in cylinder-plane contact with and without tilting of the rolling element: a) real distribution b) distribution according to a conventional slice model [Teu05]

Cell Model For geometries that cannot be mapped with sufficient accuracy using the slice model, a cell model can be used. A cell model discretizes the contact surface not only in the roller axis dimension, but in the perpendicular axis dimension. This is particularly useful for contacts in which the resulting contact surface deviates significantly from a standard point and line contact. For example, this is the case of the rib contact of a tapered roller between the rolling element end and the rib ring. In these terms, a limited sector containing the contact area of the surfaces of the two bodies in contact is divided into a defined number of square cells. For each cell, the penetration, contact point and contact normal have to be determined.

5.2.2 Mathematical determination

When using a slice model to reduce the complexity of the contact situation, the rolling element is discretised. By this means, on one hand the contact problem is reduced to the slice center plane and on the other hand each slice leads to a circular geometry. The basic geometry of the raceways of unprofiled rollers like cylindrical or tapered rollers can be defined by means of a linear or square surface (plane, cylinder, cone or sphere). However,

for profiled raceways as well as spherical, barrel or toroidal rollers, the consideration of
a PCR of the raceway leads to the geometry of a torus. For the geometry under study,
as described in Figure 4.11, two different PCR define the profile of a raceway. Thus, the
mathematical descriptions of both inner and outer ring raceways follow two intersected
toruses. In order to simplify the contact definition, it will be first defined which of the
two toruses of the raceway is in contact with the roller bearing. Afterwards, the contact
between the roller bearing and this torus will be calculated using mathematical relations.

Disregarding the tilting of the rolling element, the intersection curve of the raceway
geometry (torus) with the slice planes is a circle (as represented in the left side of Figure
5.6). This calculation must be carried out for each slice with the corresponding raceway
cutting contour.

If the tilting movement of the rolling elements relative to the raceways are taken into
account, the simplification mentioned no longer applies. Depending on the raceway geom-
etry, different blending curves can arise. In case of a torus, its intersection curve with the
slice plane is as shown in the right side of Figure 5.6.

The direct calculation of the intersection curve between the slice and the torus of a raceway
can be done if a surface (torus) is implicitly described and the counter surface (slice)
is described in parametric form [HL92]. Afterwards, the equations for the individual
coordinates (in parametric form) can be introduced in the implicit representation.

The surface of a slice can be defined in terms of a plane. In parametric form, a plane E
can be thus described by a support vector $\vec{q}$ and two direction vectors $\vec{u}$ and $\vec{v}$ with the
two parameters s and t.

$$E = \left\{ \vec{x} = (x, y, z) \in \mathbb{R}^3 \mid \vec{x} = \vec{q} + s\vec{u} + t\vec{v} \right\} \; mit \; \vec{q}, \vec{u}, \vec{v} \in \mathbb{R}^3 \; und \; s, t \in \mathbb{R} \qquad (5.1)$$

On the other hand, the torus is a surface of fourth degree and can be implicitly described
using the radii R and r. Here r is the radius of the rotated circle and R the distance
between the center of the circle and the axis of rotation. When describing the raceways of
our model, as well as a standard spherical or barrel roller bearing, the PCR of the raceway
defines the parameter r or radius of the rotated circle. On the other hand, R, the distance
between the center of the circle and the axis of rotation is defined by the distance between
the bearing axis and the center of the PCR of the raceway.

When the radii of the torus are such that $R > r$, the surface will be the familiar ring torus
as shown in Figure5.5.a. On the other hand, if $R < r$, a self-intersecting spindle torus is
built as shown in Figure 5.5.b. Depending on the geometry of the rolling bearing, the
radius r might be smaller than R, making it difficult to provide a real representation of
the contact situation. For further examples, a ring torus will be used in order to offer an
schematic representation.

The implicit equation in cartesian coordinates for a torus radially symmetric about the z-axis is:

$$\left(\sqrt{x^2+y^2}-R\right)^2 + z^2 = r^2 \tag{5.2}$$
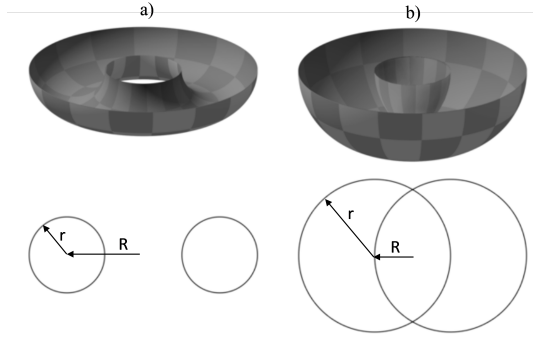
Figure 5.5: Bottom-halves and vertical cross-sections of a ring torus (a) and a spindle torus (b)

Algebraically eliminating the square root of equation (5.2), a quadratic equation can be obtained:

$$\left(x^2+y^2+z^2+R^2-r^2\right)^2 - 4R^2\left(x^2+y^2\right) = 0 \tag{5.3}$$

Inserting the plane equation (5.1) into the implicit torus equation (5.3) leads to a plane algebraic curve of fourth degree, which has fourteen coefficients in a generally standardized form. By this means, the cutting contour with a torus is an equation with five coefficients b_i as follows:

$$\left(x^2+y^2\right)^2 - b_1 x^2 + b_2 y^2 + b_3 x + b_4 y + b_5 = 0 \tag{5.4}$$

The resulting blending curves for the inner ring of a barrel roller bearing and a spherical roller bearing with $R > r$ are shown in Figure 5.6. Since for untilted barrel roller bearings the roller axis is parallel to the bearing axis, the resulting cutting contours are circles. For spherical roller bearings, the roller axis is tilted relative to the bearing axis, so that the cutting contours result in algebraic curves according to equation (5.7).

The contact point $\vec{p}_{RW}$ on the raceway section contour can be found as the point of the cutting contour with the smallest distance to the center point of the slice $\vec{p}_S$. Based on the contact point $\vec{p}_{RW}$, the penetration is then obtained in terms of a distance calculation between the cutting contour and the center of the circle. This can be solved analytically for the geometry of a torus. By this means, a non-linear system of equations with two unknowns has to be solved.
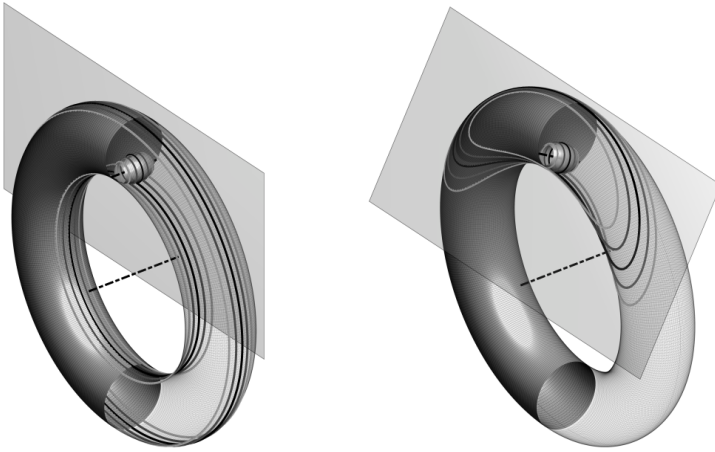
Figure 5.6: Contact geometries (gray and black solid lines) in the middle of the slice plane
           for rollers and a toroidal raceway for barrel roller (left) and spherical roller
           (right) bearings when using a slice model (five slices) without tilting of the
           roller [Kie17]   .

In order to determine the contact point $\vec{p}_{RW}$ on the raceway section contour, the points of
intersection between the body surface and the ray in the normal direction of the surface
plane at the discretized points are sought. Afterwards, the transition from the standard
geometries to the real geometries requires the scaling, distortion and shifting or rotation
of the basic geometries. With the approach of homogeneous coordinates, these transforma-
tions are all carried out by multiplying the corresponding transformation matrices, which
significantly simplifies the numerical implementation.

A ray can be parametrically defined by means of a starting point $\vec{e}$ (center of the corre-
sponding slice) and a direction vector $\vec{e}$ as follows (see Figure):

$$\vec{r}(t) = \vec{e} + t\vec{d} \tag{5.5}$$

Which can as well be written as:

$$\begin{aligned}
x(t) &= x_E + tx_D \\
y(t) &= y_E + ty_D \\
z(t) &= z_E + tz_D
\end{aligned} \tag{5.6}$$

The point of intersection between the torus and the ray and thus, the contact point $\vec{p}_{RW}$
on the raceway section contour, is obtained by inserting the ray coordinates $\vec{r}_t$ (Eq. 5.6)

into the quadratic equation of a torus (5.3). By this means, the following equation is obtained:

$$2R\sqrt{x_E^2 + 2tx_Ex_D + t^2x_D^2 + y_E^2 + 2ty_Ey_D + t^2y_D^2} =$$
$$R^2 + x_E^2 + 2tx_Ex_D + t^2x_D^2 + y_E^2 + 2ty_Ey_D + t^2y_D^2 + z_E^2 + 2tz_Ez_D + t^2z_D^2 - r^2 \tag{5.7}$$

This equation only contains the ray length parameter t as an unknown. Through several transformations, it results in a fourth degree polynomial of t, which can be solved analytically (see, for example, [Gla98]) or numerically (see, for example, [PTV07]). The fourth degree polynomial having five coefficients has the following form:

$$b_4 \cdot t^4 + b_3 \cdot t^3 + b_2 \cdot t^2 + b_1 \cdot t + b_0 = 0 \tag{5.8}$$

Solving the equation (5.7), the five coefficients of the fourth degree polynomial are defined as:

$$b_4 = dot_{dd}^2$$
$$b_3 = 4 \cdot dot_{dd} \cdot dot_{ed}$$
$$b_2 = 4(dot_{ed}^2) + 2dot_{dd} \cdot (dot_{ee} - r^2 - R^2) + 4R^2 z_D^2 \tag{5.9}$$
$$b_1 = 4 \cdot dot_{ed} \cdot (dot_{ee} - r^2 - R^2) + 8R^2 z_E z_D$$
$$b_0 = (dot_{ee} - r^2 - R^2)^2 + 4R^2 z_E^2 - 4R^2 r^2$$

Where the parameters dot_{dd}, dot_{ee} and dot_{ed} are the dot products of the vectors defined in equation (5.6). This way, they are defined as:

$$dot_{dd} = \vec{d} \cdot \vec{d} = x_D{}^2 + y_D{}^2 + z_D{}^2$$
$$dot_{ee} = \vec{e} \cdot \vec{e} = x_E{}^2 + y_E{}^2 + z_E{}^2 \tag{5.10}$$
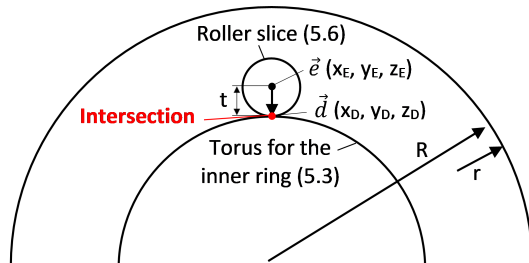$$dot_{ed} = \vec{e} \cdot \vec{d} = x_E x_D + y_E y_D + z_E z_D$$

Figure 5.7: Intersection point between the torus (equation (5.3)) and the ray of the roller slice (equation (5.6))

.

5.2.3 State Variables

The geometrical definition of the contact at each cutting geometry is defined by means of three parameters: the penetration, the contact point and the contact normal as defined in section 5.2.

Under the term *State Variables*, the calculation variables determining the contact situation are summarized. These variables describe the contact beyond the geometrical variables of penetration, contact point and contact normal. These include, for example, the surface speeds, the resulting relative and total speeds, the lubricant properties in the contact, the height of the lubricating film and the associated parameters.

The procedure for determining the gap or penetration function in the roller bearing contact is described below. The calculation is carried out in the body-fixed coordinate system of the roller. The penetration can be considered as a negative gap, so that it can be determined from the variation of the gap between the bodies at the discretized points in terms of a distance calculation between the cutting contour and the center of the circle. Based on the the contact point $\vec{p}_{RW}$ on the raceway section contour obtained after solving the equation (5.8) with the coefficients defined in equation (5.9), the determination of the contact point on the roller surface $\vec{p}_R$ can be calculated. Knowing the location of the center of the slice $\vec{p}_S$, this can be done by scaling the unit vector from $\vec{p}_S$ to $\vec{p}_{RW}$ with the slice radius r_S as follows:

$$\vec{p}_R = \frac{\vec{p}_{RW} - \vec{p}_S}{\|\vec{p}_{RW} - \vec{p}_S\|} \cdot r_S \tag{5.11}$$

Based on the contact point on the raceway $\vec{p}_{RW}$ and the contact point on the roller $\vec{p}_R$, the penetration δ results as the absolute difference between these two points:

$$\delta = \|\vec{p}_{RW} - \vec{p}_R\| \tag{5.12}$$

Knowing the contact normal to the raceway $\vec{n}_{RW}$ at the determined contact point $\vec{p}_{RW}$ and the contact normal to the corresponding slice $\vec{n}_R$ at the contact point $\vec{p}_R$, the resulting contact normal is calculated as the mean value of the surface normals:

$$\vec{n} = 0.5 \left(\frac{\vec{n}_{RW}}{\|\vec{n}_{RW}\|} + \frac{\vec{n}_R}{\|\vec{n}_R\|} \right) \tag{5.13}$$

Finally, the contact point $\vec{p}$, lying in the middle of the enclosed area between $\vec{p}_{RW}$ and $\vec{p}_R$ can be obtained as follows:

$$\vec{p} = \vec{p}_{RW} + \frac{\delta}{2} \cdot \vec{n} = \vec{p}_R - \frac{\delta}{2} \cdot \vec{n} \tag{5.14}$$

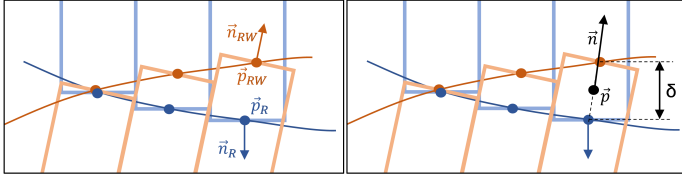An illustrative example of the variables defining the roller-raceway contact is shown in Figure 5.8.

Figure 5.8: Penetration (δ), contact points and contact normals at the raceway section ($\vec{p}_{RW}$ and $\vec{n}_{RW}$), at the roller surface ($\vec{p}_R$ and $\vec{n}_R$) and in the middle of the enclosed area ($\vec{p}$ and $\vec{n}$).

5.3 Contact force and load distribution

The load distribution along the rolling element axis can be determined with the help of a slice model as explained in section 5.2.1. In these terms, as a result of the roller-raceway contact calculation, the penetration, the contact point and the contact normal are available as a vector. Based on these vectors, the contact pressures and forces can be calculated for each individual contact with the corresponding discretization. These variables are a fundamental prerequisite for the dynamic simulation and are directly used for the calculation of the load distribution and the stiffness. They are also an important input variable for calculating the friction conditions.

The methods for the contact calculation of line contacts based on the Hertz's theory describe two infinitely long, axially parallel cylinders. This leads to an even distribution of pressure along the contact line. While the width of the contact surface and the maximum pressure can be calculated according to Hertz, there is no correlation between the applied load and the resulting deformation.

Various authors have dealt with this problem developing several solutions. TEUTSCH summarizes the most important works and compares their results with the results of two FE models [Teu05]. The method according to TRIPP [Tri85] and HOUPERT [Hou01] is used here. Within these methods, the penetration is explicitly defined as a function of the contact force ($\delta = f(Q)$). However, for the purpose of the dynamic simulation, the contact force has to be defined as a explicit function of the penetration, since the penetration is the known variable. Therefore, an approximation is carried out based on the existing geometry by means of power regression in order to obtain an equation of the following form:

$$Q_i = k_1 \cdot \delta_i^{k_2} \tag{5.15}$$

This equation has to be determined with the parameters k_1 and k_2. This resembles the form as described in [DIN11] (based on the work of PALMGREN). While TEUTSCH

determines the parameters individually for each slice on the basis of the geometry, the standard specifies values for k_1 and k_2 that are independent of the geometry and material. However, this simple approach is not suitable for taking into account the profiling of the rolling element and the raceways as well as the tilting of the rolling elements. For this purpose, it is necessary to take into account the conditions that vary over the length of the contact area.

To overcome this limitation, TEUTSCH developed an Alternative Slicing Technique (AST) model (section 5.2.1). Based on the half-space theory, the influence that a force Q_i acting on a slice i has on the deformation δ_k occurring on the slice k, is taken into account. For that purpose, an influence-number-matrix is used. The method manages with a few iterations and is therefore very well suited for its use in MBS as a compromise between accuracy and optimization of computing time [TS04].

5.4 Friction calculation

As already pointed out, the frictional forces in the contact represent an important requirement for a precise simulation of the dynamic behavior of rolling bearings. Frictional forces take place at every contact points. The basics for their calculation in the model are described in Section 2.3. However, the way of implementing these principles in the model is also decisive.

For this purpose, the frictional forces are divided into several categories, which will be individually calculated. By this means, the total resulting friction will be obtained by summing each individual force and torque. On the one hand, the frictional forces are divided into losses or traction forces. On the other hand, they can be divided into solid-body or lubricating-film forces. This approach has been successfully implemented by KIEKBUSCH [Kie17] for different types of standard rolling bearings. The definition of these categorizations is explained below.

The frictional forces influence the movement of all rolling bearing components. At the same time, the relative movement of the components to one another influences the frictional forces. Hence, there is a very strong interaction between the friction and the dynamics of the rolling bearing. In order to procure a correct description of the friction, both the resistance to movement (losses) and the adhesion behavior (traction forces) are modeled.

Mixed friction occurs in rolling bearings when the height of the lubricating film is not large enough to separate the roughness peaks of the contact partners from one another. In [ZH91], ZHOU and HOEPRICH develop a calculation approach for the efficient description of friction in mixed friction contact. By this means, they divide the normal force N of

the contact into a part that is borne by the roughness peaks (solid body load N_F) and a part that is borne by the lubricating film (lubricating film load). According to [Tal67], the calculation of the solid load-bearing component Φ is based on the specific lubricating film height Λ and two parameters (B_{ZH} and C_{ZH}), which are dependent on the surface quality:

$$\Phi = \frac{N_F}{N} = exp\left(-B_{ZH} \cdot \Lambda^{C_{ZH}}\right) \tag{5.16}$$

This overall leads to friction losses obtained as the combination of the solid body rolling torque $M_{T,S,r}$, the lubricant rolling torque $M_{T,L,r}$ and the material hysteresis $M_{T,hys}$. Moreover, the traction forces and torques are divided into the solid body sliding force $F_{T,S,s}$ and torque $M_{T,S,s}$ and the lubricant sliding force $F_{T,L,s}$ and torque $M_{T,L,s}$. For a better understanding, the different subscripts together with their description are listed in Table 5.1.

Table 5.1: Subscripts for the definition of the frictional forces and torques taking place at the contact

Subscript	Description
T	Tangential force/torque
S	Solid body force/torque
L	Lubricant force/torque
r	Rolling force/torque
s	Sliding force/torque

Within the model, first of all, the above mentioned forces and torques amounts are calculated on the basis of the *State Variables*. These are then vectorized using the contact variables. Finally, the integration or summation of the frictional forces F_T and moments M_T of the discretizatized points resulting into the total frictional force $\vec{F_T}$ and moment $\vec{M_T}$ in the contact takes place as follows:

$$\vec{F_T} = \Phi \cdot F_{T,S,s} + (1-\Phi) \cdot F_{T,L,s} \tag{5.17}$$

$$\vec{M_T} = \Phi \cdot M_{T,S,r} + M_{T,hys} + M_{T,L,r} + \Phi \cdot M_{T,S,s} + (1-\Phi) \cdot M_{T,L,s} \tag{5.18}$$

5.5 TRB Model

The MBS Model of a TRB used in this work has been developed by KIEKBUSCH [Kie17] within the software ADAMS. It is based on the peculiarities of its geometry as well as on different models previously developed. The following subsections describe the singularities

of the model, that differ from the model used for the prototype, and therefore are in need of an additional explanation.

The existing MBS Model, the routines used within the TRB Model, as well as its procedure of computation and evaluation, have been validated and presented in several studies [AAH07; SK17; KS17; KFS15; Teu05]. In particular, the state of the TRB Model used for this work has been validated by KIEKBUSCH [Kie17]. For this purpose, both frictional torque measurements and simulations were carried out with a TRB 32216. In order to confirm the contact modeling, the results for the load distribution were as well compared with the results of the calculation tool *LAGER2* of the *Forschungsvereinigung Antriebstechnik e.V.*

Within its validation, it could be shown that the developed model correctly calculates both the load distribution and the friction conditions in the rolling bearing. Based on the resulting frictional torque when varying the input parameters (temperature, angular velocity, and axial and radial load), the simulations showed very small deviations and confirmed the high model quality.

5.5.1 Rib contact

In tapered roller bearings the contact between the roller-end and the raceway rib has an important influence on the load distribution and thus the fatigue life. The reason for this is the different taper angles on the inner and outer ring raceways create an axial force component that has to be supported by the rib, as explained in Section 2.1.2. As a result, the definition of this contact has a decisive in fluence on the functionality and losses of this type of rolling bearing. Furthermore, there is an interaction between the raceway contact and rib contact in roller bearings. This, however, requires the consideration of the entire machine element and not only the individual contacts.

The geometries of the roller-end and the raceway rib are mainly responsible for the friction that occurs in the rib contact and its service life. The geometry of the raceway rib surface can be divided in three types, depending on the level of detail of the simulation: plane, cone or profiled cone. Similarly, several geometries of the roller-end can be defined with different level of detail: plane with edge radius, spherical, spherical with an edge radius or curved with an edge radius. Within the TRB model used for this work the roller-end and the raceway rib are defined in such a way, that the combination defines a torus-plane contact. These geometries can be defined as follows:

- Flat face with edge radius for the roller end (see Figure 5.9a): The profile of this geometry can be described by a straight line and a quarter circle. In 3-dimensional space, the edge radius rk results in a torus, while the straight line results in the "cover" of the torus. In practice, the rolling element will usually touch the raceway

rib with the edge radius, unless the rib does not have an opening angle and the rolling element is not skewed. It is therefore sufficient to consider the contact between the torus and the countersurface.

- Cone for the rib surface (see Figure 5.9b): The countersurface for the roller-end represents a plane that is not perpendicular to the bearing axis, but has a rib opening angle. This geometry is often used in roller bearings.

For geometries that cannot be defined with sufficient accuracy using the slice model, a cell model can be used. This happens in case of the rib contact. When using a cell model, the contact surface is discretized in two dimensions.

a) Roller end geometry   b) Rib surface geometry
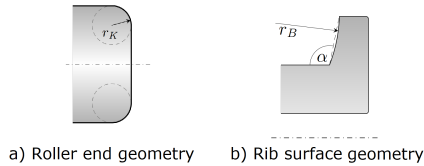
Figure 5.9: Roller end and rib surface geometries implemented in the TRB Model

5.5.2 Hydraulic losses

Liebrecht et al. examined in [LSS15b; LSS15a] the churning losses on a TRB 32208 with the help of experimental and CFD methods. They establish that the oil foaming has a decisive influence on the churning and flow losses. With the help of the effective viscosity of the lubricant-air mixture approximated from the experiments, good correspondences between the CFD simulations and the measurement results can be shown. In [LSS16] they deduced a technical-mathematical model named the $CoDaC$ (Calculation of Drag and Churning) from their investigations. With this model, the hydraulic losses appearing in TRB can be estimated on the basis of physical principles. For this purpose, they subdivide the hydraulic losses into churning losses on the roller end and roller profile, as well as the inner and outer ring and the drag losses through the rolling elements. This approach has been validated for different types of bearings [Lie18]. In [KLS17], the transferability to rolling bearings with cylindrical rolling elements in a horizontal arrangement has already been shown. Although the technical-mathematical model $CoDaC$ has not been per se implemented into the TRB model, it can be used to externally obtained the hydraulic losses and in order to add them to the resulting frictional losses.

6 Experimental testing

In order to validate the MBS generated for the new geometry, experimental tests have been conducted. For this purpose, first of all, a prototype of the new geometry has been produced. This process, as well as the parameters defining its geometry is explained in section 6.1. The experimental tests have been conducted in a test bench described in section 6.2. Within the experiments, not only the new geometry has been tested, but also a standard TRB of main dimensions d = 40 mm and D = 80 mm. With that in mind, a TRB 32208 of the company SCHAEFFLER has been chosen. By this means, a better comparison between the new geometry and a TRB can be achieved. This comparison can take place in several ways. First of all, each MBS model will be compared with its corresponding experiments in order to validate the models (presented in section 6.3). Second of all, a comparison between the simulations as well as a comparison between the experiments of both types of rolling bearing has be conducted (presented in section 6.4).

6.1 Prototyping

In order to be able to compare the new geometry with a TRB 32208, two prototypes with main dimensions comparable to a 32208 were produced (Figure 6.1). These prototypes have a cage made of a conventional polymer cage material (Polyamide 66).

Figure 6.1: Prototype of the new geometry with polymer cage

The inner geometry of the prototype corresponds to the one defined in section 4.2. Furthermore, the geometrical parameters defining this geometry accordant to Figure 4.11

are shown on Table 6.1. For the selection of these values, a first optimization of the model has been conducted, whereby different parameters have been varied in order to reduce the frictional torque. After the validation of the model, a more extensive optimization has been performed (section 7.2).

The frictional torque is used as an integral variable to validate the dynamics of the MBS model. For this purpose, the resulting frictional torque of the prototype has been compared with those of its MBS Model. These results are presented in section 6.3. Furthermore, with the purpose of quantifying the benefits of the new geometry, the experimental results of the prototype have been compared to a TRB 32208. These results are presented in section 6.4. Further simulation results of the geometry defining the prototype are featured in section 7.1.

The determination of the surface data required for the simulation was carried out using measurements obtained with a 3D confocal microscope from NanoFocus. The combined standard deviation of the roughness in the contact rolling element-raceway, which is used in the simulation, is 0.22 μm for the prototype and 0.33 μm for the tapered roller bearing. These values, as well as other roughness values are listed in Table A.3 of Annex A.1.1.

Table 6.1: Parameters defining the geometry of the prototype

Parameter	Description	Prototype
α	Contact angle	33°
γ	Taper angle	4,5°
aA	Distance from the bearing axis to the center of the PCR_R	0,25 mm
aP	Distance between contact points	8 mm
aPk	Distance from contact point to the edge	9,5 mm
B	Rolling bearing width	24,75 mm
D_{pw}	Pitch diameter	58 mm
L_{we}	Roller length	20 mm
PCR	PCR_R	43,83 mm
r	Rolling bearing bore radius	20 mm
R	Rolling bearing outside radius	40 mm
s	Osculation $(PCR_{LB} - PCR_R)$	2 mm
w	Calculation angle	10°
Z	Number of rollers	17

6.1.1 Load ratings and calculation factors

Although for standard rolling bearings the load ratings are experimentally obtained, a first approximation can be made by means of a mathematical determination. The methods and equations to be used for this determination are explained in section 2.1.4. In case of the

prototype, this can be done based on its internal geometrical parameters as described in Table 6.1. For the basic static load rating, the equation (2.10) can be used. Similarly, the basic dynamic load rating can be obtained from the equation (2.14). For the computation of the calculation factors, dependent on the contact angle of the roller, the equations listed in (2.9) and (2.13) have to be used (section 2.1.4).

Table 6.2: Load ratings and calculation factors for the prototype and a TRB 32208

Par.	Description	Prototype	TRB 32208	
D_{we}	Roller diameter	8,4 mm	10 mm	
D_{pw}	Pitch diameter	58 mm	60 mm	
L_{we}	Effective roller length	20 mm	17 mm	
α	Contact angle	33°	13,55°	
Z	Number of rollers	17	17	
			Calculated	Catalog
b_m	Load rating coefficient	1,13	1,10	
f_c	Calculation factor	86,61	88,54	
C_0	Basic static load rating	93,5 KN	104 KN	93 KN
C	Basic dynamic load rating	72,8 KN	86 KN	79 KN
X_0	Static radial load factor	0,5	0,5	0,5
Y_0	Static axial load factor	0,34	0,88	0,88
e	Limiting value of F_a/F_r for the applicability of diff. values of factors X and Y	0,97	0,37	0,37
X	Dynamic radial load factor	0,4	0,4	0,4
Y	Dynamic axial load factor	0,62	1,60	1,60

Table 6.2 summarizes the load ratings and calculation factors obtained for the geometry of the prototype as well as the additional factors needed for its mathematical determination. The length of the roller used for the calculation of the load ratings is the effective length. This means, the length of the roller that is loaded. For the prototype it has been assumed that 100% of the roller length is loaded. However, this is not true for all the load conditions studied, but rather changes with the load applied (the influence that the load has in the contact length of the roller of the prototype is presented in section 7.1). For a better comparison, the corresponding values of a TRB 32208 (with same main dimensions) are as well listed. For the TRB, both the calculated values according to DIN ISO 281 [DIN10a] and the catalog values of the SCHAEFFLER company are listed [Sch17]. It can be observed, that the mathematically determined load ratings for the TRB 32208 are slightly higher than those experimentally obtained by the SCHAEFFLER company. Therefore, although the load ratings for the prototype and the catalog values for the TRB 32208 are similar, it can be assumed that the real load ratings of the prototype are as well minimally slower

than those mathematically obtained. As a result, the load ratings of the prototype (when the whole length of the roller is loaded) are expected to be slightly slower than those of a TRB 32208.

6.2 Test bench

For the experimentally investigation of rolling bearings, a frictional torque test rig was developed at the MEGT department several years ago in the course of Aul´s work [Aul08]. This test bench has been used in this work in order to experimentally test the prototypes of the geometry under study. With the frictional torque test rig it is possible to realistically reproduce the loads occurring on a bearing in reality.

A CAD view of the test bench pointing out the main parts (black), movements (green) and loads (red) is represented in Figure 6.2. The test bench is divided into three main modules. A schematic diagram of the test bench and its three modules is shown in Figure 6.3. In the test module, the outer ring of the rolling bearing to be examined (test bearing) is accommodated in the inner ring of a hydrostatic bearing. The outer ring of the hydrostatic bearing is, in turn, fixed to the base plate. By this means, the frictional torque generated in the test bearing is transferred to the inner ring of the hydrostatic bearing. Afterwards, the rotational degree of freedom of the hydrostatic bearing is recorded with a bending beam force sensor. This can be used to determine the required holding force and thus the frictional torque.
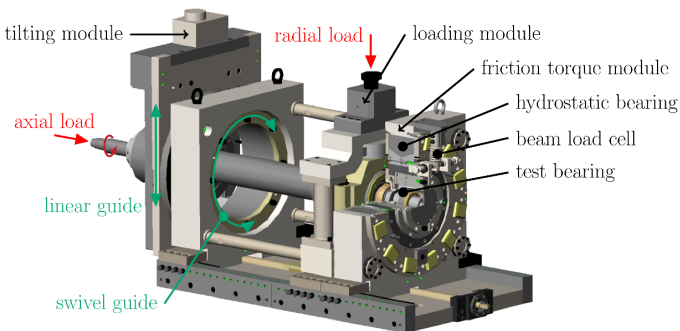

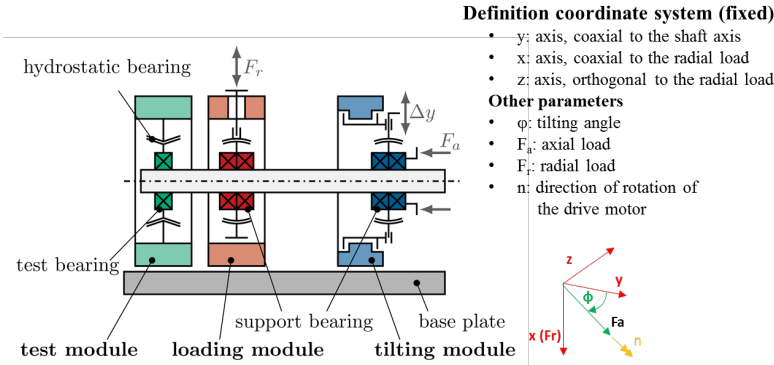Figure 6.2: CAD of the frictional torque test bench

Figure 6.3: Schematic diagram of the frictional torque test bench

The radial load on the test bearing is indirectly applied via the support bearing of the load module through a load screw. Moreover, the adjustment of the misalignment can be set independently of the bearing load. For this purpose, the tilt module has a linear guide, which is, in turn, mounted in a rotary guide. By this means, in order to achieve a tilted position of the test bearing, the support bearing of the tilt module can be moved in the radial direction. In this way, the angular position of the test bearing can be set between 0° and 90° to the radial load direction, so that tilting and skewing, as well as combined inclined positions, can be set. In addition, an axial force can also be applied via the support bearing of the tilting module by means of a hydraulic cylinder. The support bearings of the tilt and load module are accommodated in spherical calottes to compensate the tilting position.

The lubrication is carried out as oil bath lubrication with FVA reference oil No. 3. The test chamber is filled with lubricant up to half the height of the lowest rolling element at standstill. The lubricant data used in the MBS model can be found in the Annex A.1.1.

Table 6.3: Boundary conditions for verification of the simulation model

Shaft diameter	40 mm
Radial load	0 to 8 kN
Axial load	0 to 5 kN
Shaft speed	2000/4000 rpm
Tilting prototype	0 to 0.5°
Tilting TRB	0 to 2,5'

Although the new geometry is intended for high loads, the load that can be applied when using the frictional torque test bench is limited. The boundary conditions under which the experimental investigation is conducted are summarized in Table 6.3.

6.3 Model validation

In order to validate the model created as explained in section 5, experimental results have to be compared to simulated ones. For this purpose, the total frictional torque is being used as the main outcome for this comparison.

6.3.1 Previous experiments

As mentioned before, a TSRB has already been studied and compared to a TRB at the MEGT chair in Kaiserslautern. Within this work, a prototype of a TSRB as defined in the patent of JACOB [Jac08] without an optimized geometry or surface finish (Ra = 0.15µm) has been experimentally tested. This was done in order to compare it to a TRB of the same main dimensions (32314A), having an optimal flange geometry and high quality surface finish (Ra = 0.03µm). It had been observed, that the TSRB already shown a frictional torque comparable to the one of a TRB. In this study, both roller bearings (of 70mm shaft diameter) where submitted to an axial load of 20 kN and a variable radial load from -20kN to 20 kN.

The first validation of the MBS model has been done throughout the usage of the existing experimental results and comparing them to the simulated values obtained with the MBS Model. As shown in Figure 6.4 it can be observed, that the frictional torque obtained in the simulation (black line) when submitted to an axial load of 20 kN is about 5 Nm, where the radial load has a minimal influence on it. This is a similar outcome to the experimentally obtained in the original study at the MEGT chair (black line). It has to be mentioned, that this bearing is a much bigger one, than the one that has been studied afterwards. (d = 70 mm, D = 150 mm; compared to d = 40 mm, D = 80 mm).
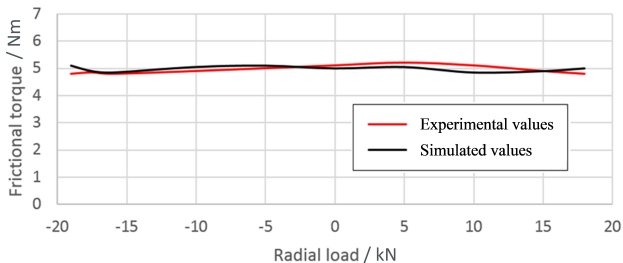

Figure 6.4: Comparison of the experimental and simulated results of the frictional torque for a tapered barrel roller bearing with the main dimensions of a 32314

6.3.2 Prototype

After the initial validation, a deeper validation based on the geometry of the prototype
has been conducted. With this purpose, the prototype, as well as a comparable TRB
32208 have been experimentally tested. The results of these experiments, compared with
its simulation, are shown in Figures 6.5 to 6.10. For all the scenarios under study, the
inner ring was rotating at an angular speed of 2000 rpm, while the outer ring was fixed.
Due to limited temperature control possibilities on the test rig, the lubricant temperature
at 2000 rpm is in the range of 50-60°C.
Figure 6.5 shows the resulting frictional torque for different radial loads at a constant
axial load of 3 kN and 4.5 kN, as well as for different axial loads when the radial load is 0
kN. It can be observed, that the lines of both the experiment and the simulation have the
same tendency for the three different load scenarios. Since the influence that the load has
in the resulting frictional torque can be correctly predicted, it can be affirmed, that the
MBS model used, together with the integrated calculation routines, are suitable.
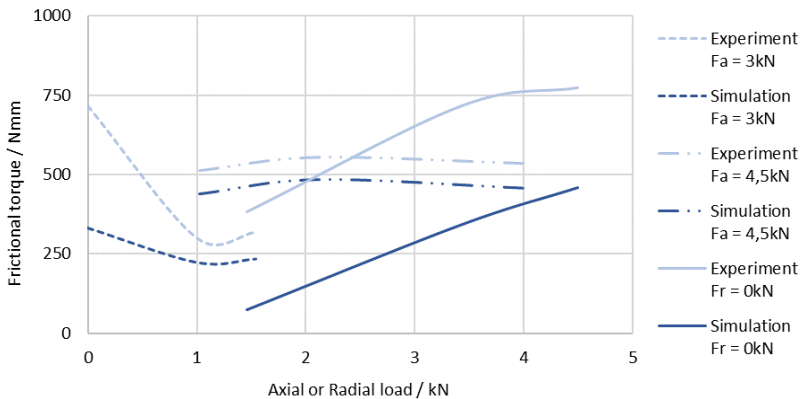
Figure 6.5: Simulation and experimental results of frictional torque for different load
            conditions for the Prototype

At pure axial load (solid line) the curves show an almost linear increase in the frictional
torque with increasing axial load. Given the comparatively lower purely axial load present,
it can be assumed that the drilling friction taking place at the prototype outweigh the other
types of friction (similar to the rib friction of the TRB), being this directly proportional
to the load.
It can also be pointed, that for the line of higher axial load (broken line) the influence
that the radial load has on the frictional torque of the prototype is minimal. This is due

to a reduction in the circumferential load zone when introducing a radial load component compared to pure axial loading. This turns into fewer rolling elements loaded, each of them more loaded in comparison to a pure axial load. However, due to the approximately degressive increase in the frictional torque, the total frictional torque remains at a comparable level or is slightly reduced.

Figure 6.6 shows the totality of the test points for both the prototype (left) and the TRB 32208 (right) at once, independent of the load scenario. The blue points represent the relation between the measured friction torque values and those obtained using the regression models integrated in the developed MBS model. With a perfect model quality, all the values would lie on the bisector, since the measured and the simulated values would be identical. The values of the regression model of the TRB show deviations that do not exceed 20% (dashed lines) for most values. On the other hand, the model of the new geometry underestimates the measurements for most of the test points studied. The deviation from the experimental results varies between 20% and 60% from the simulated frictional torque.

Figure 6.6: Accuracy of the simulation model both for the prototype and the tapered roller bearing for different dynamic bearing load

In order to understand this deviations from the simulation model better, the test points have to be studied in relation to the load scenario. Like this, a tendency might be determined. Figure 6.7 represents the accuracy of the models in terms of its deviation to the experimental results for both the prototype (green line) and the tapered roller bearing (blue line), compared to the dynamic bearing load, P. By this means, similar to the representation in Figure 6.6, it could be assumed that the model is validated when the ratio simulation to experimental results is higher than 0,8. This denotes a model accuracy

of 80%, a deviation assumable considering further uncertainties always to be considered in the experiment.

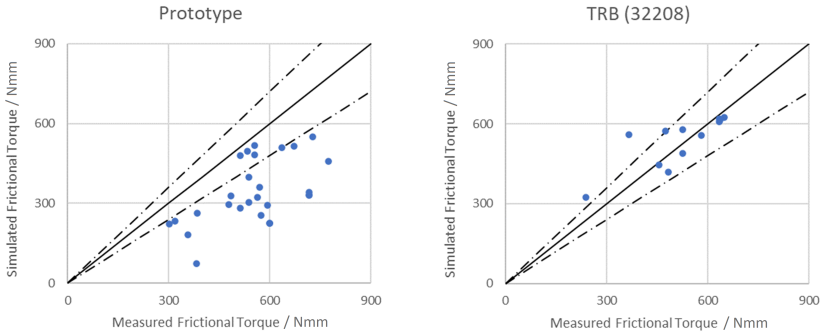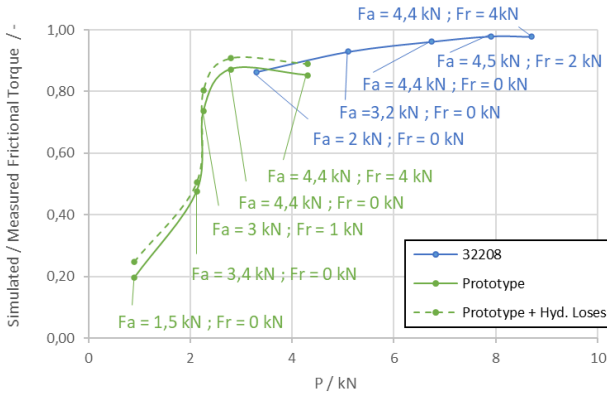Figure 6.7: Accuracy of the simulation model both for the prototype and the tapered roller bearing for different dynamic bearing load

It can be mentioned, that since the prototype has much bigger contact angle than the 32208 bearing (33° to 14°), the influence that the axial load has in the dynamic bearing load is much smaller for the prototype. Although both bearings were submitted to the same load conditions within the experimental tests, the difference of their contact angle turns into much smaller dynamic bearing loads for the prototype. Since the dynamic bearing load depends on both the axial and the radial load, similar values of P have been obtained for different load conditions. In such cases, only one point has been considered in order to represent the tendency of the curve, while the other point of similar P is individually represented. For the TRB model, which has been used for many years and has been deeply studied [Kie17; KS17], we obtain a precision of less than 10% for most of the cases. This percentage decreases with increasing load, since we have a more defined contact situation as well as less sliding in the bearing. This behavior is even more noticed for the prototype, since its model has been designed for high load conditions.

Following the recommendation by the manufacturer of the TRB, a minimum radial load of the order of $P > C_{0r}/60$ is necessary for a proper bearing operation. This turns into a minimum load for the TRB 32208 of 1,56 kN. Assuming that the minimum load required for the geometry of the prototype follows the same equation, a minimum load of 1,56 kN would be necessary for the proper operation of the prototype. According to this assumption, together with the experimental results and ultimately the tendency shown in Figure 6.7, it would be recommended to set the minimum load for the prototype to at least 2 kN.

The notable deviation between the simulation results and the experimental results for the prototype under lower dynamic bearing load could derive from several reasons. As mentioned before, similar to the TRB, the higher the load, the more defined the contact situation is as well as less sliding in the bearing. Deviations can also be attributed, for example, to the lubricant temperature, which cannot be precisely measured. In addition, there is still potential to optimize the model with regard to the consideration of the contact stiffness in order to model the real surface roughness in the simulation. The measured surfaces of the contact partners can be used in a finite element simulation to map the non-linear material behavior. The results can then be used as input variables for the multi-body simulation. Since the geometry of the prototype has not been studied before, it is impossible to know for certain, what is the weight of the hydraulic losses in the total frictional torque, in order to add those into the model. For the TRB model, the hydraulic losses are determined within the calculation routines according to the technical-mathematical approach to calculate the drag and churning losses specifically developed for this type of bearing [LSS16]. This approach has been validated for different types of bearings [Lie18]. In [KLS17], the transferability to rolling bearings with cylindrical rolling elements in a horizontal arrangement has already been shown. Based on this, the present case results exclusively in churning losses that apply to the complete set of rolling elements. Adding this information to the simulation results, a more accurate model (represented in Figure 6.7 by a green broken line) can be obtained for the prototype. The validation of the technical-mathematical approach for the geometry of the prototype is yet to be studied, and will be under consideration for future studies at the MEGT chair.

6.4 Comparison with a TRB

Based on the experimental and simulation results obtained for the prototype and the TRB 32208, the benefits of the new geometry can be quantified.
Figure 6.8 compares the resulting frictional torque of both rolling bearings for the simulation and the experiment with variation of the axial load when purely axial loaded at a speed of 2000 rpm. At two of the three load points, the measurement result for the prototype bearing has a higher value than the TRB. The maximum difference for these values is up to 37%. The reason for this is, that with the comparatively lower purely axial loads present, the drilling friction of the TRB probably outweighs the rib friction of the TRB.

Figure 6.8: Comparison of the frictional torques from the simulations and measurements
with variation of the axial load when no radial load is applied

Figure 6.9 shows the frictional torque for different radial loads at a constant axial load of 4.5
kN, again at 2000 rpm. Except for a radial load of approximately 2 kN, the measurement
results for the prototype are above those of the TRB. Therefore, in terms of frictional
torque, for a load condition of 4,5 kN in the axial direction and 2 kN in the radial direction,
the prototype is a better solution than the commonly used TRB. It is also to be mentioned,
the different equivalent dynamic bearing load P resulting from the difference in the contact
angle between the two rolling bearings. For the prototype, a load condition of 4,5 kN in
the axial direction and 2 kN in the radial direction results into a P of 3,6 kN. On the other
hand, this load conditions results into a P of 8,4 kN for the TRB 32208. In order to affirm
that the prototype is a suitable alternative for this load, other output parameters such as
the pressure distribution have to be analyzed. These boundary conditions are, therefore,
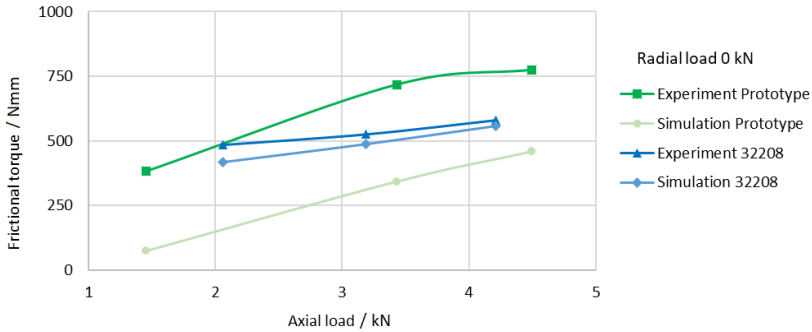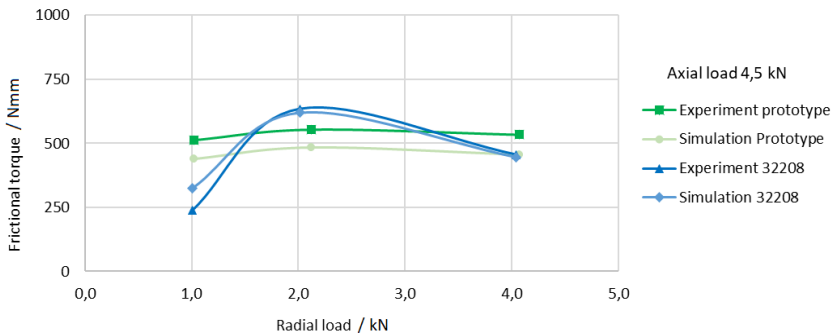the focus of the deeper analysis of the prototype behavior presented in section 7.1.

Figure 6.9: Comparison of the frictional torques from the simulations and measurements
with variation of the radial load when a constant axial load of 4,5kN is applied

Figure 6.10 shows, in logarithmic scale, the frictional torques for the two test bearings and the simulation results at different tilt angles in angular minutes. The tilting takes place in the opposite direction to the direction in which the radial load is applied. With a constant radial load of 2 kN, the axial load varies from 3,8 kN to 4,6 kN between points. The value of the axial force for each point can be seen in the graphic, being the same for both the experiment and the simulation.
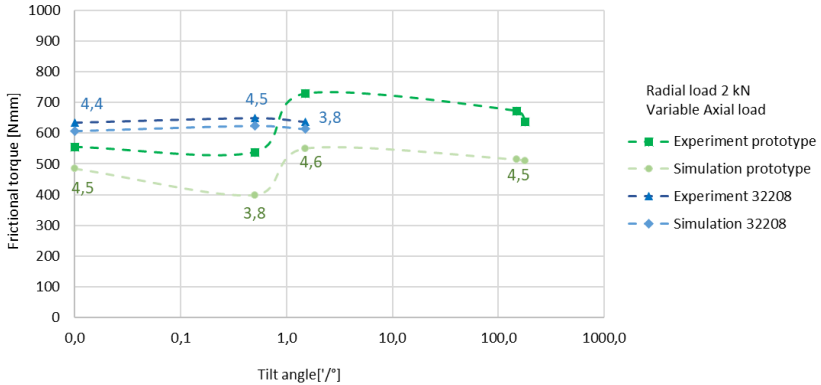
Figure 6.10: Comparison of the frictional torques from the simulations and measurements with variation of the tilt angle

According to the bearing manufacturer, the maximum tilt for a TRB must not exceed 4', which is why the last two test points (corresponding to 0.25° and 0.5° respectively) were only measured for the prototype. When looking at the results, the frictional torques for the TRB are above those of the prototype in two of the three comparable measuring points.

Generally, it should be noted that an increase in the tilt has no noticeable influence on the frictional torque, taking into consideration the differences in the axial load, which were already mentioned. In terms of the validation of the model, the curves represented in Figure 6.10 for the simulation coincide with the experimentally determined values in both amount and course, with an accuracy of 96% for the tapered roller bearing and between 76% and 87% for the prototype.

When considering all the results, it can be seen that the TSRB prototype and the TRB 32208 are on a comparable level with regard to the frictional torque. It should be noted that a comparison is only partially meaningful due to the different pressure angles (Prototype: 33 °; TRB: approximately 14 °). In addition, due to the limited load possibilities given when using the frictional torque test bench, only a limited range of boundary conditions could be experimentally analyzed.

7 Simulation results and application example

In the previous chapter, the MBS model generated for this work was validated. As a reference, only the resulting frictional torque was considered, since it is the output parameter obtained at the frictional torque test bench. Within this chapter, other output parameters obtained from the simulations are studied in order to understand the internal behavior of the rollers and raceways better. Like this, in the first section (section 7.1), output parameters such as the pressure distribution, the velocities and Slide-to-Roll ratio or the axial displacement of the rollers has been obtained and is represented for both the prototype and a TRB 32208.

Based on the results obtained for the prototype, a sensitivity analysis has been conducted and presented in section 7.2. Within the analysis, several key geometrical parameters are varied, and their influence on the rolling bearing behavior studied.

Relying on the information gathered from the simulations performed, a workflow for the optimization of the geometry under study has been developed. The key facts when optimizing the geometry are to maximize the lifetime of the rolling bearing (optimal for a specific load condition) as well as to maximize the PCR of the roller without the need of a rib at the inner ring. For this purpose, the axial displacement of the roller has to be monitored. The workflow is presented and described in section 7.3.

7.1 Prototype

The comparison between the prototype and a TRB 32208 for both the experiments and the simulations have shown several boundary conditions where the prototype showed lower frictional torque than the TRB 32208. The deeper study of other outputs obtained from the simulations focuses on the load scenario of axial load 4,5 kN. Within the validation, Figure 6.9 shows that for this load condition, the prototype behaves similar to the TRB 32208. Specifically for a radial load of 2kN, a lower frictional torque than the one obtained for the TRB 32208 was achieved for both the experiments and the simulations.

Figure 7.1 shows the pressure distribution at the outer ring for the load scenario mentioned before: axial load 4,5 kN and varying radial load. It is to be mentioned, that the slice 1, on the left side of the graphic, represents the side of the roller with the biggest diameter, which is the right side of the roller in Figure 4.11.

The three different lines for the prototype (in green) and the TRB 32208 (in blue) represent

the three radial loads of 0kN, 2kN and 4kN. Here shall be again mentioned, that the middle line of 2kN radial load has shown less frictional torque for the prototype than for the TRB 32208.

For the TRB 32208, a pressure distribution along the majority of the contact length can be observed. The length of the contact, as well as the maximum pressure, slightly increases when the radial load is increasing. On the other hand, for the prototype, there are two pressure peaks which are focused on the two contact points between the roller and the raceway of the outer ring. Because of this pressure concentration, the increment of both the contact length and the maximum pressure, when increasing the radial load, is more substantial.

In terms of the influence of the pressure in the life time of the rolling bearing, the pressure distribution shown by the prototype has a negative impact, since it is not as equally distributed as for the TRB 32208. Furthermore, the peak of the maximum pressure is bigger for the prototype than for the TRB 32208 for the three load conditions under study.
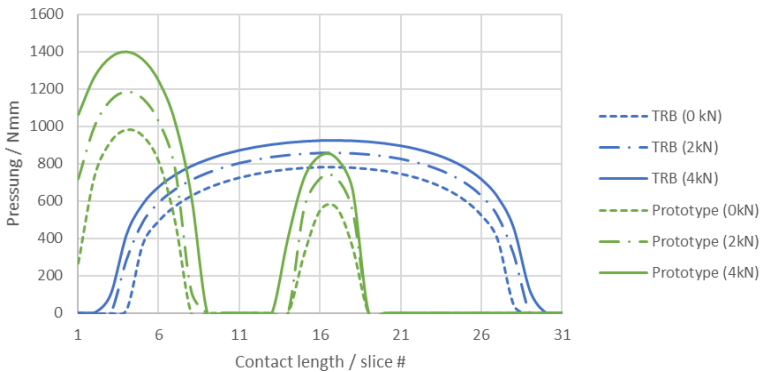
Figure 7.1: Pressure distribution on the outer ring along the contact length for the Prototype and a TRB 32208 when submitted to an axial force of 4,5kN and variable radial force

The increase in the contact length when increasing the radial force is represented in Figure 7.2 for both rolling bearings. The different course followed by the resulting frictional torque for both rolling bearing types when increasing the radial load represented in Figure 6.9 is the combination of several aspects.

On one side, the reduction in the circumferential load zone when introducing a radial load component compared to pure axial loading.

On the other side, the variation of the length of the contact loaded, which significantly

increases for the prototype from a pure axial load (with 35% of the contact length loaded) to 2kN radial load (with 50% of the contact length loaded) and remains almost constant from that point on. The contact length for a TRB 32208 remains constant from a pure axial load to an axial load of 2kN (with 80% of the contact length loaded), when loading up to 5kN in the radial direction is when a significantly increase in the length can be observed (with 88% of the contact length loaded).
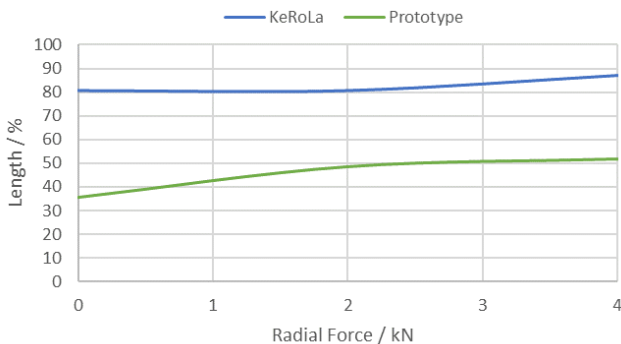
Figure 7.2: Variation of the length of the contact loaded for the Prototype and a TRB
            32208 when varying the radial force under a constant axial force of 4,5 kN

The significant difference in the loaded length affects the carrying capacity of the rolling bearing as well. As shown in equations 2.10 and 2.14, the load ratings of the rolling bearing are directly proportional to the effective roller length L_{we}, which is the length of the roller that is loaded. Therefore, the load ratings of the prototype will be reduce in between 50% and 65% of the calculated ratings listed in Table 6.2, where it is assumed for the total length to be loaded.

Figure 7.3 represents the ratio P/C for both rolling bearings for the three load scenarios considered. Although the resulting equivalent dynamic load P is different for both rolling bearings because of the difference in the contact angle (33° for the prototype and 14° for the TRB 32208), the decrease in the dynamic load rating C for the prototype turns into a similar ratio P/C for both rolling bearings.

The combination of these parameters (resulting circumferential load zone, effective roller length, and ratio P/C) for the different load scenarios results into a lower frictional torque for the prototype than for the TRB when loading with 4,5kN in the axial direction and 2kN in the radial direction.
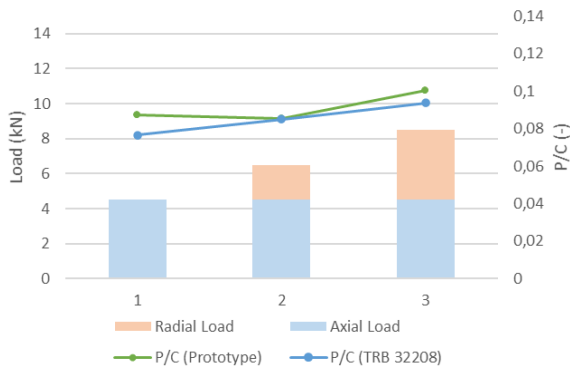
Figure 7.3: P/C ratio for the prototype (green) and a TRB 32208 (blue) for the three load scenarios under study

The relation between the velocities of the rollers and the raceways has been studied as well in order to obtain the Slide-to-Roll ratio (SRR) of the two bodies in contact and with it a description of the slip condition presenting at the contact. Figure 7.4 represents both the summation u_0 and the difference u_{rel} of the circumferential velocities.
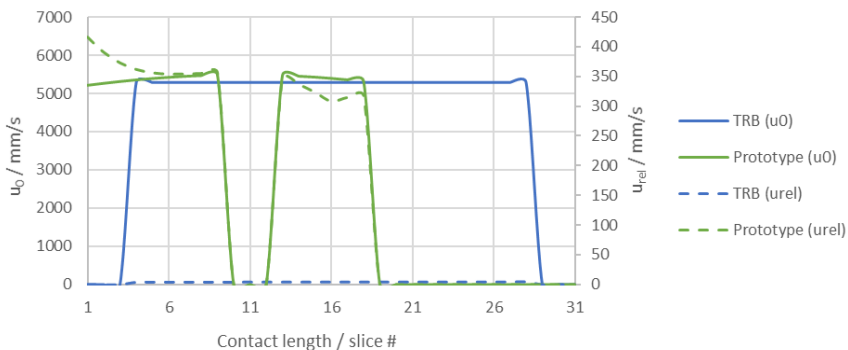
Figure 7.4: Summation (u_0) and difference (u_{rel}) of the circumferential velocities of the roller and the outer ring raceway along the contact length for the Prototype and a TRB 32208 when submitted to an axial force of 4,5kN and a radial force of 2kN

With these two parameters of velocities, the SRR can be obtained following equation (2.25) as the ratio between them. Figure 7.5 shows the resulting SRR for both rolling bearings along their contact length. According to the definition of the SRR made in section 2.3.1, a

$SRR = 0$ represents a pure rolling movement, while a SRR in between 0 and 2 represents a sliding-rolling movement. The bigger the SRR value is, the bigger the sliding friction. Therefore, it can be seen, that the sliding occurring for the prototype (right vertical axis) is bigger than for the TRB 32208 (left vertical axis), represented in a scale 100 times smaller. Furthermore, for the prototype, the sliding friction increases when moving away from each contact point. As shown in Figure 7.1 for the pressure distribution, the contact points lay at slices 4 and 16. The resulting sliding friction is, together with the drilling friction, a factor affecting the resulting higher frictional torque for the prototype. However, the sliding friction has in comparison less of an influence than the rolling and the drilling friction.
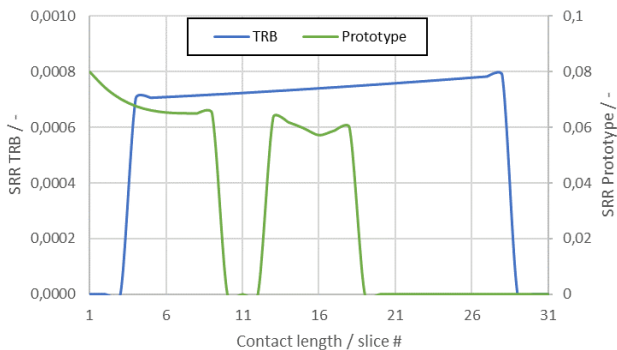
Figure 7.5: Resulting Slide-to-Roll ratio for a TRB 23308 (left axis) and the Prototype (right axis) along the contact length on the outer ring when submitted to an axial force of 4,5kN and a radial force of 2kN

7.2 Sensitivity Analysis

In order to analyze the influence that the geometrical parameters described in section 2.1.2 have on the output parameters of the simulation, a sensitivity analysis has been conducted. For this purpose, a TRB 32208 (blue for each diagram) and a reference bearing (green for each diagram) based on the geometry under study will be compared with several geometries. Within these geometries, based on the reference geometry, a specific parameter has been varied.

In the first four subsections (sections 7.2.1, 7.2.2, 7.2.3 and 7.2.4), the influence that the parameters PCR of the roller, contact angle α, osculation κ and the location of the contact points have on the main outcomes frictional torque and maximum pressure is studied and presented for six different load scenarios. Afterwards, in the last subsection of this chapter

(section 7.2.5), several dependencies and outcomes are studied. These are: the resulting axial displacement of the roller, the resulting frictional torque when increasing the axial load up to 40kN and the influence of the angular velocity.

The parameters defining the reference bearing are listed in Table 7.1. The selection of these parameters is based on several features:

- In order to have a better comparison between the TRB 32208 and the reference bearing, the parameters B, D_{pw}, L_{pw}, r, R and Z as well as a contact angle α and the resulting taper angle γ of a TRB 32208 have been chosen (see Table 4.2). By selecting the contact angle α, the load angle will have a similar influence in the behavior of both bearings.

- The location of the contact points (defined by the parameters aP and aPk) is chosen in such a way, that the contact points are centered along the contact line. This means a value for the parameters of: $aP = L_{we}/2$ and $aPk = (L_{we} - aP)/2$.

- The PCR_R of a toroidal roller bearing is considered an upper limit in terms of the axial load that the roller-raceway contact is able to absorb. Therefore, the PCR_R of the reference bearing is chosen smaller than the one of a CARB 2208. By this means, the PCR_R of a CARB 2208 (see Table 4.2) can be studied as a bearing with increased PCR_R in comparison with the reference bearing.

- The osculation s is chosen from the value of a CARB 2208 (see Table 4.2).

Table 7.1: Parameters defining the geometry of the reference bearing

Parameter	Description	Reference bearing
α	Contact angle	14°
γ	Taper angle	2,39°
aA	Distance from the bearing axis to the center of the PCR_R	62 mm
aP	Distance between contact points	8,5 mm
aPk	Distance from contact point to the edge	4,25 mm
B	Rolling bearing width	24,75 mm
D_{pw}	Pitch diameter	60 mm
L_{we}	Roller length	17 mm
PCR	PCR_R	100 mm
r	Rolling bearing bore radius	20 mm
R	Rolling bearing outside radius	40 mm
κ	Osculation	0,95
w	Calculation angle	2,5°
Z	Number of rollers	17

Table 7.2: Variations of key parameters based on the reference bearing considered for the sensitivity analysis

Parameter	Ref. Bearing	↑	↑↑	↓	↓↓	Unit
PCR_R	100	122,5	250	36	28	mm
α	14	18		10		°
κ	0,95	0,99		0,90		-
aP	8,5	10		7		mm
aPk	4,25	5,5		3		mm

The variations of the key parameters considered for the sensitivity analysis are enumerated in Table 7.2. It has to be mentioned, that only one parameter has been changed at a time, either to be increased or decreased in comparison with the reference bearing. The load scenarios considered for this analysis (bars), together with the corresponding ratio P/C for both the TRB 32208 (blue line) and the reference bearing (green line), are shown in Figure 7.6.

Similar than for the prototype, a reduction on the length of the contact loaded L_{eff}, reduces the resulting dynamic load rating C. Depending on the load condition, the effective contact length L_{eff} varies for the reference bearing between 74% and 77% of the total length of the roller L_{we}, while for the TRB 32208 this variation goes from 80% to 93%. On the other hand, the equivalent bearing load P is the same for both rolling bearings, since the contact angle defining the geometry is the same: $\alpha=$ 14°. Because of this, the resulting ratio P/C is bigger for the reference bearing than for the TRB 32208.
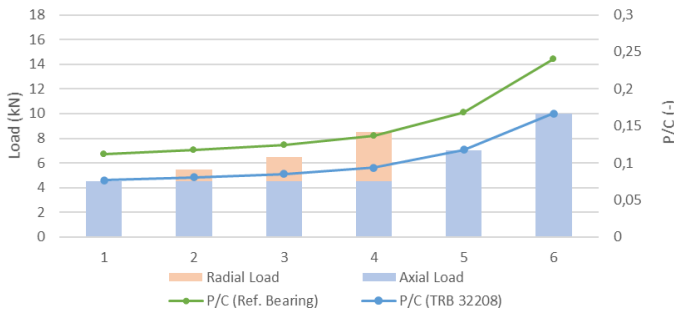
Figure 7.6: Load scenarios considered for the sensitivity analysis and the resulting ratio P/C for both rolling bearing types

7.2.1 PCR of the roller

When varying the PCR of the rollers, their crowning changes, affecting the resulting axial displacement of the roller. When increasing the PCR, a flatter roller results, increasing its axial displacement. This behavior, explained in Figure 2.8 is due to the fact that the angle between the acting axial load and the roller surface absorbing this load is decreased. On the other hand, when decreasing the PCR of the roller, a more crowned roller results, which increases the drilling friction and in turn the total resulting frictional moment.

For the geometry under study, a PCR_R of 36 mm ($\downarrow$) results into a parameter $aA = 0$ according to Figure 4.11. This means, that the distance between the bearing axis (BA) and the axis of the center of curvature (PA) is zero. Furthermore, a PCR_R of 28 mm ($\downarrow\downarrow$) results into a negative distance between the two axes.

The resulting frictional torque for the TRB 32208 (blue bars), the reference geometry (green bars) and the PCR_R variations is shown in Figure 7.7. As expected, compared to the reference bearing, an increase in the PCR_R (grey bars) turns into a reduction of the resulting frictional torque. On the other hand, a decrease of the PCR_R (yellow bars) turns into an increased frictional torque because of the rise of the drilling friction.
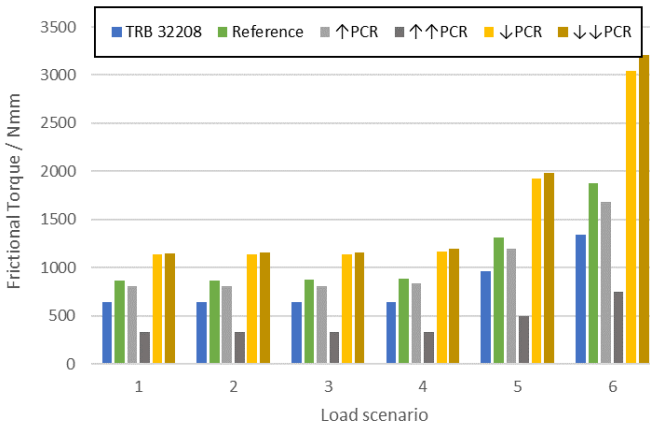
Figure 7.7: Frictional torque for the different load scenarios and rolling bearings when varying the PCR as described in Table 7.2

When looking at the resulting maximum pressure when varying the PCR_R (Figure 7.8), the pressure peaks occurring for the geometries with increased PCR_R stand out (*). These peaks result from the stress concentration in the edge area consequence of a notable axial displacement of the roller and the corresponding relocation of the contact points near the

edge of the roller. These stress peaks would have a decisive influence on the load-bearing capacity and the service life and have to be therefore avoided.
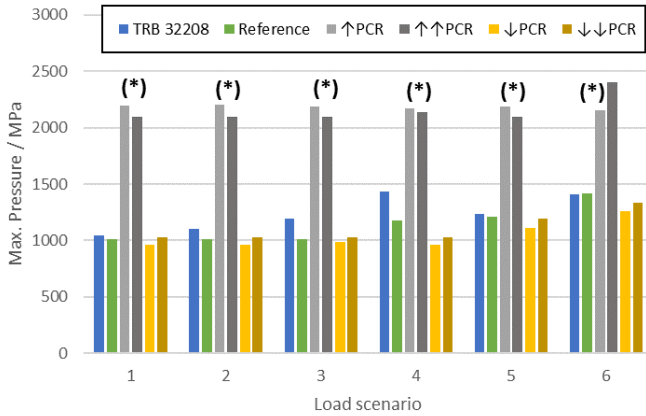
Figure 7.8: Maximum pressure for the outer ring for the different load scenarios and rolling bearings when varying the PCR (* Pressure peaks due to an stress concentration in the roller edge) as described in Table 7.2
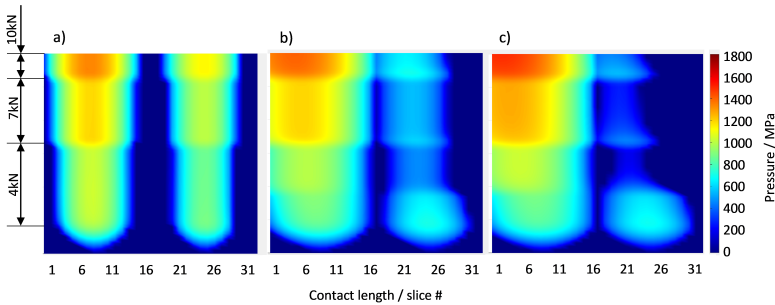
Figure 7.9: Outcome axial displacement for a bearing with a smaller $\downarrow PCR_R$ (a), the reference bearing (b), and one with a bigger $\uparrow PCR_R$ (c) when submitted to an increase in the axial load from 4kN to 7kN and finally 10kN

The resulting axial displacement for different PCR_R is illustrated in Figure 7.9. An increment in the axial displacement of the rollers, when increasing the PCR_R can be observed. This displacement is bigger when increasing the load (along the vertical). Furthermore, the higher the load is, the higher the pressure and longer the loaded length is. The axial displacement of the roller changes the original location of the contact points (displacement of the pressure peaks along the horizontal). The pressure peak resulting

from the approximation of the contact point to the roller edge can be noticed both on the reference bearing (b) and more pronounced on the bearing with $\uparrow PCR_R$ (c).

The geometry with a $PCR_R = 36mm$ ($\downarrow PCR_R$), this is a distance between the bearing axis (BA) and the axis of the center of curvature (PA) of zero ($aA = 0$), turns into a reduction of the maximum pressure (Figure 7.8). Whereas, on the other hand, a reduction of the PCR_R turning into a negative distance aA between the two axes ($\downarrow\downarrow PCR_R$) results into a reduction of the maximum pressure compared to the reference bearing, but an increase compared to the bearing with $PCR_R = 36mm$.

Conclusion   With the ultimate goal of reducing the frictional torque, the PCR_R has to be increased. Nevertheless, there is a limit on this reduction based on the axial displacement of the roller and the location of the contact points. The location of the contact points will be affected by the axial displacement. By this means, resulting stress peaks due to the proximity of the contact points to the roller edge have to be avoided. Furthermore, if the axial displacement is too big, a rib contact would be needed in order to absorb the resulting axial forces that the roller-raceway contact is not able to absorb on its own. The need of a rib, and its resulting frictional torque has to be avoided in order to reduce the overall resulting friction.

Although the levels of maximum pressure of the reference bearing are comparable to a TRB 32208, increasing the PCR_R would as well increase its maximum pressure. This parameter has to be monitored and maintained at the same order of magnitude than the one of a TRB 32208. Like this, a similar resulting lifetime and carrying capacity can be expected.

The maximum pressure occurring at the TRB 32208 is more influenced by an increase of the radial load (from load scenario 1 to 4), than the reference bearing. This is because the maximum pressure obtained for the reference bearing is already affected by a stress concentration of the roller edge (see Figure 7.9.b). The increase on the contact length when increasing the load, an effect more accentuated for the new geometry under study, has also an influence on the resulting maximum pressure.

7.2.2 Contact angle

A study of the influence of the contact angle α for the different load scenarios is shown in Figure 7.10 and Figure 7.11. The variations in the results are directly related to the resulting contact length, which is represented in lines in Figure 7.10. An increase in the contact angle α (grey) results into a reduction of the contact length L_{eff} from 75% of the total length of the roller L_{we} for the reference bearing, to around 45% for the bearing with bigger contact angle. This, in turn, reduces the frictional torque around 25%. On

the other hand, the load carrying capacity of the rolling bearing decreases significantly. Similarly, a reduction of the contact angle α (yellow) increases the contact length of up to 90% of the total length of the roller L_{we}, values even bigger than for the TRB 32208. This, therefore, increases both the frictional torque as well as the load carrying capacity. Furthermore, it can be seen that, as expected, the influence of the axial force is bigger, the smaller the contact angle is (Load scenarios 1, 5 and 6), while the influence of the radial load is minimal for all cases studied (Load scenarios 1, 2, 3 and 4).
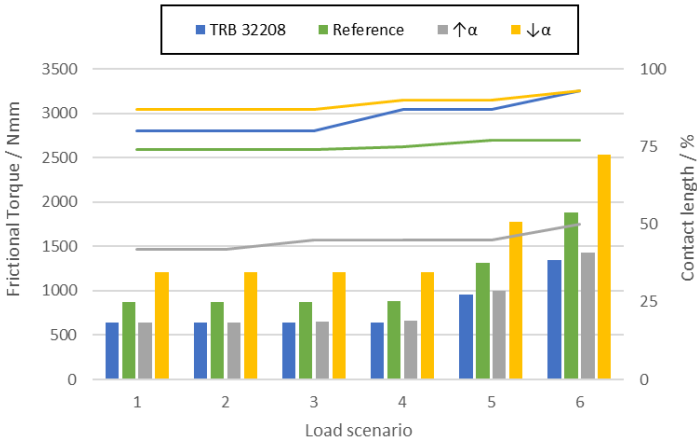
Figure 7.10: Frictional torque (bars) and contact length (lines) for the different load scenarios and rolling bearings when varying the contact angle as described in Table 7.2

Figure 7.11: Maximum pressure for the outer ring for the different load scenarios and rolling bearings when varying the contact angle as described in Table 7.2

The resulting maximum pressure, represented in Figure 7.11, is not that affected by changes on the contact angle as the frictional torque is. In terms of its dependency with the applied load, it is directly proportional to the axial load (Load scenarios 1, 2, 3 and 4). On the other hand, the influence that the radial load has on the resulting maximum pressure (Load scenarios 1, 2, 3, 4) is much more related to the contact angle, having a smaller influence for cases with bigger contact angle.

Conclusion   The contact angle α of the rollers directly affects the resulting effective length L_{eff} and therefore the carrying capacity of the rolling bearing. It has to be chosen based on the application and load condition, in a way that both the carrying capacity and ultimately the lifetime can be comparable to the ones of a TRB of same main dimensions.

7.2.3 Osculation

The osculation between the roller and the raceway defines how narrow or wide the roller-raceway contact is (see equation (2.7). Furthermore, it has a direct impact on the length of the contact between the rollers and the inner and outer ring (see Figure 2.9). Moreover, the length of the contact area directly influences the resulting frictional torque and the maximum pressure at the contact. This behavior can be observed for both the resulting frictional torque (Figure 7.12) and the maximum pressure (Figure 7.13).
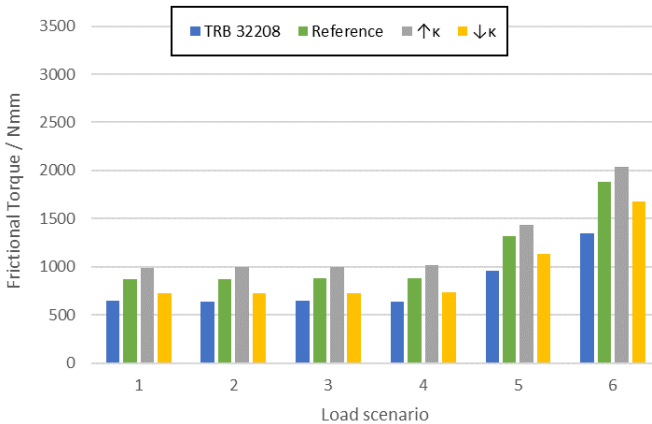
Figure 7.12: Frictional torque for the different load scenarios and rolling bearings when varying the osculation as described in Table 7.2
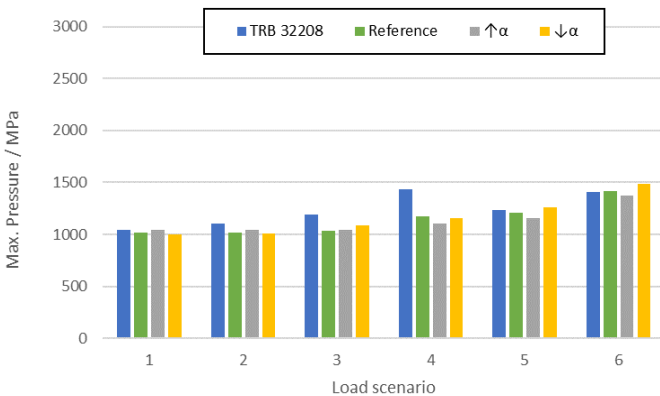
Figure 7.13: Maximum pressure for the outer ring for the different load scenarios and rolling bearings when varying the osculation as described in Table 7.2

Like this, a narrower osculation ($\uparrow \kappa$, grey bar) turns into a bigger contact length and, therefore, higher frictional torque and lower maximum pressure. On the other hand, a wider osculation ($\downarrow \kappa$, yellow bar) turns into a smaller contact length and, therefore, lower frictional torque and bigger maximum pressure.

Conclusion   The osculation has a direct impact on the length of the contact and therefore the frictional torque and maximum pressure. Although it is a successful approach to regulate these two output parameters, the contact length significantly affects the load carrying capacity as well. The goal of this work is to search for a substitute for TRBs maintaining their high carrying capacity. Therefore, the contact length (effective roller length L_{we} for the calculation of the load ratings) has to be chosen in order to obtain a resulting carrying capacity comparable to the one of a TRB of same main dimensions.

7.2.4 Contact points location

The location of the two contact points is defined via two parameters: aP defines the distance between the points and aPk the distance from one point to the roller edge (see Figure 4.11). The outcome when varying the distance between points is represented in Figure 7.14 for the frictional torque and Figure 7.15 for the maximum pressure. It has to be mentioned, that when varying the distance between points aP, the distance from one point to the roller edge aPk has been accordingly changed in order to obtained centered contact points along the roller length (following equation (4.3)). By this means, an increase of the distance between points $\uparrow aP$ up to 10mm results into a distance to the

edge $aPk = 3,5mm$. Likewise, a reduction of the distance between the points $\downarrow aP$ up to 7mm results into a distance to the edge $aPk = 5mm$.

The influence that the distance between contact points aP has on the resulting frictional torque and maximum pressure is smaller compared to the influence that other geometrical parameters have on them. However, when choosing its value, the resulting pressure distribution has to be considered in order to avoid pressure peaks and ultimately increase the carrying capacity and lifetime of the rolling bearing.

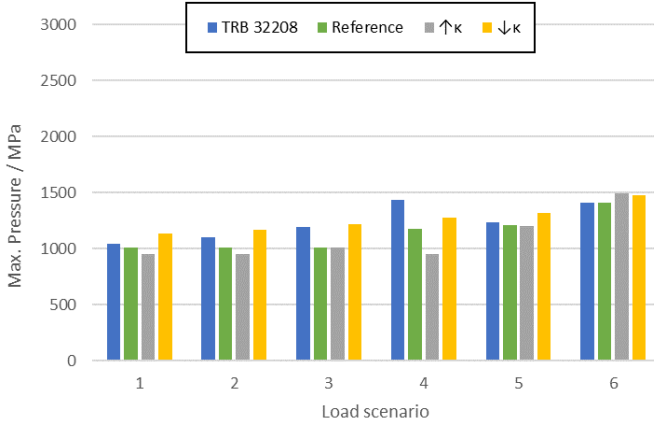Figure 7.14: Frictional torque for the different load scenarios and rolling bearings when varying the distance between points aP as described in Table 7.2

Figure 7.15: Maximum pressure for the outer ring for the different load scenarios and rolling bearings when varying the distance between points aP as described in Table 7.2

Furthermore, as mentioned by JACOB in [Jac92; Jac08], the position of the contact points are preferably to be selected in such a way that the angle which they form with respect to the central plane of the roller is bigger than 7°. By this means, the four contact points are laying outside the self-locking area, whereby the jamming of the rolling elements is excluded. With the variation of the parameter aP and consequently aPk, the angle mentioned by JACOB varies from 7,8° to 10,2°.

The results regarding the variation of the distance from one point to the edge aPk are represented in Figure 7.16 for the frictional torque and Figure 7.17 for the maximum pressure. In order to understand the results better, the pressure distribution along the contact length for the reference bearing has to be analyzed (Figure 7.9.b). If the contact points of the reference bearing are moved to the left of the figure ($\uparrow aPk$), the contact length would be decreased and the maximum pressure increased due to the stress concentration on the roller edge. On the other hand, if the contact points of the reference bearing are moved to the right of the figure ($\downarrow aPk$), the contact length would be increased and the maximum pressure due to the stress concentration on the roller edge decreased. This behavior can be observed at the resulting frictional torque and maximum pressure. By this means, a variation of $\uparrow aPk$ results into lower frictional torque and higher maximum pressure (edge stress concentration). Likewise, a reduction on its value $\downarrow aPk$ results in a higher frictional torque and lower maximum pressure.
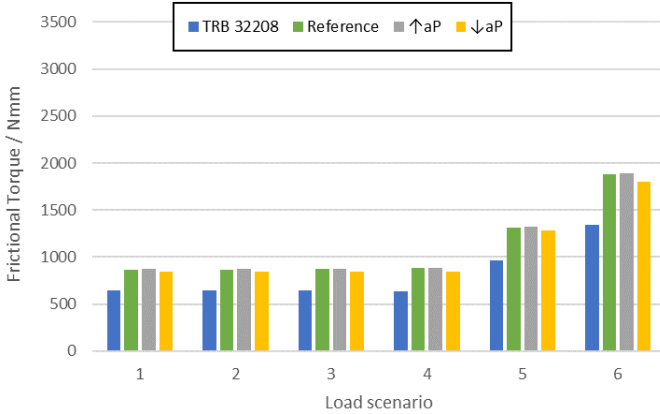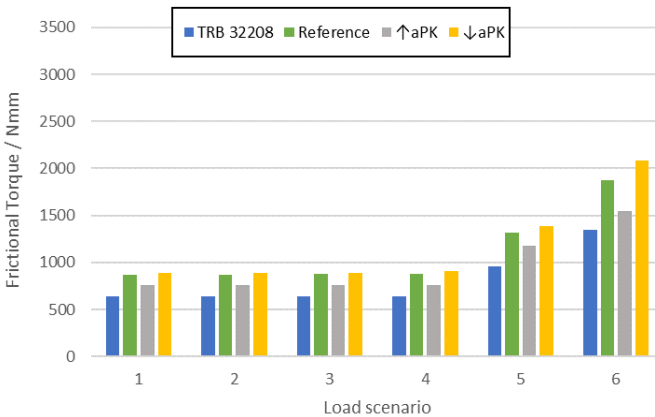

Figure 7.16: Frictional torque for the different load scenarios and rolling bearings when varying the distance from one point to the edge aPk as described in Table 7.2
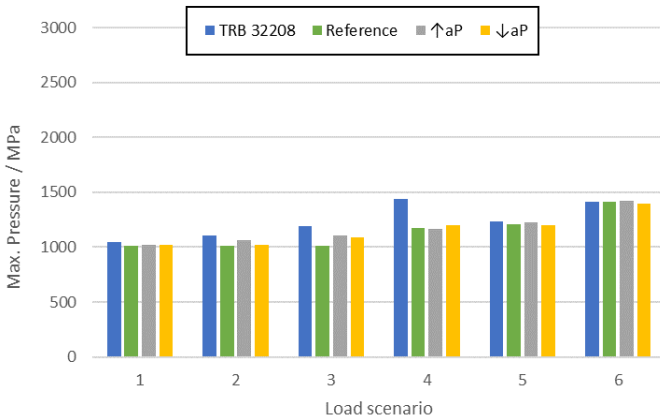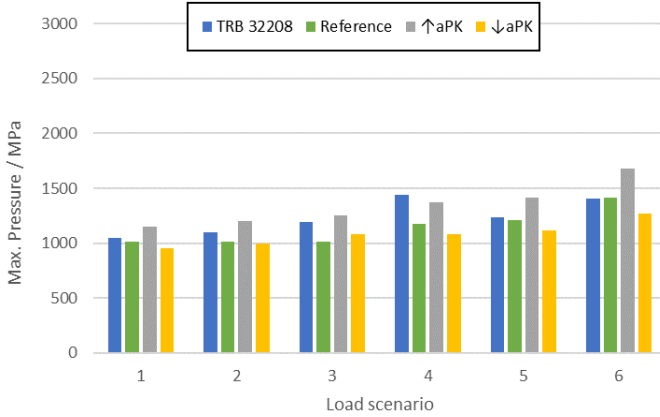
Figure 7.17: Maximum pressure for the outer ring for the different load scenarios and rolling bearings when varying the distance from one point to the edge aPk as described in Table 7.2

Conclusion The location of the contact points directly affects both the contact length and the axial displacement of the roller. It has to be chosen in a way that stress concentrations on the roller edge are avoided and, at the same time, the contact length is maximized in order to maximize the load carrying capacity. Although the distance between the contact points aP has a small influence on the resulting frictional torque and maximum pressure, its value has to be chosen accordingly to the rest of the parameters in order to obtain an even distribution of pressure and avoid stress concentrations at the roller edge. The distance from one contact point to the edge aPk has, in comparison to the distance between contact points aP, a bigger influence on the frictional torque and maximum pressure.

7.2.5 Dependencies

Beside the influence the key geometrical parameters are having on the main outputs frictional torque and maximum pressure, additional dependencies have to be considered and studied. Within this section further results will be analyzed. These are: the resulting axial displacement of the roller, the resulting frictional torque when increasing the axial load up to 40kN and the influence of the angular velocity.

Axial displacement An overview of the axial displacement taking place for different geometries when increasing the axial load is shown in Figure 7.18. Because pure axial load is applied, the rolling bearings are only displaced on the axial direction. A negative axial

displacement is considered when the roller shifts in the same direction than the axial force which is applied. In these terms, a positive axial displacement turning into the need of a rib, has to be avoided.

In discontinuous lines we can see the example of TRB with different profiles of roller according to TONG and HONG [TH17]. The roller of this study has the same main dimensions as the TRB 32208. In regards to the TRB, TONG and HONG observed that the axial displacements of all the TRBs increase almost linearly with the increase of the axial preload, with approximately the same slopes of the lines. This further implies that the same amount of added axial preload results in the same induced axial displacements regardless of the roller profiles. Furthermore, the more length of the roller is crowned, the bigger the resulting axial displacement is.
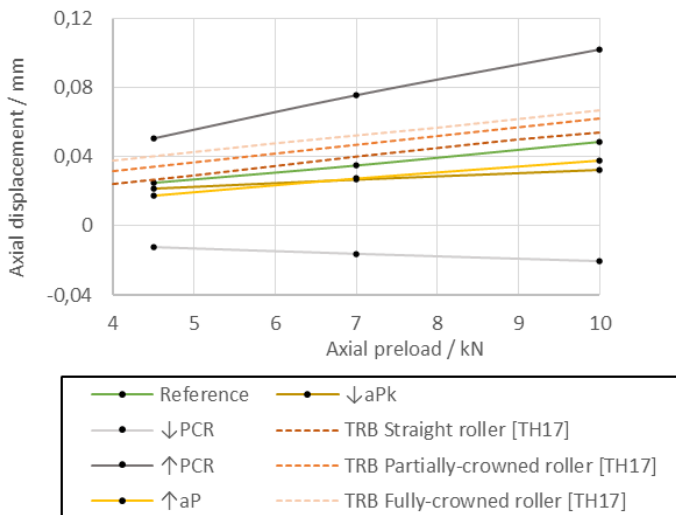
Figure 7.18: Resulting roller axial displacement when increasing the axial load for different geometries as well as different roller profiles of TRB according to [TH17]

For the new rolling bearing geometry under study, the resulting axial displacement is highly influenced by the PCR. This behavior is as well observed in the pressure distribution represented in Figure 7.9. The axial displacement shown for the reference bearing (green line) has a similar value and progression as the TRB with straight roller. When reducing the PCR (light grey line), the angle between the acting axial load and the roller surface absorbing this load is increased. Therefore, a smaller axial displacement (negative) is obtained. On the other hand, the high positive axial displacement observed for the geometry with $\uparrow PCR$ (dark grey line) results from reducing the angle between the acting axial load and the roller surface absorbing the load. This high axial displacement can lead

to instabilities on the dynamic behavior of the rolling bearing, ultimately resulting into the disengagement of the roller from the raceways.

The location of the contact points can be modified in order to reduce the axial displacement of the roller. In these terms, an increase of the distance between points aP (yellow line), as well as a reduction of the distance from one point to the roller edge aPk (brown line) turns into a diminution of the axial displacement of the roller. Furthermore, a smaller aPk significantly reduces the influence that the axial preload has on the axial displacement of the roller.

Angular velocity For all the simulation results presented before, the angular velocity was always set at 2000 rpm. However, depending on the application, this value might change. As an example, the wheel bearing of a passenger car would turn at approximately 1000 rpm for example when driving at 120 kmh. Therefore, the influence that the angular velocity has on the behavior of the rolling bearing has to be studied as well. Figures 7.19 and 7.20 represent the resulting frictional torque and maximum pressure for a TRB 32208 (blue) and the reference bearing (green) when varying the angular velocity between 1000 rpm (light line), 2000 rpm and 4000 rpm (dark line).
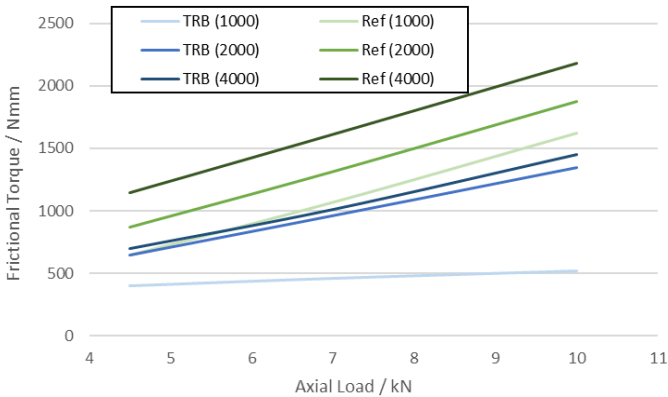
Figure 7.19: Frictional torque for the different load scenarios for the TRB 32208 (blue) and the reference bearing (green) when varying the angular velocity of the inner ring

In Figure 7.19 it can be observed, that the influence that the angular velocity has on the frictional torque is slightly different for the reference bearing and for the TRB 32208. Although for both types of bearings a higher angular velocity turns into higher frictional torques, this increment is different depending on the value of the angular velocity. This way, a much bigger increment can be observed for the TRB than for the reference bearing

when increasing from 1000 rpm to 2000 rpm. Moreover, the increment is much smaller for the TRB than for the reference bearing when increasing from 2000 rpm to 4000 rpm. This is a similar result than the one obtained by KIEKBUSCH when validating the TRB model [Kie17], with a curve frictional torque to angular velocity steeper for a higher axial force. Generally, the influence that the angular velocity has on the frictional torque for the reference bearing does not depend on the value of the angular velocity, where the three lines of the reference bearing a similar distance between them.

In terms of the maximum pressure (see Figure 7.20), the variations of the angular velocity has a minimum influence on the maximum pressure for both rolling bearings under study.
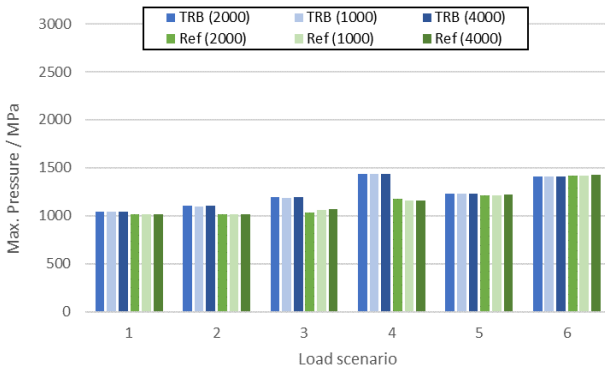
Figure 7.20: Maximum pressure for the outer ring for the different load scenarios for the TRB 32208 (blue) and the reference bearing (green) when varying the angular velocity of the inner ring

Higher load The load scenarios studied for the prototype were restricted due to the limitations of the frictional torque test bench used for its experimental tests. By this means, the maximum load condition studied in sections 6.3, 6.4 and 7.1 was of 4,5 kN on the axial direction and 4 kN on the radial direction.

In section 7.2, the highest load condition studied corresponded to a pure axial load of 10 kN, resulting into a ratio P/C of 0,17 for the TRB and 0,24 for the reference bearing. This is yet far to be consider a high load scenario.

Figures 7.21 and 7.22 represent the tendency of the resulting frictional torque and maximum pressure when increasing the axial load up to 40 kN for a TRB 32208, the reference bearing, as well as different crowning of the roller (PCR). A load condition of pure axial load of 40 kN results into a ratio P/C of 0,67 for the TRB and 0,85 for the reference bearing.
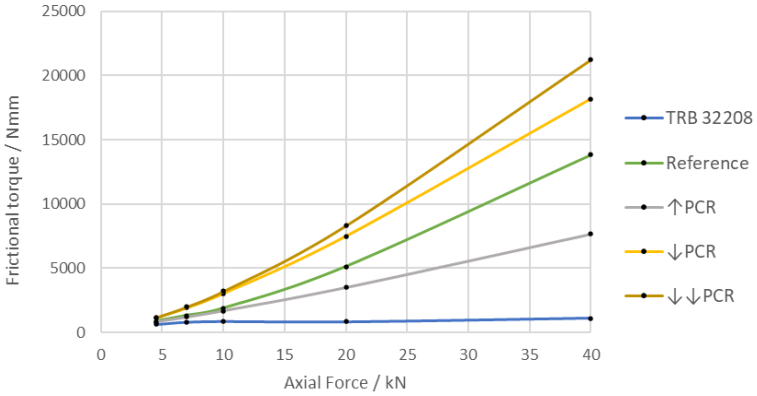
Figure 7.21: Frictional torque for different rolling bearings and higher axial load when varying the osculation at a constant angular velocity of 2000 rpm
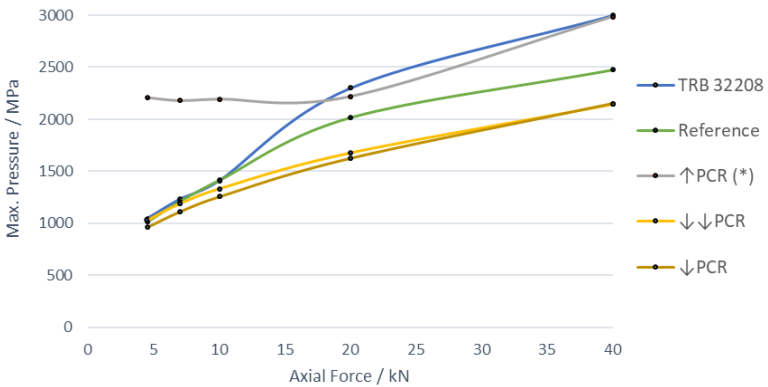
Figure 7.22: Maximum pressure for the outer ring for different rolling bearings and higher axial load when varying the osculation (* Pressure peaks due to an stress concentration in the roller edge)

In Figure 7.21 it can be observed that the resulting frictional torque for the TRB does not vary that much compared to the new geometry under study (650 Nmm for 4,5 kN up to 1100 Nmm for 40kN). Moreover, the tendency for the new geometry (slope of the lines) considerably varies when varying the PCR of the roller. This way, the frictional torque of a more crowned roller ($\downarrow PCR$ and $\downarrow\downarrow PCR$) increases faster when increasing the axial load than a flatter roller ($\uparrow PCR$). In other words, for high loads, the influence that the PCR of the roller has on the resulting friction is much bigger than for lower loads. Furthermore, the optimization of the new geometry in order to achieve a lower frictional

torque than the one obtained with a TRB is more challenging for higher load scenarios. An example of an optimization for higher loads has been studied and presented in section 7.4.1.

For the standard TRB 32208, although the frictional torque increases when increasing the axial load, its fluctuations are too small to be appreciated in this representation.

On the other hand, the resulting maximum pressure (see Figure 7.22) increases faster for the TRB than for the reference geometry, when increasing the axial force. Likewise, in contrast to the frictional torque, the maximum pressure of a more crowned roller ($\downarrow PCR$ and $\downarrow\downarrow PCR$) increases slower when increasing the axial load than a flatter roller. The results for a flatter roller ($\uparrow PCR$) can not be considered because of the pressure peaks occurring due to the stress concentrations in the roller edge.

7.3 Workflow

According to the observed influence of the different parameters on the frictional torque and the maximum pressure, every geometry has to be designed for a specific operational condition. During the optimization, the main goal is to reduce the resulting frictional torque, with a sufficient load carrying capacity, while maintaining a similar pressure compared to TRBs. Furthermore, the pressure distribution along the roller length, the axial displacement of the roller, as well as the effective contact length L_{we} have to be, among others, monitored. The effective contact length L_{we} has to be sufficient to meet the requirements of load carrying capacity, but not exceeded, since a longer length turns into a higher frictional torque.

The process of the optimization, defining the steps to follow, the input parameters to varied as well as the outcomes to monitored are presented in this section. To do so, a workflow for choosing the geometrical parameters defining the geometry for a specific load condition has been developed. A chart of this process is represented in Figure 7.23. The main steps in order to optimize the geometry are:

1. Definition of the load condition of the application

2. Choosing the contact angle α in order to maximize the lifetime by following the diagram represented in Figure 2 or similar: $\alpha = \beta = atan(F_a/F_r)$.

3. Obtaining the dynamic bearing load P following equation (2.12) and based on the axial force F_a, the radial force F_r and the contact angle α.

4. Calculating the required dynamic load rating C in order to obtained the desired lifetime as defined in equation (2.15).

5. Calculating the effective roller length L_{we} based on the previously obtained dynamic load rating C using equation (2.14).

6. Selecting the initial parameters defining the starting geometry which are:

   - The PCR of the roller which has to be maximized in order to minimize the resulting drilling friction. As a reference, the corresponding value for a toroidal roller bearing with similar main dimensions can be selected.

   - The osculation κ which has to be, first of all, maximized in order to find its minimum that results into the required effective roller length L_{we}.

   - The parameters defining the location of the contact points are selected in such a way that they are centered along the roller length. This is following equations (4.2) and (4.2).

7. With the initial parameters chosen, together with the contact angle α previously obtained, a first simulation can be run.

8. The axial displacement of the roller can be obtained and analyzed.

9. According to the obtained axial displacement, it has to be considered whether a rib contact is needed or not in order to absorb the resulting axial force.

10. If the axial displacement is such, that a rib contact is needed, the PCR has to be decreased, a new simulation has to be conducted and the new axial displacement calculated (number 8).

11. If the axial displacement of the roller is admissible (does not affect the stability of the dynamic behavior of the rolling bearing), the pressure distribution has to be analyzed then.

12. If stress concentrations appear at the roller edge, the location of the contact points has to be modified and the new pressure distribution obtained.

13. Based on the pressure distribution along the roller, the length of the contact that is loaded has to be calculated L_{we}.

14. If the effective roller length L_{we} obtained exceeds the requirements calculated at number 5, the osculation κ of the rolling bearing has to be reduced.

15. If the effective roller length obtained L_{we} meets the requirements calculated at number 5 (sufficient L_{we} but not excessively exceed), the optimal solution for minimizing the frictional torque while maintaining the load carrying capacity needed, has been achieved.

Once the optimal geometry has been obtained, the resulting frictional torque and maximum pressure can be calculated. The frictional torque will be the minimum that can be obtained for this geometry and load condition. Depending on the boundary conditions, the resulting frictional torque may still not be lower than the resulting one for a TRB with same main dimensions.

If the frictional torque has been reduced above the one of a TRB, the maximum pressure can be compared afterwards. If the maximum pressure is higher than what is desired, the osculation can be modified again. An increase of the osculation κ will reduce the maximum pressure, but at the same time increase the frictional torque. The osculation κ has to be therefore varied in order to find the compromise between the two output parameters that meet the requirements.
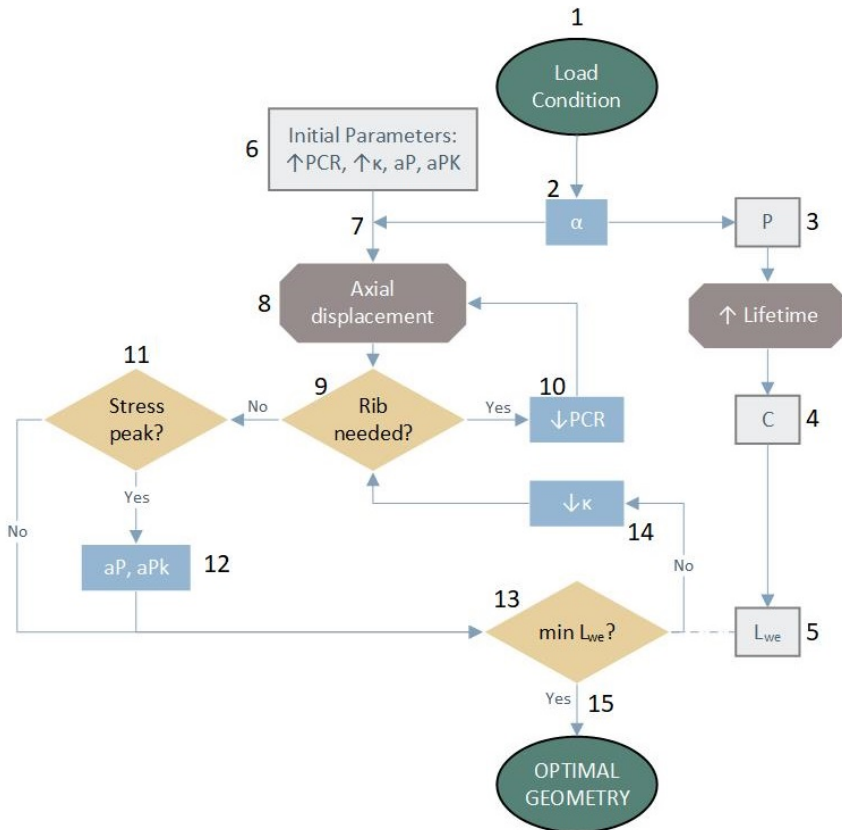
Figure 7.23: Workflow for the optimization of the roller geometry of the new rolling bearing

7.4 Application Example

7.4.1 Fundamentals of differential and pinion bearings

In the powertrain of vehicles, relative speeds between the driven outer and inner curve wheels must be balanced. This task is performed by differential gears. The main bearings of axle drives are subject to very high loads because the entire vehicle power is transmitted via these bearing points in the smallest possible installation space.

Figure 7.24 shows a conventional gear unit for such an application [Sch21]. Two bearing arrangements using either tandem angular contact ball bearings (upper half, green) or tapered roller bearings (bottom half, red) can be seen. On the left, the pinion bearings of the input shaft are designed in an O-arrangement. This rolling bearings are mainly subjected to an axial load. On the right, the differential bearings of the shaft system with the two outputs are designed in a X-arrangement. A clear source of frictional loss has been identified in the bearing arrangement using tapered roller bearings. The bearing power loss is generally lower for the differential bearings versus the pinion bearings [Mer19].
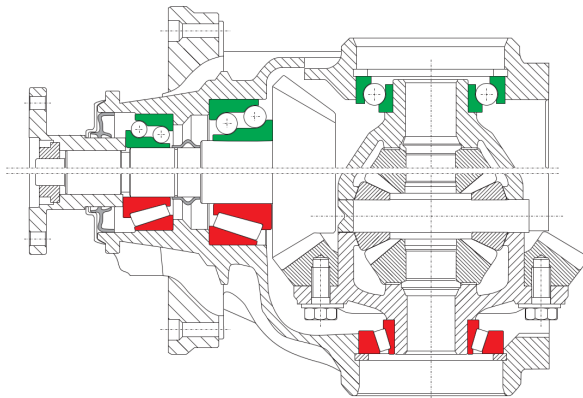
Figure 7.24: Wheel drive differential with conventionally used TRB (upper half) and tandem angular contact ball bearings (bottom half) to improve the driveline efficiency. [Sch21]

With the introduction of tandem angular contact ball bearings, the frictional losses could be significantly reduced. Tandem angular contact ball bearings have been successfully used as an alternative to tapered roller bearings for several applications, including the axle gear of passenger cars. This bearing, compared to a TRB, has the advantage of considerably less friction losses [Pla11; Boh12; Sch21].

In another comparative study on such a gear unit, the decrease in the preload of the pinion

shaft in a system with tapered roller bearings is examined in more detail. Here, a significant decrease in the preload is observed during a running-in process. It is assumed that this is caused by smoothing of the contact points at the roller-rib contact. Furthermore, the same elaboration confirms that the use of tandem angular contact ball bearings can lead to a significant increase in efficiency due to a point contact instead of a line contact between rolling elements and raceways in such a gear. However, it is noted that this effect decreases with increasing torque on the pinion shaft [Pet04].

Ball bearings have, however, the disadvantage of less carrying capacity than TRB. Therefore, although it is a better solution in case of passenger cars, its load rating is insufficient to be used in highly loaded rolling bearings, such as heavy-duty trucks.

As an application example, a pinion bearing for heavy truck commercial vehicles has been considered and studied. With the goal of decreasing the high frictional losses resulting in the pinion bearing, the new rolling bearing geometry has been optimized for this specific application. In section 7.4.2, the rolling bearing technical data of a commonly used TRB for pinion shafts in commercial vehicles is presented. Furthermore, the boundary conditions of this application are listed. In section 7.4.3, the optimization of the new rolling bearing geometry for this specific application, based on the workflow defined in section 7.3, is conducted.

7.4.2 Boundary conditions

A commonly used tapered roller bearing as pinion bearing for commercial vehicles is the TRB 31313-A. Its main dimensions and dynamic load are listed in Table 7.3.

In [Mer19] Merckling studied the loads and speeds representing the most typical working conditions of a pinion TRB for heavy truck commercial vehicles. Based on these, he established the key load conditions most significantly impacting the weighted life and weighted power loss. Based on his founding, the boundary conditions that will be studied for the pinion bearing are:

- Axial load: 15-60 kN

- Angular velocity: 550-1600 rpm

For the purpose of the optimization of the new rolling bearing geometry, intermediate values have been chosen. Like this, the parameters used for its optimization based on the workflow presented in section 7.3 are 35 kN axial load and 1100 rpm.

In [Mer19] Merckling presented the resulting frictional torque when running under such boundary conditions as well. However, he did not explain the lubricant conditions used within his study in detail. Therefore, as a starting point, the lubricant conditions of the simulation will be varied in order to obtain a similar frictional torque like the one obtained

by MERCKLING for 35 kN and 1100 rpm. These parameters, together with the material parameters are listed in Annex A.1.2. A comparison of the frictional torque obtained with the MBS Model and the measured results obtained by MERCKLING is shown in Figure 7.25.
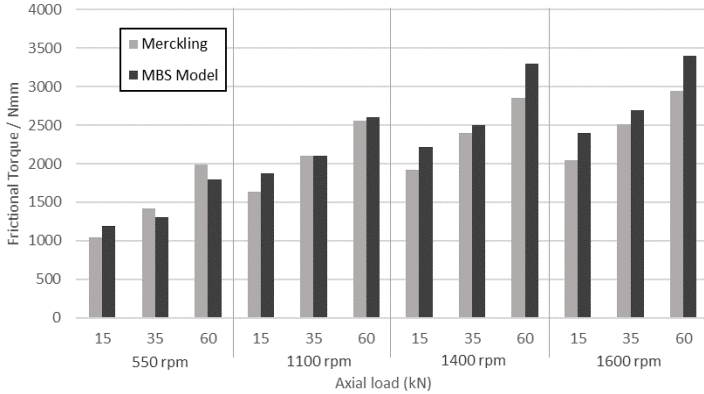
Figure 7.25: Comparison of the frictional torque of a pinion TRB obtained with the MBS Model and the measured results obtained by MERCKLING [Mer19]

Table 7.3: Main dimensions and performance data of a TRB 31313 [Sch17]

Parameter	Description	TRB 31313
α	Contact angle	24,5°
γ	Taper angle	4,165 mm
B	Rolling bearing width	33 mm
D_{pw}	Pitch diameter	102,5 mm
D_{we}	Roller diameter	18,0 mm
L_{we}	Roller length	24,2 mm
r	Rolling bearing bore radius	32,5 mm
R	Rolling bearing outside radius	70 mm
Z	Number of rollers	13
C	Dynamic load rating	163 kN

7.4.3 Optimization and simulation results

The optimization of the new geometry followed many steps. The initial parameters, as well as the intermediate parameters of the optimization, together with their resulting axial displacement, stress concentrations or effective contact length can be found in Annex A.2.1.

The information known about the application example is limited. In terms of the load conditions, the maximum radial force to which the rolling bearing is subjected for cases of combined load is unknown. Therefore, the contact angle α is chosen from the TRB 31313. Similarly, the limitations of space are unidentified. Therefore, the length of the roller, defining the rolling bearing width, is chosen from the TRB 31313.

The final parameters of the optimized geometry, based on the workflow described in Figure 7.23, are listed in Table 7.4. By this means, the resulting frictional torque of the new geometry is minimized, while the main dimensions of a TRB 31313 are maintained.

Table 7.4: Parameters defining the optimal geometry of the new rolling bearing type for its use as a pinion bearing

Parameter	Description	Value
α	Contact angle	24,5°
γ	Taper angle	4,165°
aA	Distance from the bearing axis to the center of the PCR_R	20,28 mm
aP	Distance between contact points	12,1 mm
aPk	Distance from contact point to the edge	8 mm
B	Rolling bearing width	33 mm
D_{pw}	Pitch diameter	102,5 mm
D_{we}	Roller diameter	18,0 mm
L_{we}	Roller length	24,2 mm
PCR	PCR_R	90 mm
r	Rolling bearing bore radius	32,5 mm
R	Rolling bearing outside radius	70 mm
κ	Osculation	0,95
w	Calculation angle	3,26°
Z	Number of rollers	13

However, with this optimization, the resulting frictional torque is not lower than the one of a TRB 31313, but 367% higher. The reason for that is, among others, the lower PCR that has to be chosen in order to obtain a minimum axial displacement, which leads to the removal of the rib contact. This limitation is due to the high axial load which is applied. The bigger the axial load acting on the roller, the smaller the PCR has to be, in order for the roller-raceway contact to be able to absorb the acting axial force.

Considering the possibility of varying the original main geometrical parameters defining the TRB 31313, two approaches in order to increase the PCR of the roller and, therefore, decrease the frictional torque have been studied. The first approach is to increase the roller length. The second approach is to increase the contact angle α.

On one hand, the smaller the ratio between the PCR of the roller and the roller length

L_{we} is, the higher the provided axial self-orientation ability of the rollers during operation is. Therefore, the longer the roller length is (in other words, the distance between the contact points aP), the bigger the PCR of the roller can be. By increasing the length of the roller, the total bearing roller width increases as well. In order to be able to do that, the space limitations have to be considered.

On the other hand, the angle between the acting axial load and the roller surface absorbing this load is increased by increasing the contact angle α. Therefore, the resulting axial displacement of the roller is reduced. The load conditions studied within this example are pure axial load. In order to increase the contact angle α, the combined load conditions have to be identified and studied as well.

The roller geometries resulting from these changes are illustrated in Figure 7.26. The optimization process followed for these geometries is described in Annex A.2.2 and A.2.3. The resulting optimal geometrical parameters are listed in Table 7.5.
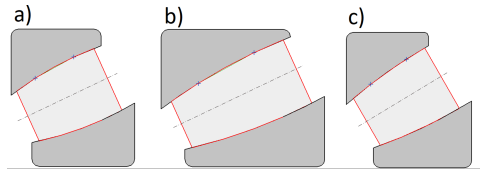
Figure 7.26: Representation of different roller geometries with the same main dimensions than a TRB 31313 (a), with increased roller length (b) and with increased contact angle α (c)

An overview of the different frictional torques for each geometry, compared to a TRB is shown in Figure 7.27. Although the resulting frictional torque for the new geometry is slightly reduced when the contact angle α and the roller length L_{we} are increased, its value is still far away from the frictional torque obtained when using a TRB as a pinion bearing. The characteristic geometry of the roller under study results into an asymmetric pressure distribution along the roller length (Figure A.2 in Annex A.2.1). This means a higher pressure peak occurs at one of the contact points compared to the other one. This might therefore result into a bigger skewing of the roller and the corresponding frictional losses. The crowing of the roller results furthermore into a different skewing moment at the inner ring than at the outer ring, which results into an undesired skewing of the roller as well. Furthermore, in comparison with a TRB, where the axial displacement of the roller is limited by the rib of the inner ring, the possibility of the roller of the new geometry to move along its z-axis might result into an undesired tilting of the rollers.

Table 7.5: Parameters defining the optimal geometries of the new rolling bearing type with increased length of the roller and contact angle for its use as a pinion bearing

Parameter	Description	$\uparrow L_{we}$	$\uparrow \alpha$
α	Contact angle	24,5°	30
γ	Taper angle	4,165°	5,018°
aA	Distance from the bearing axis to the center of the PCR_R	46,6 mm	15,6
aP	Distance between contact points	15 mm	12,1
aPk	Distance from contact point to the edge	9,5 mm	8
B	Rolling bearing width	40 mm	33
D_{pw}	Pitch diameter	102,5 mm	102,5 mm
D_{we}	Roller diameter	18,0 mm	18,0 mm
L_{we}	Roller length	30 mm	24,2 mm
PCR	PCR_R	120 mm	80 mm
r	Rolling bearing bore radius	32,5 mm	32,5 mm
R	Rolling bearing outside radius	70 mm	70 mm
κ	Osculation	0,95	0,97
w	Calculation angle	3,48°	4,20°
Z	Number of rollers	13	13
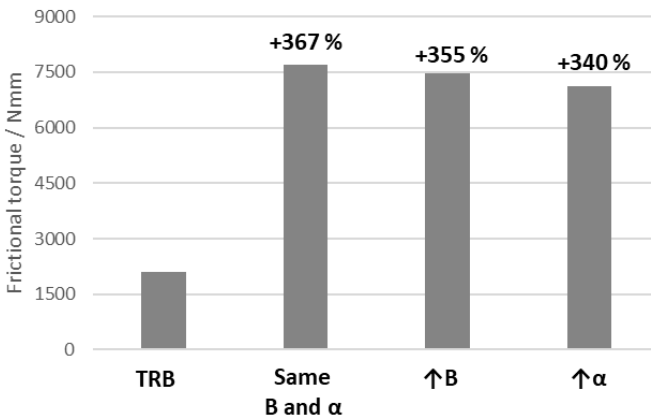
Figure 7.27: Resulting frictional torque for the different geometries of the new rolling bearing type studied and its comparison with a TRB 31313 when subjected to a pure axial load of 35 kN and an angular velocity of 1100 rpm. From the left to the right: a TRB 31313, an optimal geometry with same main geometrical parameters than a TRB 31313, an optimal geometry with increased L_{we} compared to a TRB 31313, an optimal geometry with increased α compared to a TRB 31313

In order to understand the dynamic behavior of the new rolling bearing geometry better, the skewing and tilting values of a roller are analyzed and compared to the roller of a TRB 31313. The results are presented in Figure 7.28. It can be observed, that both the skewing and the tilting of the roller are bigger within the new rolling bearing geometry. This is, together with the resulting drilling friction, the main reason for the higher frictional torque observed for this rolling bearing type compared to a TRB 31313.
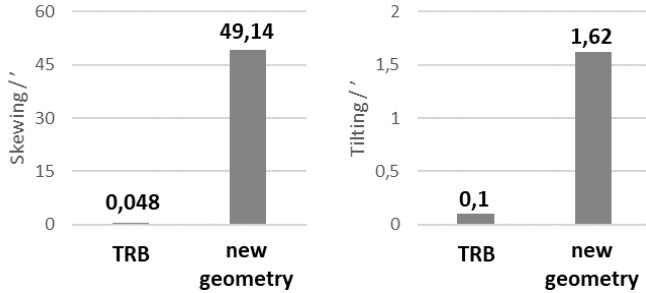
Figure 7.28: Resulting skewing and tilting of the roller for the TRB 31313 and the new geometry with same main dimensions as the TRB 31313 when subjected to a pure axial load of 35 kN and an angular velocity of 1100 rpm

8 Summary and Outlook

8.1 Summary

Rolling bearings belong among the most reliable and most used machine elements. They are used wherever relatively moving parts need to be supported or guided. In the attempt to reduce the fuel-consumption and the CO_2-output of any kind of vehicle, each rolling bearing system is thought over and optimized. Up till today for many applications rolling bearings with high frictional losses, e.g., tapered roller bearing, could have been replaced by bearing designs with significantly lower frictional losses. Partly this has been realized via new types of bearings, which do show appropriate performance characteristics. The relatively high friction losses occurring at the rib contact of TRBs are a spotlight for the engineers in this area of work. This study focuses on the development of a new type of rolling bearing, based on the existing TRB, without the need of a rib contact.

In these terms, a new rolling bearing geometry has been described and a MBS Model of it has been created and experimentally validated. For this purpose, several parameters defining the geometry of a roller have been studied and their influence on main outcomes like pressure distribution and frictional torque analyzed within the scope of a sensitivity analysis. Moreover, various patents defining new rolling bearing types and the correlations between their geometrical parameters have been considered. Thus, the geometry of the new rolling bearing type is characterized by a conical crowned roller with two contact points per raceway along the roller length. Thanks to the crowned profile of the roller, the angle between the acting axial load and the roller surface absorbing this load is increased in comparison to a TRB. By this means, the need of a rib contact at the inner ring does not longer exist, alongside its resulting frictional losses.

Most of the correlations observed between the parameters are transferable to other rolling bearing types. However, some of them, especially those concerning the location of the contact points, are unique to this geometry. Hereunder some of the most important correlations between geometrical characteristics and outcomes are enumerated:

- The contact length of the roller influences many outcomes. Such as, the longer the contact length is:

– The higher the load carrying capacity is.

– The higher the resulting frictional torque is.

– The lower the maximum pressure is.

- The contact length, on the other hand, is influenced by the geometry of the roller in various ways:

    – The narrower the osculation κ is, the longer the contact length is.

    – The bigger the contact angle α is in comparison to the load angle, the shorter the contact length is.

- Furthermore, the frictional torque is influenced by the crowning (PCR) of the roller and its resulting drilling friction. The bigger the PCR of the roller is, the higher the drilling friction is, therefore the higher the resulting frictional torque is.

- The axial displacement is the main parameter that has to be analyzed in order to prove the correct dynamic behavior of the rolling bearing. By this means, it can be analyzed if the profiling of the roller (the roller-raceway contact) can absorb the axial force on its own. If this is not the case, a rib contact would be needed. In general terms, the smaller the ratio between the PCR of the roller and the roller length L_{we} is, the higher the provided axial self-orientation ability of the rollers is. Therefore, the axial displacement of the roller can be reduced by:

    – Reducing the PCR of the roller. By this means, the angle between the acting axial load and the roller surface absorbing this load is increased, therefore, the axial displacement is decreased.

    – Increasing the distance between contact points aP, therefore, increasing the roller length.

With the results obtained in the sensitivity analysis and the correlations described before, a workflow for the optimization of the new rolling bearing geometry for a specific application has been developed. Based on this workflow, an optimization of an application example has been conducted.

An alternative for a TRB is still searched for in applications where high frictional losses take place due to a high frictional torque occurring in the roller-rib contact and at the same time a high load carrying capacity is needed. The higher frictional losses occurring in the roller-rib contact take place when a high axial load is acting on the roller. For this purpose, a pinion bearing of the differential gearbox of a heavy-duty commercial vehicle has been studied. Based on the most typical working conditions of a pinion TRB, the new

rolling bearing geometry has been optimized.

For the new rolling bearing geometry, the following occurs: the bigger the axial load acting on the roller is, the smaller the PCR has to be, in order for the roller-raceway contact to be able to absorb the acting axial force. Therefore, the resulting drilling friction can not be minimized as much as required. All this makes it impossible for the new rolling bearing geometry to deliver lower frictional torque than a TRB when high axial load is acting on the rolling bearing, which is the case for the chosen application example. The comparison of simulation results for both a pinion TRB and a pinion of the new rolling bearing geometry shows much higher frictional losses for the new geometry than for the TRB. Therefore it has been proven, that this geometry is not a suitable substitute for the specific application.

The results and knowledge gathered in this project are not amenable to direct commercial exploitation. However, selected results and findings can be used for the further development of a tapered spherical roller bearing or any other type of roller bearing.

8.2 Outlook

The most important sources of the high resulting frictional torque of the new geometry are the drilling friction of its characteristic crowned profile together with the skewing and tilting of the roller. The rotation of the roller among the axes perpendicular to the rotation axis result into undesired friction and have to be minimize. In order to optimize the dynamic behavior of the rollers of the geometry studied in this work in terms of its resulting skewing and tilting, several modifications and improvements can be carried out on its geometrical definition and MBS Model.

First of all, it has been observed, that the pressure distribution of the new geometry showed a higher pressure peak at one of the contact points compared to the other. The contact point with the higher pressure was located closer to the bigger diameter of the roller for the cases studied. This behavior is more pronounce for the application example considered. Furthermore, the contact area at this point was as well bigger. A possible solution in order to obtain a more symmetrical distribution of pressure along the roller length would be to provide a different osculation value for the two contact points. Like this, the contact point closer to the bigger diameter of the roller would have a wider osculation than the other contact point, therefore a more symmetrical pressure distribution can be achieved, avoiding the corresponding slippage.

Another possibility in order to reduce the skewing of the rollers is to have a different contact situation for the inner ring than for the outer ring. By providing a different frictional torque for both contacts (inner vs. outer ring), a possible skewing of the roller

can be reduced and, therefore, the total frictional torque minimized.

Moreover, the guidance that the cage provides, together with the friction resulting from its contact with the roller, should be studied in more detail. For this purpose, a comparative consideration of cage modeling strategies and designs, as well as its influence in the resulting skewing and tilting of the roller and ultimately frictional losses, is suggested.

A Annex

A.1 Boundary conditions for the MBS Model

The general boundary conditions for all simulations conducted in the framework of the work are listed in Table A.1.

Table A.1: General boundary conditions parameters for the MBS Model

Parameter	Description	Value	Units
E	Young´s modulus	208000	N/mm^2
ν	Poisson´s ratio	0,3	-
ρ	Density	7850	kg/m^3
$T_{\ddot{O}L}$	Lubricant temperature	50-60	°C
$\nu_{\ddot{O}L}$	Lubricant viscosity	57,01-36,88	mm^2/s
$\rho_{\ddot{O}L}$	Lubricant density	0,87-0,85	g/ml

A.1.1 Specific boundary conditions for the prototype and a TRB 32208

Specific boundary conditions for the definition of the profile of a TRB 32208 are listed in Table A.2 based on Figure A.1.

The parameters defining the surface quality of the rollers and raceways as well as the mixed friction parameters according to Zhou and Hoeprich [ZH91] for both the Prototype and a TRB 32208 are listed in Table A.3.
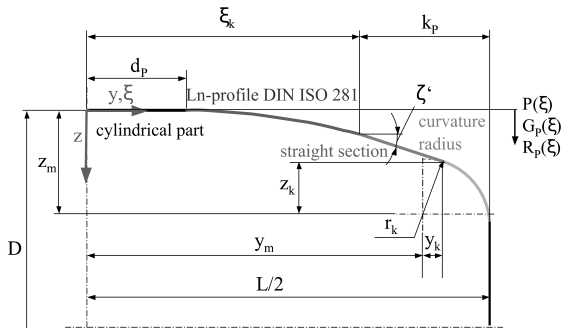
Figure A.1: Parameters for the logarithmic profile according to [Teu05]

Table A.2: Parameters for the logarithmic profile according to [Teu05]

Parameter	Value	Units
a_p	0,0005	-
c_p	15,5	mm
d_p	0	mm
k_p	2,0	mm
r_k	0,8	mm

Table A.3: Boundary condition parameters for the Prototype and a TRB 32208

| | | Values | | |
Description	Parameter	Prototype	TRB 32208	Units
	$s_{q,RW}$	0,14	0,22	μm
Roughness	$s_{q,R}$	0,17	0,24	μm
	$s_{q,Rib}$	-	0,26	μm
	$s_{q,R-end}$	-	0,28	μm
Combined roughness stan-	σ_{RW}	0,22	0,33	μm
dard deviation	$\sigma_{R-end-Rib}$	-	0,38	μm
Raceway contact mixed	B_{ZH}	1,7	2,27	-
friction parameters	C_{ZH}	0,8	1,05	-
Roller end - rib contact	B_{ZH}	-	1,78	-
mixed friction parameters	C_{ZH}	-	1,01	-

A.1.2 Specific boundary conditions for the application example of a pinion bearing

Specific boundary conditions for the application example of a pinion bearing are listed in Table A.4.

Table A.4: Boundary condition parameters for the pinion bearing

Description	Parameter	Value	Units
Roughness	$s_{q,RW}$	0,09	μm
	$s_{q,R}$	0,12	μm
Combined roughness standard de-	σ_{RW}	0,13	μm
viation			
Raceway contact mixed	B_{ZH}	1,85	-
friction parameters	C_{ZH}	0,85	-
Lubricant temperature	$T_{\ddot{O}L}$	50	°C
Lubricant viscosity	$\nu_{\ddot{O}L}$	38,95	mm^2/s
Lubricant density at 15°	$\rho_{\ddot{O}L}$	0,86	g/ml

A.2 Optimization process of the application example of a pinion bearing

A.2.1 Optimization for a geometry with the same main dimensions as a TRB 31313

The initial parameters for the optimization of the pinion bearing conducted in section 7.4 are listed in Table A.5. The parameters B, D_{pw}, D_{we}, L_{pw}, r, R and Z as well as the contact angle α and the resulting taper angle γ have been chosen from the TRB 31313 in order to be optimized. The PCR_R of a toroidal roller bearing with similar main dimensions like a TRB 31313 has been selected: a CARB 2213. The osculation κ has been, first of all, maximized: $\kappa = 0{,}99$. Following the indications listed in section 7.3, the parameters defining the location of the contact points (aP and aPK) are selected in such a way, that they are centered along the roller length. This matches the following equations (4.2) and (4.3).

Table A.5: Initial parameters for the optimization of a pinion bearing

Parameter	Description	Value
α	Contact angle	24,5°
γ	Taper angle	4,165°
aA	Distance from the bearing axis to the center of the PCR_R	115,89 mm
aP	Distance between contact points	12,1 mm
aPk	Distance from contact point to the edge	6,05 mm
B	Rolling bearing width	33 mm
D_{pw}	Pitch diameter	102,5 mm
D_{we}	Roller diameter	18,0 mm
L_{we}	Roller length	24,2 mm
PCR	PCR_R	200 mm
r	Rolling bearing bore radius	32,5 mm
R	Rolling bearing outside radius	70 mm
κ	Osculation	0,99
w	Calculation angle	4,4°
Z	Number of rollers	13

After the selection of the initial parameters, the first optimizations have been conducted. The results of these simulations are listed in Table A.6. Within the first stages, the PCR of the roller leading to an acceptable axial displacement, where no rib contact is needed, is searched for. These first optimization stages (geometries 1, 2, 3 and 4) are equivalent to the steps 8, 9 and 10 of the workflow presented in section 7.3. For a better understanding

of the resulting axial displacement, the corresponding effective length (rolling length that is loaded) has been monitored as well.

Once the axial displacement of the roller is decreased to a limit where no rib contact is needed (0,047 mm for this example), the second optimization step can be conducted (geometries 4, 5, and 6). This corresponds to the steps 11 and 12 of the workflow. First of all, the stress peaks occurring when the contact point is too close to the end have to be avoided. For this purpose, the location of the contact points (aPk) is varied and the resulting maximum pressure analyzed. The pressure distribution of geometries 4, 5 and 6 is represented in Figure A.2. Afterwards, the osculation κ has been decreased in order to reduce the resulting frictional torque. For this purpose, the corresponding effective roller length L_{we} has to be monitored as well. The effective roller length L_{we} has to be chosen in order to provide the needed load carrying capacity.

Table A.6: Parameters defining the geometries of the optimization process

Geom.	PCR (mm)	aPk (mm)	κ (-)	Axial disp. (mm)	L_{we} (mm)
#1	200	6,05	0,99	2	4,68
#2	150	6,05	0,99	0,85	5,46
#3	100	6,05	0,99	0,07	15,61
#4	90	6,05	0,99	0,047	17,95
#5	90	8	0,99	0,024	22,64
#6	90	8	0,95	0,024	17,95
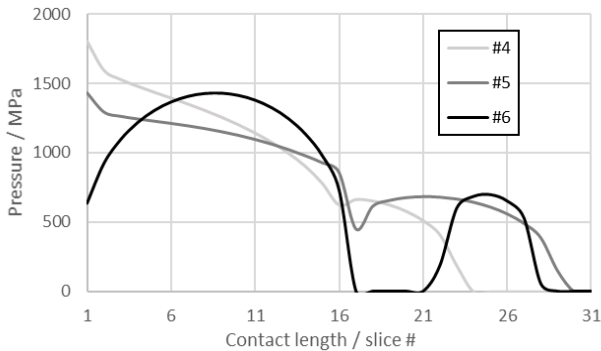
Figure A.2: Pressure distribution along the contact length for different geometries as described in Table A.6

A.2.2 Optimization for a geometry with longer L_{we} than a TRB 31313

The optimization process followed for a geometry with longer L_{we} than a TRB 31313 is the same as the previously explained one (Annex A.2.1). The parameters chosen for each optimization step are listed in Table A.7. The pressure distribution of geometries 23, 24 and 25 is presented in Figure A.3.

Table A.7: Parameters defining the geometries of the optimization process for a geometry with longer L_{we}

Geom.	PCR (mm)	aPk (mm)	κ (-)	Axial disp. (mm)	L_{we} (mm)
#21	200	7,5	0,99	0,85	4,84
#22	150	7,5	0,99	0,18	10,65
#23	120	7,5	0,99	0,052	21,29
#24	120	9,5	0,99	0,032	26,13
#25	120	9,5	0,95	0,032	17,95
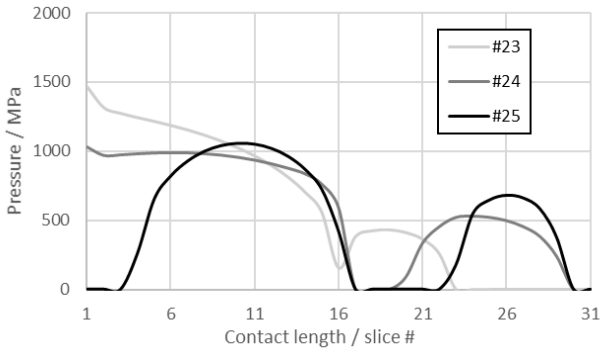
Figure A.3: Pressure distribution along the contact length for different geometries as described in Table A.7

A.2.3 Optimization for a geometry with bigger α than a TRB 31313

The optimization process followed for a geometry with bigger α than a TRB 31313 is the same as the previously explained one (Annex A.2.1). The parameters chosen for each optimization step are listed in Table A.8. The pressure distribution of geometries 34, 35 and 36 is presented in Figure A.4.

Table A.8: Parameters defining the geometries of the optimization process for a geometry with bigger α

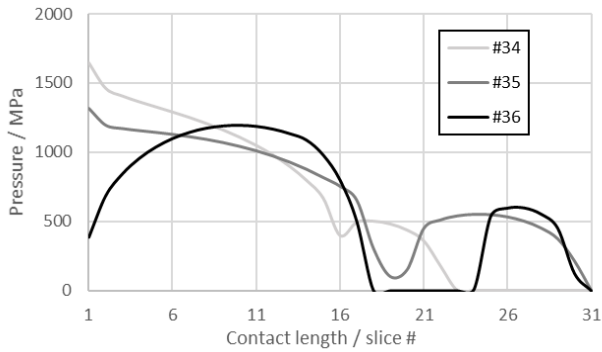| Geom.	PCR (mm)	aPk (mm)	κ (-)	Axial disp. (mm)	L_{we} (mm)
#31	200	6,05	0,99	1,22	3,90
#32	150	6,05	0,99	0,55	5,46
#33	120	6,05	0,99	0,35	6,25
#34	90	6,05	0,99	0,038	17,17
#35	90	8	0,99	0,033	18,74
#36	90	8	0,97	0,033	17,95

Figure A.4: Pressure distribution along the contact length for different geometries as described in Table A.8

Bibliography

[Ara97]   ARAMAKI, H.: "Rolling Bearing Analysis Program Package "BRAIN"", in: *Motion & Control* 3 (1997), pp. 15–24.

[ANS97]   ARAMAKI, H.; NAKANO, Y.; SHODA, Y.: "Rolling Bearing Analysis Codes "BRAIN" - The Estimation of Rolling Bearing Performance for an Automotive Application", in: *SAE International Congress and Exposition* (1997).

[Aul08]   AUL, E.: *Analyse von Relativbewegungen in Wälzlagersitzen*, Kaiserslautern: TU Kaiserslautern, 2008.

[AAH07]   AUL, V.; AUGUSTINO, R.; HAEHNEL, T., et al.: "MKS-Studie", in: *Forschungsvereinigung Antriebstechnik, FVA-Heft 8222* (2007).

[Aul14]   AUL, V.: "Kontaktmodelle zur dynamischen Simulation vollrolliger Zylinderrollenlager", Dissertation, Technische Univerität Kaiserslautern, 2014, Maschinenelemente und Getriebetechnik Berichte, Bd. 14/2014, ISBN: 978-3-943995-55-8.

[BK12]   BAEK, H.-K; KANG, H. Y.: "Development of a Low Friction Chain Drive System for Gasoline Engines", in: *SAE 2012 International Powertrains, Fuels & Lubricants Meeting, 18. September 2012, Malmo, Sweden*, ed. by SOCIETY OF AUTOMOTIVE ENGINEERS, 2012.

[BH05]   BODENSTEIN, F.; HABERHAUER, H.: *Maschinenelemente: Bodenstein F, Haberhauer H (2005) Maschinenelemente. Springer, Berlin, Heidelberg, New York*, 2005.

[Boh12]   BOHR, A.: "Nachhaltigkeit durch neue Wälzlager", in: *Tribologie und Schmierungstechnik* 1.59 (2012).

[BEH95]   BRÄNDLEIN, J.; ESCHMANN, P.; HASBARGEN, L., et al.: *Die Wälzlagerpraxis: Handbuch für die Berechnung und Gestaltung von Lagerungen*, 3. Auflage / neu bearb. von J. Brändlein, Vereinigte Fachverlage GmbH, 1995.

[CH15]   CZICHOS, H.; HABIG, K.-H.: *Tribologie-Handbuch: Tribometrie, Tribomaterialien, Tribotechnik*, 4., vollständig überarbeitete und erweiterte Auflage, Wiesbaden: Springer Fachmedien, 2015.

[Dah16]   DAHIWAL, R.: *Entwicklung eines Berechnungsmoduls zur Dynamiksimula-tion und Betriebsanalyse von Zylinderrollenlagern unter Berücksichtigung der Umgebungskonstruktion in Simpack. Forschungsvorhaben Nr. 625 II. Abschlussbericht*, vol. XXX, Forschungsheft, FVA Forschungsvereinigung Antriebstechnik e.V, 2016.

[DIN11]   DIN 26281: *Wälzlager – Dynamische Tragzahlen und nominelle Lebens-dauer - Berechnung der modifizierten nominellen Referenz Lebensdauer für Wälzlager*, 2011.

[DIN10a]   DIN ISO 281: *Wälzlager – Dynamische Tragzahlen und nominelle Lebens-dauer*, 2010.

[DIN78]   DIN ISO 355: *Wälzlager - Metrische Kegelrollenlager*, 1978.

[DIN10b]   DIN ISO 611: *Wälzlager - Übersicht*, 2010.

[DIN94]   DIN ISO 635-1: *Wälzlager - Pendelrollenlager - Beiblatt 1: Tonnenlager. Merkmal-Kennungen und vereinfachte Darstellung*, 1994.

[DIN09a]   DIN ISO 635-2: *Wälzlager - Pendelrollenlager - Zweireihig, zylindrische und kegelige Bohrung*, 2009.

[DIN09b]   DIN ISO 76: *Wälzlager - Statische Tragzahlen*, 2009.

[DH61]   DOWSON, D.; HIGGINSON, G. R.: "New Roller-Bearing Lubrication For-mula", in: *Engineering* 192.4972 (1961), pp. 158–159.

[FKS11]   FIEDLER, S.; KIEKBUSCH, T.; SAUER, B.: "Investigation of inner contact and friction conditions of a spherical roller bearing using multi-body simulation", in: *Periodica Polytechnica Mechanical Engineering* 55.2 (2011), p. 79.

[FKS12]   FIEDLER, S.; KIEKBUSCH, T.; SAUER, B.: "Influence of Inner Geometry on Friction Torque in Spherical Roller Bearings", in: *Proceedings of the Eighth International Conference on Mechanical Engineering (GÉPÉSZET)*, 2012.

[Gla98]   GLASSNER, A. S., ed.: *Graphics gems*, San Diego, CA: Academic Press, 1998.

[Gre19]   GREHN, M.: "Rollenlager", pat. DE 10 2017 128 800 A1, 2019.

[HB96]   HABERHAUER, H.; BODENSTEIN, F.: *Maschinenelemente: Gestaltung, Berech-nung, Anwendung*, Zehnte, vollständig neubearbeitete Auflage, Springer-Lehrbuch, Berlin, Heidelberg: Springer Berlin Heidelberg, 1996.

[HSN15]   HAHN, B.; SMOLENSKI, M.; NEUKIRCHNER, J.: "Investigations of New Cage Designs for the Main Bearings in Multi-Megawatt Wind Power Plants", in: *2nd Conference for Wind Power Drives (CWD)*, 2015, pp. 321–333.

[Hah05]   HAHN, K.: "Dynamik-Simulation von Wälzlagerkäfigen", Diss. TU Kaiserslautern, 2005.

[HL92]   HOSCHEK, J.; LASSER, D.: *Grundlagen der geometrischen Datenverarbeitung*, 2., neubearb. und erw. Aufl., Stuttgart: Teubner, 1992.

[Hou09a]   HOUPERT, L.: "CAGEDYN: A Contribution to Roller Bearing Dynamic Calculations Part I: Basic Tribology Concepts", in: *Tribology Transactions* 53.1 (2009), pp. 1–9.

[Hou09b]   HOUPERT, L.: "CAGEDYN: A Contribution to Roller Bearing Dynamic Calculations Part II: Description of the Numerical Tool and Its Outputs", in: *Tribology Transactions* 53.1 (2009), pp. 10–21.

[Hou10]   HOUPERT, L.: "CAGEDYN: A Contribution to Roller Bearing Dynamic Calculations. Part III: Experimental Validation", in: *Tribology Transactions* 53.6 (2010), pp. 848–859.

[Hou01]   HOUPERT, L.: "An Engineering Approach to Hertzian Contact Elasticity—Part I", in: *Journal of Tribology* 123.3 (2001), p. 582.

[ISF05]   IOANNIDES, E.; STACKE, L.-E.; FRITZSON, D., et al.: "Multibody Rolling Bearing Calculations (Computer Programm BEAST)", in: *Proceedings of World Tribologie Congress III (WTC 2005)*, 2005.

[Jac08]   JACOB, M.: "Wälzlager", pat. DE102007021523A1, 2008.

[Jac92]   JACOB, W.: "Gelenklager", pat. DE 3904456C2, 1992.

[Kel85]   KELLSTRÖM, M.: "Radial roller bearing", pat. EP0175858, 1985.

[KB76]   KELLSTRÖM, M.; BLOMQVIST, S.: "Roller bearings comprising rollers with positive skew angle", pat. US3990753, 1976.

[KKL16]   KELLSTRÖM, M.; KULLIN, J.; LÖFQVIST, A.: "Angular contact self-aligning toroidal rolling element bearing", pat. EP 3020987A1, 2016.

[Kie17]   KIEKBUSCH, T.: "Strategien zur dynamischen Simulation von Wälzlagern", Dissertation, Technische Universität Kaiserslautern, 2017, Maschinenelemente und Getriebetechnik Berichte, Bd. 23/2017, ISBN: 978-3-95974-043-2.

[KFS15]   KIEKBUSCH, T.; FRUTH, T.; SAUER, B.: *Analyse des dynamischen Verhaltens von Wälzlagern in WEA unter Berücksichtigung der Umgebungsverformung: VDI-Bericht, vol 2242, pp 83–96, 6. VDI-Fachtagung „Schwingungen von Windenergieanlagen"*, Bremen, 2015.

[KLS17]   KIEKBUSCH, T.; LIEBRECHT, J.; SAUER, B.: *Dynamiksimulation von Wälzlagern unter Berücksichtigung der Plansch- und Schleppverluste*, 2017.

[KS17]   KIEKBUSCH, T.; SAUER, B.: *Calculation of the dynamic behaviour of rolling bearings with detailed contact calculations: Proceedings of the EUROMECH Colloquium 578 in Rolling Contact Mechanics for Multibody System Dynamic*, Funchal, Madeira, Portugal, 2017.

[Koc08]   KOCH, O.: "Dreidimensionale Simulation von kombiniert belasteten Radialzylinderrollenlagern", Dissertation, Ruhr-Universität Bochum, 2008.

[KPW09a]   KOCH, O.; PLANK, R.; WEBER, J.: "Analytisches Modell zur Berechnung und Minimierung der Wälzlagerreibung: Analytical Model for Calculation and Minimization of Bearing Friction", in: *Gleit- und Wälzlagerungen : Gestaltung, Berechnung, Einsatz ; Wiesloch bei Heidelberg, 9. und 10. Juni 2009*, ed. by VEREIN DEUTSCHER INGENIEURE, VDI Berichte, Düsseldorf: VDI Verlag, 2009, pp. 67–78.

[KPW09b]   KOCH, O.; PLANK, R.; WEBER, J.: "Wälzlageroptimierung durch dreidimensionale dynamische Simulation: Bearing Optimization due to Three-Dimensional Dynamic Simulation", in: *Gleit- und Wälzlagerungen : Gestaltung, Berechnung, Einsatz ; Wiesloch bei Heidelberg, 9. und 10. Juni 2009*, ed. by VEREIN DEUTSCHER INGENIEURE, vol. 2069, VDI Berichte, Düsseldorf: VDI Verlag, 2009, pp. 43–51.

[Kor11]   KORYCIAK, J.: "Einfluss der Ölmenge auf das Reibmoment von Wälzlagern mit Linienberührung:" in: *VDI-Tagung Gleit- und Wälzlagerungen, Schweinfurt* (2011).

[KD11]   KRUG, U.; DITTMAR, R.: "Anwendung reibungsoptimierter Kegelrollenlager:" in: *VDI-Tagung Gleit- und Wälzlagerungen, Schweinfurt* (2011).

[Lie18]   LIEBRECHT, J.: "Technisch-mathematischer Ansatz zur Berechnung der hydraulischen Verluste in Wälzlagern.", Dissertation, Technische Universität Kaiserslautern, 2018, Maschinenelemente und Getriebetechnik Berichte, Bd. 30/2018, ISBN: 978-3-95974-103-3.

[LSS15a]   LIEBRECHT, J.; SI, X.; SAUER, B., et al.: "Untersuchungen von hydraulischen Verlusten an Kegelrollenlagern", in: *Tribologie und Schmierungstechnik* 62.3 (2015), pp. 14–21.

[LSS16]   LIEBRECHT, J.; SI, X.; SAUER, B., et al.: "Technisch-mathematischer Ansatz zur Berechnung der Plansch- und Strömungsverluste am Kegelrollenlager.", in: *Tribologie und Schmierungstechnik* 63.4 (2016), p. 5.

[LSS15b]   LIEBRECHT, J.; SI, X.; SAUER, B., et al.: "Investigation of Drag and Churning Losses on Tapered Roller Bearings", in: *Strojniški vestnik – Journal of Mechanical Engineering* 61.6 (2015), pp. 399–408.

[Lun39]   LUNDBERG, G.: "Elastische Berührung zweier Halbräume", in: *Forschung im Ingenieurwesen* 10.5 (1939), pp. 201–211.

[Mag12]   MAGYAR, B.: ""Tribo-dynamische Untersuchungen von Zylinderschneckengetrieben"", Diss. Technische Universität Kaiserslautern, 2012.

[Mer19]   MERCKLING, J.: "Pinion Fuel Efficient Tapered Roller Bearings for Heavy Truck Commercial Vehicles", in: *ATZheavy duty worldwide* 12.2 (2019), pp. 40–43.

[MEG15]   MORALES-ESPEJEL, G. E.; GABELLI, A. A.: "Major Step Forward in Life Modelling", in: #4 (2015), pp. 21–27.

[NHM10]   NAKAGAWA, N.; HORI, M.; MAEDA, T., et al.: "Double-row self-aligning roller bearing and device for supporting wind turbine generator main shaft", pat. EP 1 705 392 B1, 2010.

[Nak76]   NAKAMURA, T.: "Conical roller bearing", pat. US 3 951 483, 1976.

[Nak06]   NAKHIMOVSKI, I.: "Contributions to the Modeling and Simulation of Mechanical Systems with Detailed Contact Analysis", Diss. Linköpings universitet, 2006.

[Neu17]   NEUKIRCHNER, J.: "Kegelrollenlager mit korrigierter Lauffläche", pat. DE 10 2017 113 933 A1, 2017.

[PO12]   PABST, A.; OSWALD, A.: "Kegelrollenlager", pat. DE 10 2012 204 280 A1, 2012.

[Pet04]   PETERY, G. VON: "Lager für Achsgetriebe von BMW", in: *ATZ - Automobiltechnische Zeitschrift* 106.12 (2004), pp. 1096–1100.

[Pla11]   PLANK, R.: "Effizienzsteigerung von Fahrzeugantrieben durch optimierte Lagerungen.", in: *VDI-Tagung Gleit- und Wälzlagerungen, Schweinfurt* (2011).

[PTV07]   PRESS, W. H.; TEUKOLSKY, S. A.; VETTERLING, W. T., et al.: *Numerical recipes: The art of scientific computing*, 3rd ed., Cambridge, UK and New York: Cambridge University Press, 2007.

[Rei28]   REICHLE, P.: "Selbst einstellende Schrägrollenlagerung", pat. DE 462 623, 1928.

[Reu87]   REUSNER, H.: *Das logarithmische Profil–Qualitätsmerkmal moderner Zylinderrollenlager: – Qualitätsmerkmal moderner Zylinderrollenlager*, 1987.

[SK17]   SAUER, B.; KIEKBUSCH, T.: *Dynamic simulation of the interaction between raceway and rib contact of cylindrical roller bearings: STLE Annual Meeting, Atlanta, USA*, 2017.

[Sch17] Schaeffler Technologies AG & Co. KG, ed.: *Wälzlager*, Herzogenaurach, 2017.

[Sch21] Schaeffler Technologies GmbH: *Increase Fuel Mileage up to 2.5 % with FAG Tandem Angular Contact Ball Bearings in Your Final Drive*, ed. by FAG, Herzogenaurach (Germany), 2021.

[SKF14] SKF Gruppe, ed.: *Wälzlager*, 2014.

[Soc31] Soc. An. Officine di Villar Perosa: "Selbsteinstellendes Rollenlager", pat. 537156, 1931.

[SF01] Stacke, L.-E.; Fritzson, D.: "Dynamic behaviour of rolling bearings: Simulations and experiments", in: *Proceedings of the Institution of Mechanical Engineers, Part J: Journal of Engineering Tribology* 215.6 (2001), pp. 499–508.

[SFN99] Stacke, L.-E; Fritzson, D.; Nordling, P.: "BEAST—a rolling bearing simulation tool", in: *Proceedings of the Institution of Mechanical Engineers, Part K: Journal of Multi-body Dynamics* 213.2 (1999), pp. 63–71.

[SRW21] Stahl, T.; Rumpel, R.; Wirth, P., eds.: *Neue Lösungen für noch weniger Reibung*, vol. 2378, VDI Berichte, Bremen, 2021.

[SS08] Steinhilper, W.; Sauer, B., eds.: *Konstruktionselemente des Maschinenbaus 1: Grundlagen der Berechnung und Gestaltung von Maschinenelementen*, 7th ed., Springer-Lehrbuch, Berlin and Heidelberg: Springer Verlag, 2008.

[SS12] Steinhilper, W.; Sauer, B.: *Konstruktionselemente des Maschinenbaus 2: Grundlagen von Maschinenelementen für Antriebsaufgaben*, Berlin, Heidelberg: Springer, 2012.

[Tal67] Tallian, T. E.: "On Competing Failure Modes in Rolling Contact", in: *A S L E Transactions* 10.4 (1967), pp. 418–439.

[Teu05] Teutsch, R.: "Kontaktmodelle und Strategien zur Simulation von Wälzlagern und Wälzführungen. Diss., TU Kaiserslautern", Dissertation, Technische Universität Kaiserslautern, 2005, Maschinenelemente und Getriebetechnik Berichte, Bd. 1/2005,

[TS04] Teutsch, R.; Sauer, B.: "An Alternative Slicing Technique to Consider Pressure Concentrations in Non-Hertzian Line Contacts", in: *Journal of Tribology* 126.3 (2004), pp. 436–442.

[TH15] Tong, V.; Hong, S.: "Characteristics of tapered roller bearings in relation to roller profiles", in: *J Mech Sci Technol 29, 2913–2919* (2015).

[TH17] Tong, V.; Hong, S.: "Optimization of partially crowned roller profiles for tapered roller bearings", in: *J Mech Sci Technol 31, 641–650* (2017).

[Tri85]   TRIPP, J. H.: "Hertzian contact in Two and Three Dimensions", in: *NASA Technical Paper Series* 2473 (1985).

[Wan15]   WANG, D.: "Berechnung der Wälzlagerreibung aufgrund weiterentwickelter Rheologischer Fluidmodelle.", Diss. Universität Hannover, 2015.

[WJO15]   WANG, D.; JURKSCHAT, T.; OTTO, M., et al.: *Low Friction, Lager 2 (Wälzlager Reibungsberechnung): Erweiterung der Berechnung der Wälzlagerreibung in FVA-Software: Abschlussbericht zum FVA-Forschungsvorhaben 701 I (Heft 1157)*, Frankfurt/Main: Forschungsvereinigung Antriebstechnik e.V., 2015.

[WP13]   WANG, D.; POLL, G.: *Low Friction Powertrain - Teilprojekt G2.1 (Teil 2): Wirkungsgradoptimiertes Getriebe: Abschlussbericht (Heft 1007-2)*, Frankfurt/Main: Forschungsvereinigung Verbrennungskraftmaschinen e.V., 2013.

[Woh10]   WOHLGEMUTH, M.: "Ein Beitrag zur Lebensdauerverlängerung von feststoffgeschmierten Rillenkugellagern", Diss, TU Kaiserslautern, 2010.

[YDH00a]   YANG, Y.; DANYLUK, S.; HOEPRICH, M.: "A Study on Rolling Element Skew Measurement in a Tapered Roller Bearing with a Specialized Capacitance Probe", in: *Journal of Tribology* 122.3 (2000), pp. 534–538.

[YDH00b]   YANG, Y.; DANYLUK, S.; HOEPRICH, M.: "Rolling Element Skew in Tapered Roller Bearings", in: *Tribology Transactions* 43.3 (2000), pp. 564–568.

[YDH99]   YANG, Y.; DANYLUK, S.; HOEPRICH, M.: "On the measurement of skew of tapered roller bearings", in: *Tribology Letters* 6.3-4 (1999), pp. 221–223.

[ZQH88]   ZHANG, Z.; QIU, X.; HONG, Y.: "EHL analysis of rib-roller end contact in tapered roller bearings", in: *Tribology Transactions* 31.4 (1988), pp. 461–467.

[ZH91]   ZHOU, R. S.; HOEPRICH, M. R.: "Torque of Tapered Roller Bearings", in: *Journal of Tribology* 113.3 (1991), pp. 590–597.

Own Publications for the Dissertation

[1] HERWEG, S.; HUBER, F.; WELLER, R.; ATAMER, S.; SAUER, B.; KIEKBUSCH, T.; MARMOL,M.: Detaillierte Mehrkörpersystem-Simulationen des hochbelasteten Nocken-Rollen-Kontakts. 5. ATZ-Fachtagung „Reibungsminimierung im Antriebsstrang" (ATZlive), Esslingen, 29.-30. November 2016

[2] HERWEG, S.; HUBER, F.; ATAMER, S.; WELLER, R.; STEINER, R.; SAUER, B.; KIEKBUSCH, T.; WIESKER, S.; MARMOL, M.: Experimental investigations and simulations on cam-roller-friction. 18. Internationales Stuttgarter Symposium 2018

[3] HERWEG, S.; HUBER, F.; ATAMER, S.; WELLER, R.; STEINER, R.; SAUER, B.; WIESKER, S.; MARMOL, M.: Experimentelle und simulative Untersuchungen zum Einfluss der Lageabweichungen im Nocken-Rollen-Kontakt auf die Ventiltriebskräfte. In: Forschung im Ingenieurwesen 82 (2018) Nr. 4, Seite 273-283; ISSN: 0015-7899; DOI: 10.1007/s10010-018-0279-8

[4] MARMOL, M.; SAUER, B.; KIEKBUSCH, T.: Development of new rolling bearing for heavy-duty truck applications. In: Berns K. et al. (eds) Commercial Vehicle Technology 2018. Proceedings. Springer Vieweg, Wiesbaden. $https://doi.org/10.1007/978-3-658-21300-8_28$

[5] MARMOL, M.; SAUER, B.; KIEKBUSCH, T.: Comparative study of a simulative bearing design with an experimentally determined data of a prototype bearing. Forsch Ingenieurwes 85, 1015–1027 (2021). $https://doi.org/10.1007/s10010-021-00494-7$

Student Works for the Dissertation

1. Franck, C.: Gegenüberstellung von Approximationsverfahren zur Interpolation von 2D und 3D-Freiformgeometrien zur Abstandsberechnung. Studienarbeit, TU Kaiserslautern (Nr. 988), 2018.
2. Happersberger, T.: FE-Modellaufbau und Modelanalyse zur Untersuchung der Lastverteilung in Abhängigkeit der Geometrie der Wälzlager. Projektarbeit, TU Kaiserslautern (Nr. 1118), 2021
3. Henn, A.: Erweiterung einer Eingabeoberfläche zur automatisierten Modellerzeugung für die Mehrkörpersimulation von Kegelrollenlagern. Studienarbeit, TU Kaiserslautern (Nr. 1144), 2021.
4. Mut, E.: Analyse des Störgrößeneinflusses auf die Messergebnisse eines Zwei-Achs-Kraftaufnehmers. Bachelorarbeit, TU Kaiserslautern (Nr. 951), 2017
5. Pazouki, Hossein.: Bearing Stiffness Analysis Considering Different Housing Types. Masterarbeit, TU Kaiserslautern (Nr. 955), 2017.
6. Wingertszahn, P.: Simulative Bestimmung der Kontaktwärmeleitzahl im rauen Kontakt. Studienarbeit, TU Kaiserslautern (Nr. 967), 2017.

Curriculum Vitae

Personal Details

Name:	Margarita Mármol
Nationality:	Spanish

Education

School education

2002 - 2008	Instituto Complutense
	Completion: General Matriculation Standard

University studies

2008 - 2014	Universidad Carlos III de Madrid
	Industrial Engineering
	Completion: Master of Science

Professional Contribution

06/2014 - 03/2015	European Technology Innovation Center
	John Deere
	Intern
05/2015 - 12/2021	Lehrstuhl für Maschinenelemente und Getriebetechnik
	Technische Universität Kaiserslautern
	Research assistant

Postgraduate dissertations at the Chair of Machine Elements, Gears and Tribology (MEGT) at the TU Kaiserslautern

1. Gäthje, Heino: Bewertung der Naßbagger und der sich anschließenden Transportkette im Schelfbereich unter Anwendung eines EDV-Modells. Dissertation, Universität Kaiserslautern, 1981
2. Kahle, Ulrich: Das Micro-CAD-System ein Beitrag zur Einführung einer rechnerunterstützen Konstruktionsweise in kleinen und mittleren Unternehmen. Dissertation, Universität Kaiserslautern, 1983
3. Kreutz, Sax: Simulation von Vergleichmässigungsprozessen auf stirnseitig abgebauten Massenschüttgutkreislagerplätzen mit Hilfe eines elektrischen Analogiemodells und eines gleichwertigen digitalen Modells. Dissertation, Universität Kaiserslautern, 1983
4. Rende, Hikmet: Ein Beitrag zur Untersuchung der elastischen Nachgiebigkeiten der verspannten Teile von Schraubenverbindungen. Dissertation, Universität Kaiserslautern, 1984
5. Sponagel, Stefan: Gummi-Metall-Bauteile. Dissertation, Universität Kaiserslautern, 1987
6. Spaltofski, Ralf: Ein Beitrag zur Beurteilung der Trageigenschaften und des Reibungsverhaltens von nicht-newtonschen Flüssigkeiten in stationär und dynamisch bewegten Gleitlagerungen. Dissertation, Universität Kaiserslautern, 1988
7. Britz, Stefan: Ein Beitrag zur Erfassung der Funktionsprinzipien dynamischer Wellendichtungen unter besonderer Berücksichtigung des Radialwellendichtrings. Dissertation, Universität Kaiserslautern, 1988
8. Hennerici, Horst: Ein Beitrag zur Berechnung der Beanspruchungen und der nichtlinearen Rückstellkräfte und -momente von dünnen Kreisringblechen als Wirkglieder von Membrankupplungen. Dissertation, Universität Kaiserslautern, 1988
9. Jiang, Fuqing: Ratterschwingungen bei selbsthemmenden Schneckengetrieben. Dissertation, Universität Kaiserslautern, 1989
10. Endemann, Ulrich: Ein Beitrag zur theoretischen und experimentelle Untersuchung hydrodynamisch arbeitender Spiralrillen-Radialgleitlager. Dissertation, Universität Kaiserslautern, 1989

11. Schlossarczyk, Jörg: Ein Beitrag zur Berechnung, Modellbildung und experimentellen Untersuchung drehelastischer Scheibenkupplungen unter Berücksichtigung des im Betrieb auftretenden Wellenversatzes. Dissertation, Universität Kaiserslautern, 1990

12. Lutz, Thomas: Ein Beitrag zur Berechnung druckbelasteter Elastomerlager. Dissertation, Universität Kaiserslautern, 1990

13. Lehnertz, Hermann: Ein Beitrag zur Berechnung hydrodynamisch arbeitender Radialgleitlager bei stationärem Betrieb mit Hilfe von Kleinrechnern. Dissertation, Universität Kaiserslautern, 1990

14. Maier, Martin: Experimentelle Untersuchung und numerische Simulation des Crashverhaltens von Faserverbundwerkstoffen. Dissertation, Universität Kaiserslautern, 1990

15. Steiner, Matthias: Ein Beitrag zur theoretischen und experimentellen Erfassung der Funktionsmechanismen von axialen Gleitringdichtungen. Dissertation, Universität Kaiserslautern, 1992

16. Stopp, Ralf: Elastomere Werkstoffe für Formdichtungen. Ein Beitrag zur Dimensionierung von Dichtsystemen. Dissertation, Universität Kaiserslautern, 1993

17. Joo, Kwang-Taek: Beitrag zum Einfluß mechanischer Parameter auf das Spurverhalten von dreirädrigen fahrerlosen Transportfahrzeugen. Dissertation, Universität Kaiserslautern, 1993

18. Fritzsche, Ralf: Ein Beitrag zur Untersuchung des Verhaltens von Radialwellendichtringen aus Elastomer- und Polytetrafluoräthylen-Material bei speziellen Betriebsbedingungen. Dissertation, Universität Kaiserslautern, 1994

19. Becker, Matthias: Ein Beitrag zur Untersuchung der Temperaturentwicklung in einer drehelastischen Scheibenkupplung bei dynamischer Beanspruchung unter besonderer Berücksichtigung des im Betrieb auftretenden Winkelversatzes. Dissertation, Universität Kaiserslautern, 1994

20. Helfrich, Axel: Bestimmung der Kenngrößen von nicht-newtonschen Schmierstoffen für die Dimensionierung hydrodynamisch arbeitender Gleitlager. Dissertation, Universität Kaiserslautern, 1995

21. Mattheis, Fritz: Ein Beitrag zur theoretischen und experimentellen Untersuchung von Flachdichtungen am Beispiel von polymerbeschichteten Metallblechen. Dissertation, Universität Kaiserslautern, 1995

22. Koch, Jürgen: Das Gleitlager endlicher Breite eine Lösung der Reynoldsschen Differentialgleichung. Dissertation, Universität Kaiserslautern, 1995

23. Spieth, Gottfried: Mechanische und werkstofftechnische Untersuchung von Verbindungen mit Schrauben aus thermoplastischem Kunststoff. Dissertation, Universität Kaiserslautern, 1995

24. Kramm, Georg: Ein Beitrag zur Modellierung von nicht-newtonschen Schmierstoffen und deren Verwendung für hydrodynamisch arbeitende Gleitlager. Dissertation, Universität Kaiserslautern, 1996

25. Berg, Michael: Untersuchungen zum Schmierstoffdurchsatz und zur Reibungsleistung dynamisch belasteter Radialgleitlager. Dissertation, Universität Kaiserslautern, 1996

26. Mán, László: Ein Beitrag zur Vorhersage von Freßschäden an tribologischen Wirkstellen. Dissertation, Universität Kaiserslautern, 1997

27. Gast, Stefan: Zielfunktionen zur Optimierung der Laufeigenschaften räumlicher Mechanismen auf der Grundlage ebener Kontaktverlustkriterien. Dissertation, Universität Kaiserslautern, 2000, Fortschritt-Berichte VDI, Reihe 1, Nr. 331

28. Ruhl, Christian: Ein Beitrag zur Wirkungsweise von Radialwellendichtungen unter Berücksichtigung von rauheitsinduzierter Hydrodynamik und radialen Verlagerungen der Gegenlauffläche. Dissertation, Universität Kaiserslautern, 2000, Fortschritt-Berichte VDI, Reihe 1, Nr. 339

29. Huber, Matthias: Ein Beitrag zur Untersuchung hydrodynamisch arbeitender Radialgleitlager unter Berücksichtigung der Schmierölverdünnung mit Rapsölmethylester. Dissertation, Universität Kaiserslautern, 2000, Fortschritt-Berichte VDI, Reihe 12, Nr. 453

30. Fuerst, Axel: Analytische Simulation von hydrodynamischen Gleitlagern in Wasserkraftanlagen. Dissertation, Universität Kaiserslautern, 2000, Fortschritt-Berichte VDI, Reihe 1, Nr. 343

31. Reif, Andreas: Entwicklung eines integrierten automatisiert schaltenden Getriebes zum Einsatz in Elektrostraßenfahrzeugen. Dissertation, Universität Kaiserslautern, 2000, Fortschritt-Bericht VDI, Reihe 1, Nr. 477

32. Lorreng, Dirk: Ein Beitrag zur Ermittlung und Beschreibung der Fließeigenschaften biologisch schnell abbaubarer Schmierstoffe. Dissertation, Universität Kaiserslautern, 2001, Fortschritt-Berichte VDI, Reihe 3, Nr. 741

33. Péteri, Szabolcs: Untersuchungen von Radialwellendichtringen unter Wellenschwingungen bei unterschiedlichen Temperaturen. Dissertation, Technische Universität Kaiserslautern, 2004, Fortschritt-Berichte VDI, Reihe 1, Nr. 379

34. Hahn, Kersten: Dynamik-Simulation von Wälzlagerkäfigen. Dissertation, Technische Universität Kaiserslautern, 2005, Skaker Verlag, Reihe Konstruktionstechnik, ISBN 3-83223-760-7

35. Teutsch, Roman: Kontaktmodelle und Strategien zur Simulation von Wälzlagern und Wälzführungen. Dissertation, Technische Universität Kaiserslautern, 2005, Maschinenelemente und Getriebetechnik Berichte Bd. 01/2005, ISBN 3-93689-073-0

36. Groß, Torsten: Ein Beitrag zur Entwicklung und Analyse serieller und paralleler Strukturen. Dissertation, Technische Universität Kaiserslautern, 2007, Maschinenelemente und Getriebetechnik Berichte Bd. 02/2007, ISBN 978-3-93943-246-3

37. Thullen, Carlo: Entwicklung und Validierung einer Universalprüfeinrichtung zur Untersuchung von dynamisch belasteten Radialwellendichtungen. Dissertation, Technische Universität Kaiserslautern, 2008, Maschinenelemente und Getriebetechnik Berichte Bd. 03/2008, ISBN 978-3-93943-289-0

38. Nicola, Andreas: Versuchsgestützte Dynamiksimulation hydraulisch gespannter Kettentriebe und Drehungleichförmigkeiten. Dissertation, Technische Universität Kaiserslautern, 2008, Maschinenelemente und Getriebetechnik Berichte Bd. 04/2008, ISBN 978-3-93943-290-6

39. Aul, Eduard: Analyse von Relativbewegungen in Wälzlagersitzen. Dissertation, Technische Universität Kaiserslautern, 2008, Maschinenelemente und Getriebetechnik Berichte Bd. 05/2008, ISBN 978-3-93943-296-8

40. Bach, Peter: Umsturzsicherheit von Doppeldeckeromnibussen. Dissertation, Technische Universität Kaiserslautern, 2008, Maschinenelemente und Getriebetechnik Berichte Bd. 06/2008, ISBN 978-3-93943-297-5

41. Scheuermann, Miguel: Dynamiksimulation zur virtuellen Produktentwicklung von Rollenschienenführungen. Dissertation, Technische Universität Kaiserslautern, 2010, Maschinenelemente und Getriebetechnik Berichte Bd. 07/2010, ISBN 978-3-94143-849-1

42. Wohlgemuth, Martin: Ein Beitrag zur Lebensdauerverlängerung von feststoffgeschmierten Rillenkugellagern. Dissertation, Technische Universität Kaiserslautern, 2010, Maschinenelemente und Getriebetechnik Berichte Bd. 08/2010, ISBN 978-3-94143-864-4

43. Leichner, Tim: Prognose der Dichtlippenfolgefähigkeit von RWDR bei dynamisch verlagerter Welle. Dissertation, Technische Universität Kaiserslautern, 2012, Maschinenelemente und Getriebetechnik Berichte Bd. 09/2012, ISBN 978-3-94143-891-0

44. Magyar, Balázs: Tribo dynamische Untersuchungen von Zylinderschneckengetrieben. Dissertation, Technische Universität Kaiserslautern, 2012, Maschinenelemente und Getriebetechnik Berichte Bd. 10/2012, ISBN 978-3-94399-503-9

45. Babbick, Till: Wandern von Wälzlagerringen unter Punktlast. Dissertation, Technische Universität Kaiserslautern, 2012, Maschinenelemente und Getriebetechnik Berichte Bd. 11/2012, ISBN 978-3-94399-505-3

46. Gastauer, Tobias: Reibungs und Verschleißuntersuchungen von Elastomerwerkstoffen für Dichtungsanwendungen. Dissertation, Technische Universität Kaiserslautern, 2012, Maschinenelemente und Getriebetechnik Berichte Bd. 12/2013, ISBN 978-3-94399-516-9

47. Gummer, Alexander: Analytische Untersuchung des Geometrieeinflusses auf das Verschleißverhalten von Antriebsketten. Dissertation, Technische Universität Kaiserslautern, 2013, Maschinenelemente und Getriebetechnik Berichte Bd. 13/2013, ISBN 978-3-94399-523-7

48. Aul, Viktor: Kontaktmodelle zur dynamischen Simulation vollrolliger Zylinderrollenlager. Dissertation, Technische Universität Kaiserslautern, 2014, Maschinenelemente und Getriebetechnik Berichte Bd. 14/2014, ISBN 978-3-94399-555-8

49. Marquart, Matthias: Ein Beitrag zur Nutzung feststoffgeschmierter Wälzlager. Dissertation, Technische Universität Kaiserslautern, 2014, Maschinenelemente und Getriebetechnik Berichte Bd. 15/2014, ISBN 978-3-94399-552-7

50. Buchmiller, Viktor: Wälzgelagerter Kurbeltrieb - Potenzial von Wälzlagern im Verbrennungsmotor. Dissertation, Technische Universität Kaiserslautern, 2015, Maschinenelemente und Getriebetechnik Berichte Bd. 16/2015, ISBN 978-3-94399-579-4

51. Kaiser, Fabian: Ein Simulationsmodell zur Analyse des Schmierfilms von Stangendichtungen. Dissertation, Technische Universität Kaiserslautern, 2015, Maschinenelemente und Getriebetechnik Berichte Bd. 17/2015, ISBN 978-3-95974-010-4

52. Bajer, Peter: Einflussgrößen auf das Schlupfverhalten von Wälzlagern in Generatorgetrieben. Dissertation, Technische Universität Kaiserslautern, 2016, Maschinenelemente und Getriebetechnik Berichte Bd. 18/2016, ISBN 978-3-95974-016-6

53. Jennewein, Barbara: Integrierter Berechnungsansatz zur Prognose des dynamischen Betriebsverhaltens von Radialwellendichtringen. Dissertation, Technische Universität Kaiserslautern, 2016, Maschinenelemente und Getriebetechnik Berichte Bd. 19/2016, ISBN 978-3-95974-015-9

54. Radnai, Benjamin: Wirkmechanismen bei spannungsbeaufschlagten Wälzlagern. Dissertation, Technische Universität Kaiserslautern, 2016, Maschinenelemente und Getriebetechnik Berichte Bd. 20/2016, ISBN 978-3-95974-029-6

55. Frölich, Daniel: Strategien und Modelle zur Simulation des Betriebsverhaltens von Radial-Wellendichtringen. Dissertation, Technische Universität Kaiserslautern, 2016, Maschinenelemente und Getriebetechnik Berichte Bd. 21/2016, ISBN 978-3-95974-030-2

56. Sappok, Daniel: Experimentelle und simulative Methoden zur Untersuchung der Verschleißvorgänge im Kettengelenk von Antriebs- und Steuerketten. Dissertation, Technische Universität Kaiserslautern, 2016, Maschinenelemente und Getriebetechnik Berichte Bd. 22/2016, ISBN 978-3-95974-033-3

57. Kiekbusch, Timo: Strategien zur dynamischen Simulation von Wälzlagern. Dissertation, Technische Universität Kaiserslautern, 2017, Maschinenelemente und Getriebetechnik Berichte Bd. 23/2017, ISBN 978-3-95974-043-2

58. Kaiser, Christian: Entwicklung einer Prüfmethodik für Modelluntersuchungen an schmutzbeaufschlagten Radial-Wellendichtringen. Dissertation, Technische Universität Kaiserslautern, 2017, Maschinenelemente und Getriebetechnik Berichte Bd. 24/2017, ISBN 978-3-95974-052-459

59. Fingerle, Thorsten: Experimentelle und simulative Untersuchung des Schlupfverhaltens von Kegelrollenlagern, Dissertation, Technische Universität Kaiserslautern, 2017, Maschinenelemente und Getriebetechnik Berichte Bd. 25/2017, ISBN 978-3-95974-054-8

60. Eckstein, Christian: Ermittlung repräsentativer Lastkollektive zur Betriebsfestigkeit von Ackerschleppern. Dissertation, Technische Universität Kaiserslautern, 2017, Maschinenelemente und Getriebetechnik Berichte Bd. 26/2017, ISBN 978-3-95974-064-7

61. Fruth, Torben: Vom tribologischen Modellversuch zum Maschinenelement: Berücksichtigung des rheologischen Verhaltens von Schmierstoffen in der Wälzlagersimulation. Dissertation, Technische Universität Kaiserslautern, 2018, Maschinenelemente und Getriebetechnik Berichte Bd. 27/2018, ISBN 978-3-95974-084-5

62. Fábián, Csaba: Verbesserung des Wirkungsgrades von Steuerkettentrieben durch bedarfsgerechte Kettenspannung. Dissertation, Technische Universität Kaiserslautern, 2018, Maschinenelemente und Getriebetechnik Berichte Bd. 28/2018, ISBN 978-3-95974-091-3

63. Oehler, Manuel: Methodische Ansätze zur Optimierung des Wirkungsgrades von Schneckengetrieben. Dissertation, Technische Universität Kaiserslautern, 2018, Maschinenelemente und Getriebetechnik Berichte Bd. 29/2018, ISBN 978-3-95974-097-5

64. Liebrecht, Jürgen: Technisch-mathematischer Ansatz zur Berechnung der hydraulischen Verluste in Wälzlagern. Dissertation, Technische Universität Kaiserslautern, 2018, Maschinenelemente und Getriebetechnik Berichte Bd. 30/2018, ISBN 978-3-95974-103-3

65. Krupp, Frederik: Reibleistungsreduzierung in Steuerkettentrieben. Dissertation, Technische Universität Kaiserslautern, 2018, Maschinenelemente und Getriebetechnik Berichte Bd. 31/2018, ISBN 978-3-95974-107-1

66. Herweg, Sören: Entwicklung und Validierung einer Methodik für erweiterte Ventiltriebssimulationen. Dissertation, Technische Universität Kaiserslautern, 2019, Maschinenelemente und Getriebetechnik Berichte Bd. 32/2019, ISBN 978-3-95974-106-4

67. Pörsch, Sascha: Ansätze zur erweiterten Lebensdauerberechnung feststoffgeschmierter Wälzlager. Dissertation, Technische Universität Kaiserslautern, 2019, Maschinenelemente und Getriebetechnik Berichte Bd. 33/2019, ISBN 978-3-95974-113-2

68. Thielen, Stefan: Entwicklung eines TEHD-Tribosimulationsmodells für Radialwellen-dichtringe. Dissertation, Technische Universität Kaiserslautern, 2019, Maschinenele-mente und Getriebetechnik Berichte Bd. 34/2019, ISBN 978-3-95974-120-0

69. Weyrich, Dominik: Tribologisches Prüfsystem für Dichtungsanwendungen. Dis-sertation, Technische Universität Kaiserslautern, 2020, Maschinenelemente und Getriebetechnik Berichte Bd. 35/2020, ISBN 978-3-95974-131-6

70. Wiesker, Sebastian: Axialschub an nadelgelagerten Stützrollen. Dissertation, Tech-nische Univer- sität Kaiserslautern, 2020, Maschinenelemente und Getriebetechnik Berichte Bd. 36/2020, ISBN 978-3-95974-136-1

71. Bechev, Dani: Prüfmethodik zur Charakterisierung der elektrischen Eigenschaften von Wälzla- gerschmierstoffen. Dissertation, Technische Universität Kaiserslautern, 2020, Maschinenelemente und Getriebetechnik Berichte Bd. 37/2020, ISBN 978-3-95974-135-4

72. Zimmermann, Florian: Optimierung der Energieeffizienz von Kettenspannsystemen. Dissertati- on, Technische Universität Kaiserslautern, 2020, Maschinenelemente und Getriebetechnik Be- richte Bd. 38/2020, ISBN 978-3-95974-138-5

73. Becker, Andre: Entwicklung einer Prüfmethodik für Verschleißuntersuchungen an Kettengelen- ken von Antriebs- und Steuerketten. Dissertation, Technische Universität Kaiserslautern, 2021, Maschinenelemente und Getriebetechnik Berichte Bd. 39/2020, ISBN 978-3-95974-143-9

74. Dahiwal, Rahul: Contribution to the Influence of Cage Wear on the Bearing Life of Solid- Lubricated Rolling Bearings. Dissertation, Technische Universität Kaiser-slautern, 2021, Maschi- nenelemente und Getriebetechnik Berichte Bd. 40/2021, ISBN 978-3-95974-151-4

75. Hofmann, Markus: Auslegung von Berechnungsverfahren am Beispiel der Simula-tion von Misch- reibung. Dissertation,Technische Universität Kaiserslautern, 2022, Maschinenelemente und Ge- triebetechnik Berichte Bd. 41/2022, ISBN 978-3-95974-174-3

76. Burkhart, Christoph: Ein Beitrag zum Verständnis des Verschleißverhaltens im System Radial- wellendichtring. Dissertation, Technische Universität Kaiserslautern, 2022, Maschinenelemente und Getriebetechnik Berichte Bd. 42/2022, ISBN 978-3-95974-184-2

77. Marmol, Margarita: Development of a new bearing geometry to reduce friction losses. Dissertation, Technische Universität Kaiserslautern, 2022, Maschinenelemente und Getriebetechnik Berichte Bd. 43/2022, ISBN 978-3-95974-189-7

MEGT

Research for Sustainability
Lehrstuhl für Maschinenelemente, Getriebe und Tribologie